

QCD Resummation Techniques

A Dissertation, Presented

by

Tibor Kúcs

to

The Graduate School

in Partial Fulfillment of the

Requirements

for the Degree of

Doctor of Philosophy

in

Physics

State University of New York

at Stony Brook

May 2004

Dissertation Director: Prof. George Sterman

State University of New York
at Stony Brook
The Graduate School

Tibor Kúcs

We, the dissertation committee for the above candidate for the Doctor of Philosophy degree, hereby recommend acceptance of this dissertation.

George Sterman

Professor, C.N. Yang Institute for Theoretical Physics, SBU
Dissertation Director

Jack Smith

Chair, C.N. Yang Institute for Theoretical Physics, SBU
Chairman of Dissertation

Michael Rijssenbeek

Professor, Department of Physics, SBU

Werner Vogelsang

Department of Physics, Brookhaven National Laboratory
Outside Member

This dissertation is accepted by the Graduate School.

Graduate School

Abstract of the Dissertation

QCD Resummation Techniques

by

Tibor Kúcs

Doctor of Philosophy

in

Physics

State University of New York

at Stony Brook

2004

Dissertation Director: Prof. George Sterman

The primary aim of high-energy QCD phenomenology is the determination of cross sections for particle collisions. One of the fundamental properties of QCD, the asymptotic freedom, suggests that the coupling constant in this high-energy regime is small. Provided that the coefficients of the perturbative expansion are small enough, the perturbation theory should give reliable results. However, in many quantities of interest the smallness of the expansion coefficients is violated due to large logarithmic enhancements. In this case the perturbation series cannot be truncated at fixed order

and, instead, it must be resummed. The development of such resummation algorithms is the main subject of the research presented in this thesis.

In the first part, we propose a resummation technique applicable to the Regge limit, which is defined for elastic scattering as the region of large energies and small momentum transfer. We develop a new systematic procedure for this limit in perturbative QCD to arbitrary logarithmic order. The formalism relies on the IR structure and the gauge symmetry of the theory. We identify leading regions in loop momentum space responsible for the singular structure of the amplitudes and perform power counting to determine the strength of these divergences. Using a factorization procedure introduced by Sen, we derive a sum of convolutions in transverse momentum space over soft and jet functions, which approximate the amplitude up to power-suppressed corrections. A set of evolution equations generalizing the BFKL equation and controlling the high energy behavior of the amplitudes to arbitrary logarithmic accuracy is derived. The general method is illustrated in the case of leading and next-to-leading logarithmic gluon reggeization and BFKL equation. We confirm the standard results at LL accuracy. At NLL order, we find an agreement with the reggeization conjecture up to two loops. However, starting at three loop order, we identify contributions violating the Regge ansatz. In addition, we calculate the evolution kernel determining the high-energy behav-

ior of the non-reggeized term in the scattering amplitude.

In the second part, we focus our attention to another intriguing problem of high-energy QCD, the resummation associated with soft radiation in dijet events which is complicated by the presence of non-global logarithms. We introduce a set of correlations between energy flow and event shapes that are sensitive to the flow of color at short distances in jet events. These correlations are formulated for a general set of event shapes, which includes jet broadening and thrust as special cases. We illustrate the method for e^+e^- dijet events, and calculate the correlation at leading logarithm in the energy flow and at next-to-leading-logarithm in the event shape.

Contents

Acknowledgements	x
1 Introduction	1
I Regge Resummation	6
2 The Method	7
2.1 Introduction	7
2.2 Kinematics and Gauge	11
2.3 Leading Regions, Power Counting	15
2.3.1 Singular contributions and reduced diagrams	15
2.3.2 Power counting	18
2.3.3 First factorized form	25
2.4 The Jet Functions	28
2.4.1 Decoupling of a soft gluon from a jet	28
2.4.2 Variation of a jet function with respect to a gauge fixing vector η	31

2.4.3	Dependence of a jet function on the plus component of a soft gluon's momentum attached to it	34
2.5	Factorization and Evolution Equations	36
2.5.1	Second factorized form	37
2.5.2	Evolution equation	41
2.5.3	Counting the number of logarithms	47
2.5.4	Solution of the evolution equations	49
2.6	Conclusions	54
3	The Applications	55
3.1	Amplitude at LL	56
3.2	Amplitude at NLL	62
3.2.1	Evolution of $\Gamma^{(n)}$ at LL	74
3.3	Gluon reggeization at NLL	76
3.3.1	Color octet and negative signature amplitude	76
3.3.2	NLL evolution equation for $J_A^{(1)}$	80
3.4	Conclusions	85
II	Resummation in Dijet Events	87
4	Event Shape / Energy Flow Correlations	88
4.1	Introduction	88
4.2	Shape/Flow Correlations	93
4.2.1	Weights and energy flow in dijet events	93
4.2.2	Weight functions and jet shapes	97
4.2.3	Low order example	99

4.3	Factorization of the Cross Section	103
4.3.1	Leading regions near the two-jet limit	104
4.3.2	The factorization in convolution form	107
4.3.3	The short-distance function	112
4.3.4	The jet functions	114
4.3.5	The soft function	118
4.4	Resummation	122
4.4.1	Energy flow	123
4.4.2	Event shape transform	126
4.4.3	The resummed correlation	130
4.4.4	The inclusive event shape	132
4.5	Results at NLL	133
4.5.1	Lowest order functions and anomalous dimensions	133
4.5.2	Checking the ξ_c -dependence	138
4.5.3	The inclusive event shape at NLL	139
4.5.4	Closed expressions	143
4.6	Numerical Results	145
4.7	Summary and Outlook	148
A		151
A.1	Power counting with contracted vertices	151
A.2	Varying the Gauge-Fixing Vector	157
A.3	Tulip-Garden Formalism	161
A.4	Feynman Rules	163
A.5	Origin of Glauber Region	165

B	167
B.1 Symmetry property of the jet functions	167
B.2 Evolution kernel	170
C	184
C.1 Eikonal Example	184
C.2 Recoil	188
Bibliography	204

Acknowledgements

It is my pleasure to thank all the people who directly or indirectly influenced the course of my research and without whom this work would have never been completed.

I wish to thank my adviser George Sterman for his patient guidance and invaluable help during my graduate career. I would also like to thank my collaborators Carola F. Berger and Maarten Boonekamp for working with me on many challenging problems. I am grateful to Zurab Kakushadze, Peter van Nieuwenhuizen, Martin Rocek, Robert Shrock, Jack Smith and George Sterman for wonderful lectures on quantum field theory, particle physics and string theory that I was lucky to attend. I am very thankful to Michael Rijssenbeek and Werner Vogelsang for making it possible to spend very fruitful research periods at CERN and BNL, respectively. My first steps in particle physics started in Prague, where Jiri Formanek, Jiri Horejsi and Jiri Chyla had very positive influence on me. I have also benefited from many physics and non-physics related conversations with my friends Lilia Anguelova, Nathan Clisby, Olindo Corradini, Alberto Iglesias, Peter Langfelder, Valer Zetocha and Kostas Zoubos during the years spent at Stony Brook.

Last but definitely not least, I am indebted to my parents and to my wife

Simona for their love and overall support during my educational period.

Chapter 1

Introduction

The birth of modern theory of strong interactions dates back to the early sixties when Gell-Mann and Zweig, [1] proposed the quark model to describe the properties of hadrons. This model suggests that all strongly interacting objects are composed of more elementary constituents named quarks. The first experimental support of this idea came in the late sixties at SLAC in a Deeply Inelastic Scattering. After this, the top priority became the hunt for a theory describing the dynamics of quarks. The distinctive feature of quarks is that they carry internal quantum number called color. Each quark can be in three color states. In the early seventies, Fritzsche, Gell-Mann and Leutwyler, Ref. [2], proposed a gauge theory describing the interaction between these quarks, called Quantum Chromodynamics (QCD). The mediator of this interaction, analogous to a photon in QED, is a gluon. At the classical level, QCD is invariant under the color $SU(3)$ local gauge transformations. The quarks transform in the fundamental representation and the gluons in the adjoint representation of this group. The process of quantization introduces

a gauge-fixing and the ghost terms into the Lagrangian. It satisfies a global residual gauge symmetry, called BRS symmetry, Ref. [3]. This symmetry proves to be very powerful in deriving identities between Green functions which are exact, i.e. they hold to all orders in perturbation theory.

The use of QCD as a perturbation theory is justified due to the property of asymptotic freedom discovered by 't Hooft, Gross, Wilczek and Politzer [4]. This property says that with increasing energies the coupling characterizing the interaction between the quarks and gluons decreases.

At the Ultra-Violet (UV) spectrum of internal momenta, the 4-D field theory is plagued by infinities. They appear since the current theory is only an effective theory valid in a certain energy regime. At sufficiently high energies it must, presumably, be embedded into some more fundamental theory. Nevertheless the theory is internally consistent, since we can remove these infinities by the process of renormalization, [5].

On the opposite end of momentum spectra, we encounter another type of divergences due to the Infra-Red (IR) region of soft momenta and collinear momenta. These divergences occur only for Green functions with external particles on-shell, when at least one of the particles is massless. Their origin is due to the degeneracy of states occurring in the soft and collinear limit, since we cannot possibly distinguish soft emissions and collinear splittings from situations when these emissions and splittings are absent. This observation suggests, that although IR divergences appear on a diagram by diagram basis, they cancel in properly averaged quantities. Namely, one needs to sum over all indistinguishable states. Already in 1937, Bloch and Nordsieck, Ref. [6], showed that this is, indeed, the case in QED when the summation over final

states is performed.

In QCD the situation is more complicated due to the self-coupling of gluons. In this case the KLN theorem, Ref. [7], which extends the summation over final state degeneracies to initial states as well, comes to our rescue. It is these quantities, which are free of IR divergences in QCD. From the experimental point of view this solution to the IR problem has a caveat, however. We can hardly expect to prepare our initial states in collision experiments to satisfy the conditions of the KLN theorem. Instead, we take one step further and invoke factorization theorems, Ref. [8]. It is exactly these theorems that enable us to turn perturbative QCD to a predictive calculational tool.

Factorization theorems claim that it is possible to separate short and long distance physics in physical quantities. A cross section for hadronic collision can be written as a convolution over functions describing long distance dynamics, which can be either Parton Distribution Functions (PDFs) or Fragmentation Functions (FFs), and functions describing short distance physics, which are partonic cross sections. The former have a physical interpretation of probabilities to find partons inside hadrons in case of PDFs, or to find hadrons inside partons in the case of FFs. These quantities cannot be completely determined from perturbative QCD and need to be fitted to experimental data. However, perturbative QCD enables us to find the evolution of the density functions with energy scale, Ref. [9]. These evolution equations resum large logarithmic corrections in this energy scale. They are the consequence of the factorized form for the cross section and the renormalization group equation stating that the physical quantities cannot depend on the scale at which we make the separation of short and long distance dynamics. Actually, under

very general assumptions, we can claim that whenever there is a factorization, there is a corresponding resummation. We will encounter concrete examples of this statement in later chapters. The main feature of the distribution functions is that they are process independent. This suggests that after fitting long distance functions in one process, we can use them in certain other processes involving the same type of hadron.

The second ingredient of the factorized cross section is the partonic cross section, which quantifies the interaction of the underlying partons in the hard process. This quantity is IR safe and calculable within perturbation theory provided the coefficients of the perturbative expansion are small. This is, however, not always the case. The coefficients are usually enhanced at kinematic edges of phase space. The reason for this is easily understood. The cancellation of IR divergences happens between virtual and real corrections. The integration in the virtual corrections spans all the energy scales: soft, hard and UV. The last one is removed by renormalization, so only the region between the soft and the hard scale remains. The phase space for real corrections depends on the kinematics considered. If we are completely inclusive then the integration region is the same as in the case of virtual corrections and there is a perfect cancellation between the two. However, once we impose kinematic constraints on the final state, then the cancellation between the two is incomplete and we can be left with large logarithms spoiling the perturbative expansion. In this case we need to resum the perturbation series.

The development of resummation procedures for various processes is the main topic of this work. It consists of two parts. In the first part we propose a systematic resummation technique applicable in the Regge limit, Ref. [10]

- [11]. This limit concerns almost forward elastic scattering of particles. In the second part of this thesis we pursue resummation of soft radiation accompanying final state jets in lepton collisions, Ref. [12].

Part I

Regge Resummation

Chapter 2

The Method

2.1 Introduction

The study of semi-hard processes within the framework of gauge quantum field theories has a long history. For reviews see Refs. [13]- [15]. The defining feature of such processes is that they involve two or more hard scales, compared to Λ_{QCD} , which are strongly ordered relative to each other. The perturbative expansions of scattering amplitudes for these processes must be resummed since they contain logarithmic enhancements due to large ratios of the scales involved. One of the most important examples is elastic $2 \rightarrow 2$ particle scattering in the Regge limit, $s \gg |t|$ (with s and t the usual Mandelstam variables). It is this process that we investigate in the next two chapters. We extend the techniques developed in Refs. [16] and [17] and devise a new systematic method for evaluation of QCD scattering amplitudes in the Regge limit to arbitrary logarithmic accuracy, Ref. [10].

The problem of the Regge limit in quantum field theory was first tackled in

the case of fermion exchange amplitude within QED in Ref. [18]. Here it was found that the positive signature amplitude takes a reggeized form up to the two loop level in Leading Logarithmic (LL) approximation. In Ref. [19] the calculations were extended to higher loops, and the imaginary part of the Next-to-Leading Logarithms (NLL) was also obtained. The analysis in Refs. [18] and [19] was performed in Feynman gauge. It was realized in Ref. [20] that a suitable choice of gauge can simplify the class of diagrams contributing at LL. The common feature of all this work was the use of fixed order calculations. To verify that the pattern of low order calculations survives at higher orders, a method to demonstrate the Regge behavior of amplitudes to all orders is necessary. This analysis was provided by A. Sen in Ref. [16], in massive QED. Sen developed a systematic way to control the high energy behavior of fermion and photon exchange amplitudes to arbitrary logarithmic accuracy. The formalism relies heavily on the IR structure and gauge invariance of QED and provides a proof of the reggeization of a fermion at NLL to all orders in perturbation theory.

The resummation of color singlet exchange amplitudes in non-abelian gauge theories in LL was achieved in the pioneering work of Ref. [21], where the reggeization of a gluon in LL was also demonstrated. The evolution equations resumming LL in the case of three gluon exchange was derived in Ref. [22]. In Ref. [17], n -gluon exchange amplitudes in QCD at LL level were studied and a set of evolution equations governing the high energy behavior of these amplitudes was obtained at LL. A different approach was undertaken in Ref. [23]. Here $n \rightarrow m$ amplitudes were studied in SU(2) Higgs model with spontaneous symmetry breaking. Starting with the tree level amplitudes, an iterative proce-

dure was developed, which generates a minimal set of terms in the perturbative expansion that have to be taken into account in order to satisfy the unitarity requirement of the theory. See also Ref. [24]. The extension of the BFKL formalism to NLL spanned over a decade. For a review see Ref. [25]. The building blocks of NLL BFKL are the emissions of two gluons or two quarks along the ladder, Ref. [26], one loop corrections to the emission of a gluon along the ladder, Ref. [27], and the two loop gluon trajectory, Refs. [28], [29], [30] and [31]. The particular results were put together in Ref. [32]. In Ref. [33], the trajectory for the fermion at NLL was evaluated by taking the Regge limit of the explicit two loop partonic amplitudes, Ref. [34].

Besides the NLO perturbative corrections to the BFKL kernel a variety of approaches have been developed for unitarization corrections, Refs. [35–37], which extend the BFKL formalism by incorporating selected higher-order corrections. The procedure proposed in this work, Refs. [10] and [11], in a way, places these approaches in an even more general context. In principle, it makes it possible to find the scattering amplitudes to arbitrary logarithmic accuracy and to determine the evolution kernels to arbitrary fixed order in the coupling constant. The formalism contains all color structures and, of course, the construction of the amplitude to any given level requires the computation of the kernels and the solution of the relevant equations.

The first part of the thesis is organized as follows. In Chapter 2, we develop the general algorithm. In Sec. 2.2 we discuss the kinematics of the partonic process under study and the gauge used. In Sec. 2.3 we identify the leading regions in internal momentum space, which produce logarithmic enhancements in the perturbation series. After identifying these regions, we perform power

counting to verify that the singularity structure of individual diagrams is at worst logarithmic. The leading regions lead to a factorized form for the amplitude (First Factorized Form). It consists of soft and jet functions, convoluted over soft loop momenta, which can still produce logarithms of $s/|t|$. In Sec. 2.4 we study the properties of the jet functions appearing in the factorization formula for the amplitude. We show how the soft gluons can be factored from the jet functions. In Sec. 2.5 we demonstrate how to express systematically the amplitude as a convolution in transverse momenta. In this form all the large logarithms are organized in jet functions and the soft transverse momenta integrals do not introduce any logarithms of $s/|t|$ (Second Factorized Form). We derive evolution equations that enable us to control the high energy behavior of the scattering amplitudes.

In Chapter 3, we illustrate the general method valid to all logarithmic accuracy in the case of LL and NLL in the amplitude and we examine the evolution equations at the same level. In Sec. 3.1, we resum the amplitude at LL and we find the LL gluon Regge trajectory. In Sec. 3.2, we analyze the amplitude at NLL order. We confirm the LL BFKL evolution equation. In Sec. 3.3, we address the problem of NLL evolution equations and the gluon reggeization at this accuracy. We confirm the Regge hypothesis at two loop level. However, we identify contributions violating the Regge ansatz starting at three loop order.

Some technical details are discussed in appendices A.1 - B.2. The first appendix treats power counting for regions of integration space where internal loop momenta become much larger than the momentum transfer. In Appendix A.2 we illustrate the origin of special vertices encountered due to the resum-

mation. In Appendix A.3 we show a systematic expansion for the amplitude leading to the first factorized form. In Appendix A.4 we list the Feynman rules used throughout the text. In Appendix A.5 we demonstrate the origin of extra soft momenta configurations (Glauber region) which need to be considered in the analysis of amplitudes in the Regge limit. In Appendix B.1, we study some symmetry properties of jet functions and finally in Appendix B.2, we give details on the derivation of the color octet NLL evolution equations.

2.2 Kinematics and Gauge

We analyze the amplitude for the elastic scattering of massless quarks

$$q(p_A, r_A, \lambda_A) + q'(p_B, r_B, \lambda_B) \rightarrow q(p_A - q, r_1, \lambda_1) + q'(p_B + q, r_2, \lambda_2), \quad (2.1)$$

within the framework of perturbative QCD in the kinematic region $s \gg -t$ (*Regge limit*), where $s = (p_A + p_B)^2$ and $t = q^2$ are the usual Mandelstam variables. We stress, however, that the results obtained below apply to arbitrary elastic two-to-two partonic process. We pick process (2.1) for concreteness only. The arguments in Eq. (2.1) label the momenta, p_i , the colors, r_i , and polarizations, λ_i , for $i = A, B, 1, 2$, respectively, of the initial and final state quarks. We choose to work in the center-of-mass (c.m.) where the momenta of the incoming quarks and the momentum transfer have the following com-

ponents ¹

$$\begin{aligned}
p_A &= \left(\sqrt{\frac{s}{2}}, 0^-, 0_\perp \right), \\
p_B &= \left(0^+, \sqrt{\frac{s}{2}}, 0_\perp \right), \\
q &= (0^+, 0^-, q_\perp).
\end{aligned} \tag{2.2}$$

Strictly speaking $q^\pm = \pm|t|/\sqrt{2s}$, so the q^\pm components vanish in the Regge limit only.

In the color basis

$$\begin{aligned}
b_{\mathbf{1}} &= \delta_{r_A, r_1} \delta_{r_B, r_2}, \\
b_{\mathbf{8}} &= -\frac{1}{2N_c} \delta_{r_A, r_1} \delta_{r_B, r_2} + \frac{1}{2} \delta_{r_A, r_2} \delta_{r_B, r_1},
\end{aligned} \tag{2.3}$$

with N_c the number of colors, we can view the amplitude for process (2.1) as a two dimensional vector in color space

$$A = \begin{pmatrix} A_{\mathbf{1}} \\ A_{\mathbf{8}} \end{pmatrix}, \tag{2.4}$$

where $A_{\mathbf{1}}$ and $A_{\mathbf{8}}$ are defined by the expansion

$$A_{r_A r_B, r_1 r_2} = A_{\mathbf{1}} (b_{\mathbf{1}})_{r_A r_B, r_1 r_2} + A_{\mathbf{8}} (b_{\mathbf{8}})_{r_A r_B, r_1 r_2}. \tag{2.5}$$

Since the amplitude is dimensionless and all particles are massless, its compo-

¹We use light-cone coordinates, $v = (v^+, v^-, v_\perp)$, $v^\pm = (v^0 \pm v^3)/\sqrt{2}$.

nents can depend, in general, on the following variables

$$A_i \equiv A_i \left(\frac{s}{\mu^2}, \frac{t}{\mu^2}, \alpha_s(\mu^2), \epsilon \right) \quad \text{for } i = \mathbf{1}, \mathbf{8}, \quad (2.6)$$

where μ is a scale introduced by regularization. We use dimensional regularization in order to regulate both infrared (IR) and ultraviolet (UV) divergences with $D = 4 - 2\epsilon$ the number of dimensions. Choosing the scale $\mu^2 = s$, the strong coupling, $\alpha_s(\mu)$, is small. However, in general, an individual Feynman diagram contributing to the process (2.1) at r -loop order can give a contribution as singular as $(s/t) \alpha_s^{r+1} \ln^{2r}(-s/t)$. In Sec. 2.5.3 we will confirm that there is a cancellation of all terms proportional to the i -th logarithmic power for $i = r + 1, \dots, 2r$ at order α_s^{r+1} in the perturbative expansion of the amplitude. Hence at r loops the amplitude is enhanced by a factor $(s/t) \alpha_s^{r+1} \ln^r(-s/t)$, at most. In order to get reliable results in perturbation theory we must, nevertheless, resum these large contributions. In the k -th non-leading logarithmic approximation one needs to resum all the terms proportional to $(s/t) \alpha_s^{r+1} \ln^{-j}(-s/t)$, $j = 0, \dots, k$ at r -loop level.

We perform our analysis in the Coulomb gauge, where the propagator of a gluon with momentum k has the form

$$-i \delta_{ab} \frac{N_{\alpha\beta}(k, \bar{k})}{k^2 + i\epsilon} \equiv -i \delta_{ab} \frac{1}{k^2 + i\epsilon} \left(g_{\alpha\beta} - \frac{k_\alpha \bar{k}_\beta + \bar{k}_\alpha k_\beta - k_\alpha k_\beta}{k \cdot \bar{k}} \right), \quad (2.7)$$

in terms of the vector

$$\bar{k} = k - (k \cdot \eta) \eta, \quad (2.8)$$

with

$$\eta = \left(\frac{1}{\sqrt{2}}, \frac{1}{\sqrt{2}}, 0_{\perp} \right), \quad (2.9)$$

an auxiliary four-vector defined in the partonic c.m. frame. The numerator of the gluon propagator satisfies the following identities

$$\begin{aligned} k^{\alpha} N_{\alpha\beta}(k, \bar{k}) &= k^2 \frac{k_{\beta} - \bar{k}_{\beta}}{k \cdot \bar{k}}, \\ \bar{k}^{\alpha} N_{\alpha\beta}(k, \bar{k}) &= 0. \end{aligned} \quad (2.10)$$

The first equality in Eq. (2.10) is the statement that the nonphysical degrees of freedom do not propagate in this gauge. For use below, we list the components of the gluon propagator:

$$\begin{aligned} N^{+-}(k) = N^{-+}(k) &= \frac{k^{+}k^{-} - k_{\perp}^2}{k \cdot \bar{k}}, \\ N^{++}(k) = N^{--}(k) &= \frac{k^{+}k^{-}}{k \cdot \bar{k}}, \\ N^{\pm i}(k) = N^{i\pm}(k) &= \pm \frac{(k^{-} - k^{+})k^i}{2k \cdot \bar{k}}, \\ N^{ij}(k) = N^{ji}(k) &= g^{ij} - \frac{k^i k^j}{k \cdot \bar{k}}. \end{aligned} \quad (2.11)$$

We note that these are symmetric functions under the transformation $k^{\pm} \rightarrow -k^{\pm}$, except for the components $N^{\pm i} = N^{i\pm}$, which are antisymmetric under this transformation. It was demonstrated in Ref. [38] that QCD is renormalizable in Coulomb gauge, by considering a class of gauges which interpolates between the covariant (Landau) and the physical (Coulomb) gauge.

2.3 Leading Regions, Power Counting

In order to resum the Regge logarithms, we need to identify the regions of integration in the loop momentum space that give rise to singularities in the limit $t/s \rightarrow 0$. We follow the method developed in Refs. [39,40], which begins with the identification of the relevant regions in momentum space.

2.3.1 Singular contributions and reduced diagrams

The singular contributions of a Feynman integral come from the points in loop momentum space where the integrand becomes singular due to the vanishing of propagator denominators. However, in order to give a true singularity the integration variables must be trapped at such a singular point. Otherwise we can deform the integration contour away from the dangerous region. These singular points are called pinch singular points. They can be identified with the following regions of integration in momentum space,

1. soft momenta, with scaling behavior $k^\mu \sim \sigma \sqrt{s}$ for all components ($\sigma \ll 1$),
2. momenta collinear to the momenta of the external particles, with scaling behavior
 $k^+ \sim \sqrt{s}$, $k^- \sim \lambda \sqrt{s}$, $|k_\perp| \sim \lambda^{1/2} \sqrt{s}$ for the particles moving in the + direction and
 $k^+ \sim \lambda \sqrt{s}$, $k^- \sim \sqrt{s}$, $|k_\perp| \sim \lambda^{1/2} \sqrt{s}$ for the particles moving in the - direction,
3. so-called Glauber or Coulomb momenta, Ref. [41], with scaling behavior

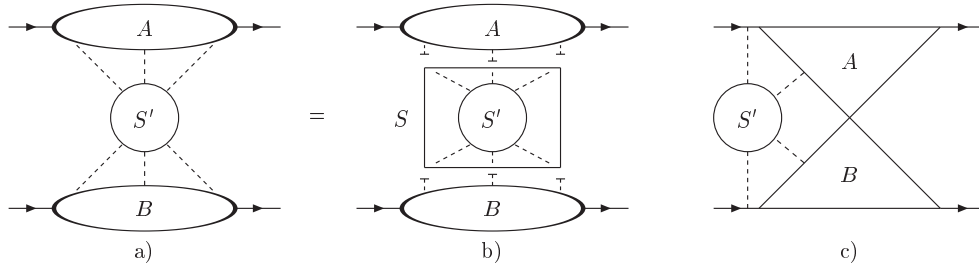


Figure 2.1: The reduced diagrams a) and c) contributing to the amplitude. Diagram b) represents a decomposition of diagram a) for the purpose of power counting.

$k^\pm \sim \sigma^\pm \sqrt{s}$, $|k_\perp| \sim \sigma \sqrt{s}$, where $\lambda \lesssim \sigma^\pm \lesssim \sigma$, and where the scaling factors λ, σ satisfy the strong ordering $\lambda \ll \sigma \ll 1$ (The origin of this region is illustrated in Appendix A.5.),

4. hard momenta, having the scaling behavior $k^\mu \sim \sqrt{s}$ for all components.

The extra gauge denominators $1/(k \cdot \bar{k})$ originating from the numerators of the gluon propagator, Eq. (2.7), do not alter the classification of the pinch singular points mentioned above. Actually, only the subsets 1 and 3 in the above classification can be produced due to the extra gauge denominators.

With every pinch singular point, we may associate a reduced diagram, which is obtained from the original diagram by contracting all hard lines (subset 4) at the particular singular point. As shown in Refs. [39, 40, 42] the reduced diagram corresponding to a given pinch singular point must describe a real physical process, with each vertex of the reduced diagram representing a real space-time point. This physical interpretation suggests two types of reduced diagrams contributing to the process (2.1), shown in Fig. 2.1.

The jet $A(B)$ contains lines whose momenta represent motion in the $+$ ($-$) direction. The lines included in the blob S' and the lines coming out of it are all soft (configurations 1 and 3 in the classification of loop momenta described above). These two oppositely moving (virtual) jets may interact through the exchange of soft lines, Fig. 2.1a, and/or they can meet at one or more space-time points, Fig. 2.1c.

Having found the most general reduced diagrams giving the leading behavior of the amplitude for process (2.1) in the Regge limit, we can estimate the strength of the IR divergence of the integral near a given pinch singular point. First we restrict ourselves to cases involving subsets 1 and 2 from the classification of loop momenta above. To do so, we count powers in the scaling variables λ and σ .

The scaling behavior of these loop momenta implies that every soft loop momentum contributes a factor σ^4 , every jet loop momentum gives rise to the power λ^2 , every internal soft boson (fermion) line provides a contribution σ^{-2} (σ^{-1}) and every internal jet line (fermionic or bosonic) scales as λ^{-1} . In addition, there can be suppression factors arising from the numerators of the propagators associated with internal lines and from internal vertices. As pointed out in Ref. [39], in physical gauges each three-point vertex connecting three jet lines is associated with a numerator factor that vanishes at least linearly in the components of the transverse jet momenta, and therefore provides a suppression $\lambda^{1/2}$.

We are now ready to estimate the power of divergence corresponding to the reduced diagrams describing our process. First we restrict ourselves to the case shown in Fig. 2.1a. As indicated schematically in Fig. 2.1b, we can

perform the power counting for the jets and for the soft part separately. All soft propagators and all soft loop momenta are included in the soft subdiagram S . The superficial degree of IR divergence of the reduced diagram R from Fig. 2.1a and Fig. 2.1b can then be written as

$$\omega(R) = \omega(A) + \omega(B) + \omega(S), \quad (2.12)$$

where the external lines and loops of S' are included in S . For $\omega(R) > 0$ the overall integral is finite, while $\omega(R) \leq 0$ corresponds to an IR divergent integral. When $\omega(R) = 0$, the integral diverges logarithmically. Here we set $\lambda \sim \sigma$ for power counting purposes. We come back to the effect of relaxing this condition in connection with a discussion of item 3, Glauber regions, in our list of singular momentum configurations.

2.3.2 Power counting

In this subsection, we consider the case when all vertices in a diagram are elementary only, that is, without contracted sub-diagrams carrying large loop momenta. In Appendix A.1 we show that our conclusions are unchanged by contracted vertices.

We perform the power counting for the soft part S first. Let f, b be the number of fermion, boson lines external to S' and let $E = f + b$. The superficial degree of divergence for S , found by summing powers of σ , can be written

$$\omega(S) = 4(E - 2) - 2b - f + 2 + \omega(S'), \quad (2.13)$$

where the first term is due to loop integrations linking S' to the jets, while the second and the third terms originate from propagators associated with the bosonic and fermionic lines, respectively, connecting the jets A , B and the soft part S' . The term $+2$ is introduced because we are resumming only leading power corrections proportional to s/t and therefore we exclude the overall factor s/t from the power counting. Since the lines entering S' are soft, we obtain the superficial degree of divergence for S' simply from dimensional analysis. It is given by

$$\omega(S') = 4 - b - 3f/2. \quad (2.14)$$

Combining Eqs. (2.13) and (2.14), the superficial degree of infrared divergence for the soft part S is then

$$\omega(S) = b + 3f/2 - 2. \quad (2.15)$$

Before carrying out the jet power counting, we introduce some notation. Let E_A be the number of soft lines attached to jet A ; I is the total number of jet internal lines; v_α is the number of α -point vertices connecting jet lines only; w_α has a meaning similar to v_α , with the difference that every vertex counted by w_α has at least one soft line attached to it. These are the vertices that connect the jet A to the soft part S . Finally, L denotes the number of loops internal to jet A . As noted above, we will perform the power counting for the case when the scaling factor for the soft momenta, σ , is of the same order as the scaling factor for jet A momenta. When the scaling factors are

different we encounter subdivergencies, which can be analyzed the same way as described below. We also assume that there are no internal and external ghost lines included in the jet function. Later we will discuss the effect of adding ghost lines.

The superficial degree of divergence for jet A can now be expressed as

$$\omega(A) = 2L - I + v_3/2. \quad (2.16)$$

The last term represents the suppression factor associated with the three point vertices. We denote the total number of vertices internal to jet A by

$$v = \sum_{\alpha} (v_{\alpha} + w_{\alpha}). \quad (2.17)$$

Next we use the Euler identity relating the number of loops, internal lines and vertices of jet A

$$L = I - v + 1, \quad (2.18)$$

and the relation between the number of lines and the number of vertices

$$2I + E_A + 2 = \sum_{\alpha} \alpha (v_{\alpha} + w_{\alpha}). \quad (2.19)$$

Using Eqs. (2.16)-(2.19) we arrive at the following form for the superficial degree of divergence for jet A

$$\omega(A) = 1 - (E_A + w_3)/2 + \sum_{\alpha \geq 5} (\alpha - 4)(v_{\alpha} + w_{\alpha})/2. \quad (2.20)$$

Since every vertex counted by w_α connects at least one external soft line, we have the condition

$$E_A \geq w_3 + \sum_{\alpha \geq 4} w_\alpha. \quad (2.21)$$

The equality holds when there is no vertex with two or more soft lines attached to it. Combining Eqs. (2.20)-(2.21) we arrive at the following lower bound on the superficial degree of divergence for jet A :

$$\omega(A) \geq 1 - E_A + \sum_{\alpha \geq 4} w_\alpha/2 + \sum_{\alpha \geq 5} (\alpha - 4)(v_\alpha + w_\alpha)/2. \quad (2.22)$$

The third and the last term in Eq. (2.22) are always positive or zero and hence

$$\omega(A) \geq 1 - E_A. \quad (2.23)$$

A similar result holds for jet B , and therefore the superficial degree of collinear divergence for jets A and B is

$$\omega(A) + \omega(B) \geq 2 - E, \quad (2.24)$$

with $E = E_A + E_B$ as in Eq. (2.13). Combining the results for soft and jet power counting, Eqs. (2.15) and (2.24), respectively in Eq. (2.12), we finally obtain the superficial degree of IR divergence for the reduced diagram in Fig. 2.1a,

$$\omega(R) \geq f/2. \quad (2.25)$$

This condition says that we can have at worst logarithmic divergences, provided no soft fermion lines are exchanged between the jets A and B . We

can therefore conclude that a reduced diagram from Fig. 2.1a containing elementary vertices can give at worst logarithmic enhancements in perturbation theory. In order for the divergence to occur, the following set of conditions must be satisfied:

1. There is an exchange of soft gluons between the jets A and B only, with no soft fermion lines attached to the jets.
2. The jets A and B contain 3 and 4 point vertices only, see Eq. (2.22).
3. Soft gluons are connected to jets only through 3 point vertices, Eq. (2.22), and at most one soft line is attached to each vertex inside the jets, Eq. (2.21).
4. In the reasoning above we have assumed that there is no suppression factor associated with the vertices where soft and jet lines meet. In order for this to be true, the soft gluons must be connected to the jet $A(B)$ lines via the $+(-)$ components of the vertices.

Next we consider adding ghost lines to the jet functions. As we review in Appendix A.4, the propagator for a ghost line with momentum k is proportional to $1/(k \cdot \bar{k})$. Hence every internal ghost line belonging to the jet gives a contribution which is power suppressed as $1/s$. Since the numerator factors do not compensate for this suppression, we can immediately conclude that the jet functions cannot contain internal or external ghost lines at leading power.

So far we have not taken into account the possibility when the soft loop momenta are pinched by the singularities of the jet lines. This situation allows different components of soft momenta to scale differently. For example, a

minus component of soft momentum can scale as the minus component of jet A momentum λ , while the rest of the soft momentum components may scale as σ , where $\lambda \ll \sigma \ll 1$. The origin of these extra pinches is illustrated in Appendix A.5.

Let us see what happens when we attach the ends of a gluon line with this extra pinch to jet A at one end and the soft subdiagram S at the other end. The integration volume for this soft loop momentum scales as $\lambda\sigma^3$. The soft gluon denominator gives a factor σ^{-2} . If this soft gluon is connected to the soft part at a 4-point vertex, there is no new denominator in the soft part. On the other hand, if the soft gluon is attached to the soft part via a 3-point vertex then the extra denominator including the numerator suppression factors scales as σ^{-1} . The new jet line scales as λ^{-1} as long as the condition $\lambda^{1/2} \gtrsim \sigma$ is obeyed; otherwise, we have the scaling σ^{-2} for the extra jet line. For $\lambda^{1/2} \gtrsim \sigma$ the Glauber region produces logarithmic infrared divergence. When $\lambda^{1/2} \lesssim \sigma$, the overall scaling factor λ/σ^2 indicates power suppressed contribution.

Let us now investigate another possibility, when the soft gluon connects jet A and jet B directly and its momentum is pinched by the singularities of the jet A and the jet B lines. Denoting the scaling factors of jet A and jet B as λ_A and λ_B , respectively, the integration volume provides the factor $\lambda_A\lambda_B\sigma^2$ and the soft gluon denominator contributes the power σ^{-2} . The extra jet A and jet B denominators scale as λ_A^{-1} and λ_B^{-1} , provided $\lambda_A^{1/2} \gtrsim \sigma$ and $\lambda_B^{1/2} \gtrsim \sigma$. For $\lambda_{A,B}^{1/2} \lesssim \sigma$ both extra jet denominators provide the scaling factor σ^{-2} . When $\lambda_{A,B}^{1/2} \gtrsim \sigma$, the power counting suggests logarithmically divergent integrals.

We have therefore verified that when the softest component of a soft line satisfies the ordering $\sigma^2 \lesssim \lambda \lesssim \sigma$, the Glauber (Coulomb) momenta produce

logarithmically IR divergent integrals and need to be taken into an account when identifying enhancements in perturbation series. The analysis demonstrated above for the case of one Glauber gluon can be extended to the situation with arbitrary number of Glauber gluons. This follows from dimensional analysis, in a similar fashion as the treatment of purely soft loop momenta above.

We conclude that the reduced diagram in Fig. 2.1a is at most logarithmically IR divergent, modulo the factor $s/|t|$. The reduced diagram in Fig. 2.1b loses one small denominator compared to the reduced diagram in Fig. 2.1a and since we are working in physical gauge, this loss cannot be compensated by a large kinematical factor coming from the numerator. Hence the reduced diagram in Fig. 2.1b is power suppressed compared to the reduced diagram in Fig. 2.1a, and we do not need to consider it at leading power.

Finally, let us discuss the scale of the soft momenta. In the case of soft exchange lines, each gluon propagator supplies a factor $1/(\sigma^2 s)$, which we want to keep at or below the order t in the leading power approximation. Thus the size of the scale is fixed to be $\sigma \sim \sqrt{|t|}/\sqrt{s}$. In the case of soft lines which are attached to jet A or to jet B only, the scaling factor lies in the interval $(\sqrt{|t|}/\sqrt{s}, 1)$. In the case of Glauber momenta, we again need $\sigma \sim \sqrt{|t|}/\sqrt{s}$. Then the condition $\lambda^{1/2} \gtrsim \sigma$, which is necessary for the logarithmic enhancement, implies that the scaling factors for $+$ and $-$ components of the Glauber (Coulomb) momenta can go down to $|t|/s$, the scale of the small components of jet momenta. Additionally, we should note that soft and jet sub-diagrams that do not carry the momentum transfer may approach the mass shell ($\lambda, \sigma \rightarrow 0$). Such lines produce true infrared divergences, which

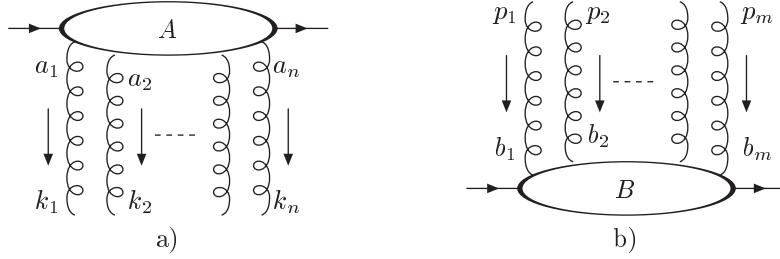


Figure 2.2: Jet A moving in the $+$ direction (a) and jet B moving in the $-$ direction (b).

we assume are made finite by dimensional regularization to preserve the gauge properties that we will use below. The same power counting as above shows that these divergences are also at worst logarithmic.

2.3.3 First factorized form

The analysis of the previous subsection suggests the following decomposition of the leading reduced diagram from Fig. 2.1a. Let us denote the $(n + 2)$ -point and $(m + 2)$ -point Green functions, 1PI in external soft gluon lines, corresponding to jet A , $J_{(A)\mu_1\dots\mu_n}^{(n) a_1\dots a_n}(p_A, q, \eta; k_1, \dots, k_n)$, Fig. 2.2a, and to jet B , $J_{(B)\nu_1\dots\nu_m}^{(m) b_1\dots b_m}(p_B, q, \eta; p_1, \dots, p_m)$, Fig. 2.2b, respectively. The jet function $J_{(A)}^{(n)}$ ($J_{(B)}^{(m)}$) also depends on the color of the incoming and outgoing partons r_A , r_1 (r_B , r_2), as well as on their polarizations λ_A , λ_1 (λ_B , λ_2), respectively. In order to avoid making the notation even more cumbersome we do not exhibit this dependence explicitly. In addition the dependence of $J_{(A)}^{(n)}$ and $J_{(B)}^{(m)}$ on the renormalization scale μ and the running coupling $\alpha_s(\mu)$ is understood. The jet functions also depend on the following parameters: the gauge fixing vector η , Eq. (2.9), of the Coulomb gauge, the four momenta of the external

soft gluons attached to jet A (B), k_1, \dots, k_n (p_1, \dots, p_m), and the Lorentz and color indices of the soft gluons attached to the jet A (B), μ_1, \dots, μ_n ; a_1, \dots, a_n (ν_1, \dots, ν_m ; b_1, \dots, b_m). The momenta of the soft gluons attached to the jets A and B satisfy the constraints $\sum_{i=1}^n k_i = q$ and $\sum_{j=1}^m p_j = q$.

According to the results of the power counting, the soft gluons couple to jet A via the minus components of their polarizations, and to jet B via the plus components of their polarizations. Therefore, only the following components survive in the leading power approximation

$$\begin{aligned}
J_A^{(n) a_1 \dots a_n}(p_A, q, \eta, v_B; k_1, \dots, k_n) &\equiv \left(\prod_{i=1}^n v_B^{\mu_i} \right) J_{(A) \mu_1 \dots \mu_n}^{(n) a_1 \dots a_n}(p_A, q, \eta; k_1, \dots, k_n), \\
J_B^{(m) b_1 \dots b_m}(p_B, q, \eta, v_A; p_1, \dots, p_m) &\equiv \left(\prod_{i=1}^m v_A^{\nu_i} \right) J_{(B) \nu_1 \dots \nu_m}^{(m) b_1 \dots b_m}(p_B, q, \eta; p_1, \dots, p_m),
\end{aligned} \tag{2.26}$$

where we have defined light-like momenta in the plus direction $v_A = (1, 0, 0_\perp)$ and in the minus direction $v_B = (0, 1, 0_\perp)$. We can now write the contribution to the reduced diagram in Fig. 2.1a, and hence to the amplitude for process (2.1), in the form

$$\begin{aligned}
A &= \sum_{n,m} \int \left(\prod_{i=1}^{n-1} d^D k_i \right) \int \left(\prod_{j=1}^{m-1} d^D p_j \right) J_A^{(n) a_1 \dots a_n}(p_A, q, \eta, v_B; k_1, \dots, k_n) \\
&\times S_{a_1 \dots a_n, b_1 \dots b_m}^{(n,m)}(q, \eta, v_A, v_B; k_1, \dots, k_n; p_1, \dots, p_m) \\
&\times J_B^{(m) b_1 \dots b_m}(p_B, q, \eta, v_A; p_1, \dots, p_m),
\end{aligned} \tag{2.27}$$

where the sum over repeated color indices is understood. Corrections to Eq. (2.27) are suppressed by positive powers of t/s . The jet functions $J_{A,B}$ are de-

fined in Eq. (2.26) in the leading power accuracy. The internal loop momenta of the jets A , B and of the soft function S are integrated over. The soft function will, in general, include delta functions setting some of the momenta k_1, \dots, k_n and color indices a_1, \dots, a_n of jet function J_A to the momenta p_1, \dots, p_m and to the color indices b_1, \dots, b_m of jet function J_B . The construction of the soft function S is described in Appendix A.3. For a given Feynman diagram there exist many reduced diagrams of the type shown in Fig. 2.1a, and one has to be careful in systematically expanding this diagram into the terms that have the form of Eq. (2.27). This systematic method can be achieved using the “tulip-garden” formalism first introduced in Ref. [44] and used in a similar context in Ref. [16]. For convenience of the reader we summarize this procedure in Appendix A.3.

Let us now identify the potential sources of the enhancements in $\ln(s/|t|)$ of the amplitude given by Eq. (2.27). If we integrate over the internal momenta of the jet functions then we can get $\ln((p_A \cdot \eta)^2/|t|)$ from J_A and $\ln((p_B \cdot \eta)^2/|t|)$ from J_B . In addition, according to the results of the power-counting, Eq. (2.23), we know that the jet function with n external soft gluons diverges as $1/\lambda^{n-1}$. After performing the integrals over the minus components of the external soft gluon lines attached to jet A and over the plus components of the external soft gluons connected to jet B , these divergent factors are potentially converted into logarithms of $\ln((p_A \cdot \eta)^2/|t|)$ and $\ln((p_B \cdot \eta)^2/|t|)$, respectively. Our goal will be to separate the full amplitude into a convolution over parameters that do not introduce any further logarithms of the form $\ln(s/|t|)$. This task will be achieved in Sec. 2.5.1. In the following section, we analyze the characteristics of the jet functions.

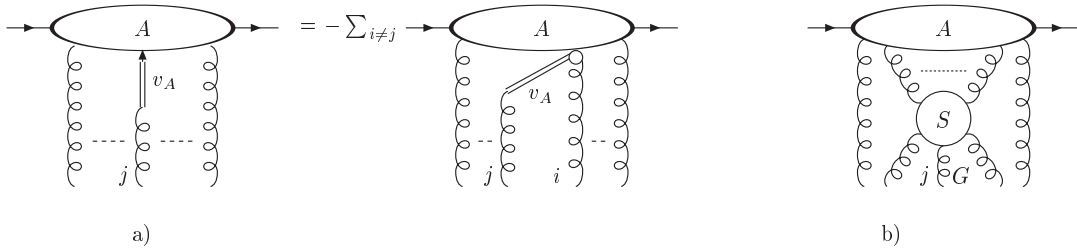


Figure 2.3: a) Decoupling of a K gluon from jet A . b) Leading contributions resulting from the attachment of a G gluon to jet A .

2.4 The Jet Functions

In this section we study the properties of the jet functions A , B given by Eq. (2.26) since, as Eq. (2.27) suggests, they will play an essential role in later analysis. Since the methods for both jet functions are similar we restrict our analysis to jet A only; jet B can be worked out in the same way. In Sec. 2.4.1 we examine the properties of jet A when the minus component of one of its external soft gluon momenta is of order $\sqrt{|t|}$. In Sec. 2.4.2 we find the variation of jet A with respect to the gauge fixing vector η , and finally in Sec. 2.4.3 we examine the dependence of jet A on the plus component of a soft gluon momentum attached to this jet.

2.4.1 Decoupling of a soft gluon from a jet

According to the results of power counting above, soft gluons attach to lines in jet A via the minus components of their polarization. Following the technique of Grammer and Yennie [45] we decompose the vertex at which the j th gluon is connected to jet A . We start with a trivial rewriting of J_A in Eq. (2.26)

$$J_A^{(n) a_1 \dots a_n} = \left(\prod_{i \neq j}^n v_B^{\mu_i} \right) v_B^{\mu_j} g_{\mu_j}^{\nu_j} J_{(A) \mu_1 \dots \nu_j \dots \mu_n}^{(n) a_1 \dots a_n}. \quad (2.28)$$

We now decompose the metric tensor into the form $g^{\mu\nu} = K^{\mu\nu}(k_j) + G^{\mu\nu}(k_j)$ where for a gluon with momentum k_j attached to jet A , $K^{\mu\nu}$ and $G^{\mu\nu}$ are defined by

$$\begin{aligned} K^{\mu\nu}(k_j) &\equiv \frac{v_A^\mu k_j^\nu}{v_A \cdot k_j - i\epsilon} \\ G^{\mu\nu}(k_j) &\equiv g^{\mu\nu} - K^{\mu\nu}(k_j). \end{aligned} \quad (2.29)$$

The K gluon carries scalar polarization. Since the jet A function has no internal tulip-garden subtractions (they are contained in the soft function S), we can use the Ward identities of the theory [46], which are readily derived from its underlying BRS symmetry [47], to decouple this gluon from the rest of the jet A after we sum over all possible insertions of the gluon. The result is

$$\begin{aligned} J_A^{(n) a_1 \dots a_j \dots a_n}(p_A, q, v_B, \eta; k_1, \dots, k_i, \dots, k_j, \dots, k_n) &= -\frac{1}{v_A \cdot k_j - i\epsilon} \\ \times \sum_{i \neq j}^n (-i g_s f^{c_i a_i a_j}) J_A^{(n-1) a_1 \dots c_i \dots \underline{a}_j \dots a_n}(p_A, q, v_B, \eta; k_1, \dots, k_i + k_j, \dots, \underline{k}_j, \dots, k_n). \end{aligned} \quad (2.30)$$

The notation \underline{a}_j and \underline{k}_j indicates that the jet function $J_A^{(n-1)}$ does not depend on the color index a_j and the momentum k_j , because they have been factored out. In Eq. (2.30), g_s is the QCD coupling constant and $f^{c_i a_i a_j}$ are the structure constants of the $SU(3)$ algebra. The pictorial representation of this

equation is shown in Fig. 2.3a. The arrow represents a scalar polarization and the double line stands for the eikonal line. The Feynman rules for the special vertices and the eikonal lines in Fig. 2.3a are listed in Appendix A.4. Strictly speaking the right-hand side of Eq. (2.30) and Fig. 2.3a contain contributions involving external ghost lines. However, from the power counting arguments of Sec. 2.3.2 we know that when all lines inside of the jet are jet-like, the jet function can contain neither external nor internal ghost lines. Therefore Eq. (2.30) is valid up to power suppressed corrections for this momentum configuration.

The idea behind the K - G decomposition is that the contribution of the soft G gluon attached to the jet line in the leading power is proportional to $v_B^\mu G_{\mu\nu} v_A^\nu = 0$. In order to avoid this suppression, the G gluon must be attached to a soft line. The general reduced diagram corresponding to the G gluon attached to jet A is depicted in Fig. 2.3b. The lines coming out of S as well as the lines included in it are soft. The letter G next to the j th gluon in Fig. 2.3b reminds us that this gluon is a G -gluon attaching to jet $J_{(A)\mu}$ via the $G^{+\mu}(k_j)$ vertex.

The reasoning described above applies to the case when all components of soft momenta are of the same order. In the situation of Coulomb (Glauber) momenta, this picture is not valid anymore, since the large ratio k_\perp/k^- coming from the $G^{+\perp}$ component can compensate for the suppression due to the attachment of the G part to a jet A line via the transverse components of the vertex.

2.4.2 Variation of a jet function with respect to a gauge fixing vector η

In this subsection we find the variation of the jet function $J_A^{(n)}$ with respect to a gauge fixing vector η . The motivation to do this can be easily understood. We consider the jet function with one soft gluon attached to it only, $J_A^{(1)}(p_A, q, v_B, \eta)$. Let us define

$$\xi_A \equiv p_A \cdot \eta \quad \text{and} \quad \zeta_B \equiv \eta \cdot v_B. \quad (2.31)$$

In these terms, jet function $J_A^{(1)}$ can depend on the following kinematical combinations: $J_A^{(1)}(p_A, q, v_B, \eta) = J_A^{(1)}(\xi_A, p_A \cdot v_B, \zeta_B, t)$. Using the identity $p_A \cdot v_B = 2 \xi_A \zeta_B$ and the fact, that the dependence of J_A on the vector v_B is introduced trivially via Eq. (2.26), we conclude that

$$J_A^{(1)}(p_A, q, v_B, \eta) = \zeta_B \bar{J}_A^{(1)}(\xi_A, t). \quad (2.32)$$

Our aim is to resum the large logarithms of $\ln(p_A^+)$ that appear in the perturbative expansion of the jet A function. In order to do so, we shall derive an evolution equation for $p_A^+ \partial J_A^{(1)} / \partial p_A^+$. Since p_A appears in combination with η only, we can trace out the p_A^+ dependence of $J_A^{(1)}$ by tracing out its dependence on η . This can be achieved by varying the gauge fixing vector η . The idea goes back to Collins and Soper [44] and Sen [43]. We will generalize the result to $J_A^{(n)}$ in Sec. 2.5.2.

We consider a variation that corresponds to an infinitesimal Lorentz boost in a positive $+$ direction with velocity $\delta\beta$. Thus, for the gauge fixing vector

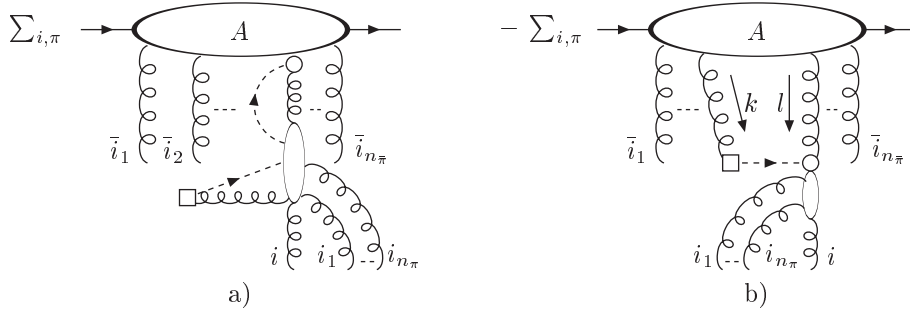


Figure 2.4: The result of a variation of jet function $J_A^{(n)}$ with respect to a gauge fixing vector.

$\eta = (1, 0, 0, 0)^2$, Eq. (2.9), the variation is: $\delta\eta \equiv \tilde{\eta} \delta\beta \equiv (0, 0, 0, 1) \delta\beta$. It leaves invariant the norm $\eta^2 = 1$ to order $\mathcal{O}(\delta\beta)$. The precise relation between the variation of the jet A function with respect to p_A^+ and $\delta\eta^\alpha$ is

$$p_A^+ \frac{\partial J_A^{(1)}}{\partial p_A^+} = -\tilde{\eta}^\alpha \frac{\partial J_A^{(1)}}{\partial \eta^\alpha} + \zeta_B \frac{\partial J_A^{(1)}}{\partial \zeta_B} = -\tilde{\eta}^\alpha \frac{\partial J_A^{(1)}}{\partial \eta^\alpha} + J_A^{(1)}. \quad (2.33)$$

We have used the chain rule in the first equality and the simple relation $\zeta_B \partial J_A^{(1)} / \partial \zeta_B = J_A^{(1)}$, following from Eq. (2.32), in the second one.

In order for Eq. (2.33) to be useful, we need to know what the variation of jet A with respect to the gauge fixing vector η is. The result of this variation for $J_A^{(n)}$ is shown in Fig. 2.4. It can be derived using either the formalism of the effective action, Ref. [48], or a diagrammatic approach first suggested in Ref. [44] and performed in axial gauge. We give an argument how Fig. 2.4 arises in Appendix A.2. Here we only note that the form of the diagrams in Fig. 2.4 is a direct consequence of a 1PI nature of the jet functions. The

²For the moment we use Cartesian coordinates.

explicit form of the boxed vertex

$$-i S^\alpha(k) \equiv -i(\eta \cdot k \tilde{\eta}^\alpha + \tilde{\eta} \cdot k \eta^\alpha), \quad (2.34)$$

as well as of the circled vertex is given in Fig. A.2 of Appendix A.4, while their origin is demonstrated in Appendix A.2. The dashed lines in Fig. 2.4 represent ghosts, and these are also given in Fig. A.2 of Appendix A.4. The four vectors η , given in Eq. (2.9), and

$$\tilde{\eta} = \left(\frac{1}{\sqrt{2}}, -\frac{1}{\sqrt{2}}, 0_\perp \right), \quad (2.35)$$

appearing in Eq. (2.34) are defined in the partonic c.m. frame, Eq. (2.2). We list the components of $S_\mu N^{\mu\alpha}(k)$

$$\begin{aligned} S_\mu(k) N^{\mu\pm}(k) &= k^\mp \left(\frac{k_+^2 - k_-^2}{2k \cdot \bar{k}} \pm 1 \right), \\ S_\mu(k) N^{\mu i}(k) &= \frac{k_-^2 - k_+^2}{2k \cdot \bar{k}} k^i, \end{aligned} \quad (2.36)$$

for later reference.

In Fig. 2.4, we sum over all external gluons. This is indicated by the sum over i . In addition, we sum over all possible insertions of external soft gluons $\{i_1, \dots, i_{n_\pi}\} \in \{1, \dots, n\} \setminus \{i\}$. This summation is denoted by the symbol π . We note that at lowest order, with only a gluon i attached to the vertical blob in Fig. 2.4b, this vertical blob denotes the transverse tensor structure

depending on the momentum k_i of this gluon

$$i \left(k_i^2 g^{\alpha\beta} - k_i^\alpha k_i^\beta \right). \quad (2.37)$$

It is labeled by a gluon line which is crossed by two vertical lines, Fig. A.2. The ghost line connecting the boxed and the circled vertices in Fig. 2.4b can interact with jet A via the exchange of an arbitrary number of soft gluons. We do not show this possibility in Fig. 2.4b for brevity.

Let us now examine what the important integration regions for a loop with momentum k in Fig. 2.4b are. The presence of the ghost line and of the nonlocal boxed vertex requires that in the leading power the loop momentum k must be soft. It can be neither collinear nor hard. This will enable us to factor the gluon with momentum k from the rest of the jet according to the procedure described in Sec. 2.4.1.

2.4.3 Dependence of a jet function on the plus component of a soft gluon's momentum attached to it

In this subsection we want to find the leading regions of the object $k_j^+ \partial J_A^{(n)} / \partial k_j^+$. This information will be essential for the analysis pursued in the next sections. For a given diagram contributing to $J_A^{(n)}$ we can always label the internal loop momenta in such a way that the momentum k_j flows along a continuous path connecting the vertices where the momentum k_j enters and leaves the jet function $J_A^{(n)}$. When we apply the operation $k_j^+ \partial / \partial k_j^+$ on a particular graph corresponding to $J_A^{(n)}$, it only acts on the lines and vertices which form this path. The idea is illustrated in Fig. 2.5a. The gluon with momentum k at-

taches to jet A via the three-point vertex v_1 . Then the momentum k flows through the path containing the vertices v_1, v_2, v_3 and the lines l_1, l_2 . The action of the operator $k^+ \partial / \partial k^+$ on a line or vertex which carries jet-like momentum gives a negligible contribution, since the $+$ component of this lines momentum will be insensitive to k^+ . In order to get a non-negligible contribution, the corresponding line must be soft. In Fig. 2.5a, lines l_1 and l_2 must be soft in order to get a non-suppressed contribution from the diagram after we apply the $k^+ \partial / \partial k^+$ operation on it. This, with the fact that the external soft gluons carry soft momenta, also implies that the lines l_3, \dots, l_6 must be soft. This reasoning suggests that in general a typical contribution to $k_j^+ \partial J_A^{(n)} / \partial k_j^+$ comes from the configurations shown in Fig. 2.5b. It can be represented as

$$\begin{aligned}
J_A^{(n) a_1 \dots a_n} &= \int \left(\prod_{i=1}^{n'-1} d^D k'_i \right) j^{(n, n') a_1 \dots a_n, a'_1 \dots a'_{n'}}(v_A, q, \eta; k_1, \dots, k_n; k'_1, \dots, k'_{n'}) \\
&\times J_A^{(n') a'_1 \dots a'_{n'}}(p_A, q, \eta, v_B; k'_1, \dots, k'_{n'}). \tag{2.38}
\end{aligned}$$

The function $j^{(n, n')}$ contains the contributions from the soft part S and from the gluons connecting the jet $J_A^{(n')}$ and S in Fig. 2.5b. The jet function $J_A^{(n')}$ has fewer loops than the original jet function $J_A^{(n)}$. Now applying the operation $k_j^+ \partial / \partial k_j^+$ to Eq. (2.38), the operator $k_j^+ \partial / \partial k_j^+$ acts only to the function $j^{(n, n')}$. Hence we can write

$$\begin{aligned}
k_j^+ \frac{\partial}{\partial k_j^+} J_A^{(n) a_1 \dots a_n} &= \int \left(\prod_{i=1}^{n'-1} d^D k'_i \right) k_j^+ \frac{\partial}{\partial k_j^+} j^{(n, n') a_1 \dots a_n, a'_1 \dots a'_{n'}}(v_A, q, \eta; \\
&k_1, \dots, k_n; k'_1, \dots, k'_{n'}) J_A^{(n') a'_1 \dots a'_{n'}}(p_A, q, \eta, v_B; k'_1, \dots, k'_{n'}). \tag{2.39}
\end{aligned}$$

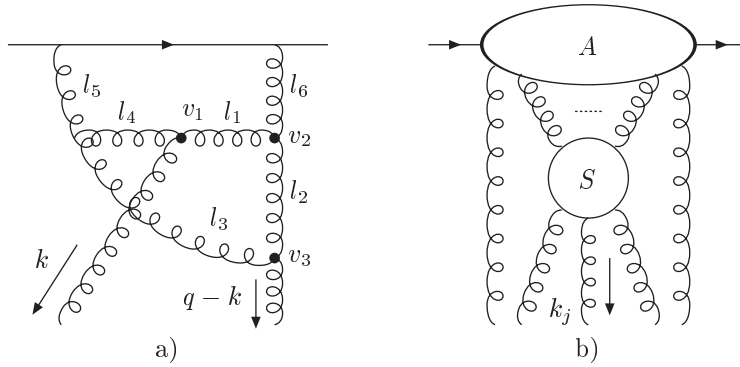


Figure 2.5: a) Momentum flow of the external soft gluon inside of jet A . b) Typical contribution to $k_j^+ \partial J_A^{(n)} / \partial k_j^+$.

We conclude that the contribution to $k_j^+ \partial J_A^{(n)} / \partial k_j^+$ can be expressed in terms of jet functions $J_A^{(n')}$ which have fewer loops than the original jet function.

2.5 Factorization and Evolution Equations

We are now ready to obtain evolution equations which will enable us to resum the large logarithms. First, in Sec. 2.5.1, we will put Eq. (2.27) into what we call the second factorized form. Then, in Sec. 2.5.2, we derive the desired evolution equations. In Sec. 2.5.3, we will show the cancellation of the double logarithms and finally in Sec. 2.5.4, we demonstrate that the evolution equations derived in Sec. 2.5.2 are sufficient to determine the high-energy behavior of the scattering amplitude.

2.5.1 Second factorized form

The goal of this subsection is to rewrite Eq. (2.27) into the following form [16]

$$\begin{aligned}
A &= \sum_{n,m} \int \left(\prod_{i=1}^{n-1} d^{D-2} k_{i\perp} \right) \left(\prod_{j=1}^{m-1} d^{D-2} p_{j\perp} \right) \\
&\times \Gamma_A^{(n) a_1 \dots a_n} (p_A, q, \eta, v_B; k_{1\perp}, \dots, k_{n\perp}; M) \\
&\times S'_{a_1 \dots a_n, b_1 \dots b_m}^{(n,m)} (q, \eta, v_A, v_B; k_{1\perp}, \dots, k_{n\perp}; p_{1\perp}, \dots, p_{m\perp}; M) \\
&\times \Gamma_B^{(m) b_1 \dots b_m} (p_B, q, \eta, v_A; p_{1\perp}, \dots, p_{m\perp}; M), \tag{2.40}
\end{aligned}$$

where $\Gamma_A^{(n)}$ and $\Gamma_B^{(m)}$ are defined as the integrals of the jet functions $J_A^{(n)}$ and $J_B^{(m)}$, over the minus and plus components, respectively, of their external soft momenta, with the remaining light-cone components of soft momenta set to zero,

$$\begin{aligned}
\Gamma_A^{(n) a_1 \dots a_n} (p_A, q, \eta, v_B; k_{1\perp}, \dots, k_{n\perp}; M) &\equiv \prod_{i=1}^{n-1} \left(\int_{-M}^M dk_i^- \right) \\
&\times J_A^{(n) a_1 \dots a_n} (p_A, q, \eta, v_B; k_{1\perp}, \dots, k_{n\perp}, k_1^+ = 0, \dots, k_n^+ = 0, k_1^-, \dots, k_n^-), \\
\Gamma_B^{(m) b_1 \dots b_m} (p_B, q, \eta, v_A; p_{1\perp}, \dots, p_{m\perp}; M) &\equiv \prod_{i=1}^{m-1} \left(\int_{-M}^M dp_i^+ \right) \\
&\times J_B^{(m) b_1 \dots b_m} (p_B, q, \eta, v_A; p_{1\perp}, \dots, p_{m\perp}, p_1^- = 0, \dots, p_m^- = 0, p_1^+, \dots, p_m^+). \tag{2.41}
\end{aligned}$$

In Eq. (2.40), S' is a calculable function of its arguments and M is an arbitrary scale of the order $\sqrt{|t|}$. The functions $\Gamma_{A,B}$ and S' depend individually on this scale, but the final result, of course, does not. Based on the discussion at the end of Sec. 2.3.3, one can immediately recognize that all the large logarithms

are now contained in the functions Γ_A and Γ_B . The convolution of Γ_A, Γ_B and S' is over the transverse momenta of the exchanged soft gluons. Since these momenta are restricted to be of the order $\sqrt{|t|}$, the integration over transverse momenta cannot introduce $\ln(s/|t|)$. This indicates that at leading logarithm approximation the factorized diagram with the exchange of one gluon only contributes. In general, when we consider a contribution to the amplitude at $L = L_A + L_B + L_{S'}$ loop level, where L_A, L_B and $L_{S'}$ is the number of loops in Γ_A, Γ_B and S' , respectively, we can get $L - L_{S'}$ logarithms of $s/|t|$ at most. Hence, the investigation of the s/t dependence of the full amplitude reduces to the study of the p_A^+ and p_B^- dependence of Γ_A and Γ_B , respectively. We formalize this statement at the end of Sec. 2.5.3 after we have proved that Γ_A (Γ_B) contains one logarithm of p_A^+ (p_B^-) per loop.

Let us now show how we can systematically go from Eq. (2.27) to Eq. (2.40). We follow the method developed in Ref. [16]. We start from Eq. (2.27) and consider the k_i^- integrals over the jet function J_A for fixed $k_i^+, k_{i\perp}$:

$$A = \sum_n \int \prod_{i=1}^{n-1} dk_i^- R_A^{a_1 \dots a_n}(k_1^-, \dots, k_n^-; \dots) J_A^{(n) a_1 \dots a_n}(p_A, q, \eta, v_B; k_1, \dots, k_n), \quad (2.42)$$

where R_A is given by the soft function S and the jet function J_B ,

$$\begin{aligned} R_A^{a_1 \dots a_n}(k_1^-, \dots, k_n^-; \dots) &= \sum_m \int \left(\prod_{j=1}^{m-1} d^D p_j \right) \\ &\times S_{a_1 \dots a_n, b_1 \dots b_m}^{(n, m)}(q, \eta, v_A, v_B; k_1, \dots, k_n; p_1, \dots, p_m) \\ &\times J_B^{(m) b_1 \dots b_m}(p_B, q, \eta, v_A; p_1, \dots, p_m). \end{aligned} \quad (2.43)$$

We next use the following identity for R_A :³

$$\begin{aligned}
R_A(k_1^-, \dots, k_{n-1}^-) &= R_A(k_1^- = 0, \dots, k_{n-1}^- = 0) \prod_{i=1}^{n-1} \theta(M - |k_i^-|) \\
&+ \sum_{i=1}^{n-1} [R_A(k_1^-, \dots, k_i^-, k_{i+1}^- = 0, \dots, k_{n-1}^- = 0) \\
&- R_A(k_1^-, \dots, k_{i-1}^-, k_i^- = 0, \dots, k_{n-1}^- = 0) \theta(M - |k_i^-|)] \\
&\times \prod_{j=i+1}^{n-1} \theta(M - |k_j^-|). \tag{2.44}
\end{aligned}$$

We have suppressed the dependence on the color indices and other possible arguments in R_A for brevity. The scale M can be arbitrary, but, as above, we take it to be of the order of $\sqrt{|t|}$. The first term on the right hand side of Eq. (2.44) has all $k_i^- = 0$. The rest of the terms can be analyzed using the K - G decomposition discussed in Sec. 2.4.1. Consider the ($i = 1$) term, say, in the square bracket of Eq. (2.44) inserted in Eq. (2.42). Let us denote it A_1 . In the region $|k_1^-| \ll M$ the integrand vanishes. On the other hand, for $|k_1^-| \sim M$ we can use the K - G decomposition for the gluon with momentum k_1 . The contribution from the K part factorizes and the integral over the component k_1^- has the form

$$\begin{aligned}
A_1 &= \int \frac{dk_1^-}{v_A \cdot k_1} [R_A^{a_1 \dots a_n}(k_1^-, k_2^- = 0, \dots, k_{n-1}^- = 0) \\
&- \theta(M - |k_1^-|) R_A^{a_1 \dots a_n}(k_1^- = 0, \dots, k_{n-1}^- = 0)] \\
&\times \sum_{i=2}^{n-1} \left(i g_s f^{a_1 c_i a_i} \int_{-M}^M \prod_{j=2}^{n-1} dk_j^- J_A^{(n-1) a_2 \dots c_i \dots a_n}(p_A, q, \eta, v_B; \right. \\
&\quad \left. k_2, \dots, k_1 + k_i, \dots, k_n) \right). \tag{2.45}
\end{aligned}$$

³Recall that $k_n = q - (k_1 + \dots + k_{n-1})$, so k_n is not an independent momentum.

Eq. (2.45) is valid when all the lines inside the jet are jet-like. In that case the contributions from the ghosts are power suppressed. The contribution corresponding to a G gluon comes from the region of integration shown in Fig. 2.3b. It can be expressed in the form of Eq. (2.42) involving some $J_A^{(n')}$ with fewer loops than in the original $J_A^{(n)}$, and an R'_A with more loops than in the original R_A . Then we can repeat the steps described above with this new integral.

Every subsequent term in the square bracket of Eq. (2.44) can be treated the same way as the first term. This allows us to express the integral in Eq. (2.42) in terms of k_i^- integrals over some $J_A^{(n')}$ s, which have the same or fewer number of loops than the original $J_A^{(n)}$,

$$\begin{aligned} & \Gamma_A^{(n') a'_1 \dots a'_{n'}} \left(p_A, q, \eta, v_B; k_1'^+, \dots, k_{n'}'^+; k_{1\perp}', \dots, k_{n'\perp}' ; M \right) \equiv \\ & \int_{-M}^M \prod_{i=1}^{n'-1} dk_i'^- J_A^{(n') a'_1 \dots a'_{n'}} \left(p_A, q, \eta, v_B; k_1', \dots, k_{n'}' \right). \end{aligned} \quad (2.46)$$

We now want to set $k_i'^+ = 0$ in order to put Eq. (2.42) into the form of Eq. (2.40). To that end, we employ an identity for $J_A^{(n')}$ (we again suppress the dependence on the color indices for brevity)

$$\begin{aligned} & J_A^{(n')} \left(p_A, q, \eta, v_B; k_1', \dots, k_{n'}' \right) = \\ & J_A^{(n')} \left(p_A, q, \eta, v_B; k_1'^+ = 0, \dots, k_{n'}'^+ = 0, k_1'^-, \dots, k_{n'}'^-, k_{1\perp}', \dots, k_{n'\perp}' \right) \\ & + \sum_{i=1}^{n'-1} \int_0^{k_i'^+} dl_i^+ \frac{\partial}{\partial l_i^+} J_A^{(n')} \left(p_A, q, \eta, v_B; k_{1\perp}', \dots, k_{n'\perp}', k_1'^-, \dots, k_{n'}'^-, \right. \\ & \left. k_1'^+, \dots, k_{i-1}'^+, l_i^+, k_{i+1}'^+ = 0, \dots, k_{n'}'^+ = 0 \right). \end{aligned} \quad (2.47)$$

Substituting the first term of Eq. (2.47) into Eq. (2.46), we recognize the definition for Γ_A , Eq. (2.41). We have shown in Sec. 2.4.3 that the contributions from the terms proportional to $\partial J_A^{(n')}/\partial l_i^+$ in Eq. (2.47) can be expressed as soft-loop integrals of some $J_A^{(n'')}$, again with fewer loops than in $J_A^{(n')}$. When we substitute this into Eq. (2.46) we may express the resulting contribution in terms of integrals which have the form of Eq. (2.42). We can now repeat all the steps mentioned so far, with this new integral. By this iterative procedure we can transfer the k_i^- integrals in Eq. (2.42) to $J_A^{(n)}$ and also set $k_i^+ = 0$ inside $J_A^{(n)}$. In a similar manner, we can analyze the p_j^+ integrals in Eq. (2.27), and express them in terms of Γ_B defined in Eq. (2.41). This algorithm, indeed, leads from the first factorized form of the considered amplitude, Eq. (2.27), to the second factorized form, Eq. (2.40).

2.5.2 Evolution equation

We have now collected all the ingredients necessary to derive the evolution equations for quantities defined in Eq. (2.41). Consider $\Gamma_A^{(n)}$. We aim to find an expression for $p_A^+ \partial \Gamma_A^{(n)} / \partial p_A^+$. As discussed in Sec. 2.4.2 this will enable us to resum the large logarithms of $\ln(p_A^+)$ and eventually the logarithms of $\ln(s/|t|)$. According to Eq. (2.41), in order to find $p_A^+ \partial \Gamma_A^{(n)} / \partial p_A^+$, we need to study $p_A^+ \partial J_A^{(n)} / \partial p_A^+$. Using the identities $p_A \cdot v_B = 2 \xi_A \zeta_B$, $p_A \cdot k_i = 2 \xi_A \xi_i$, where $\xi_i \equiv k_i^- \eta^+$ and ξ_A, ζ_B are defined in Eq. (2.31), we conclude that

$$J_A^{(n)} = \zeta_B^n \bar{J}_A^{(n)} (\xi_A, \{\xi_i\}_{i=1}^{n-1}, t, \{q_\perp \cdot k_{i\perp}\}_{i=1}^{n-1}, \{k_{i\perp} \cdot k_{j\perp}\}_{i,j=1}^{n-1}). \quad (2.48)$$

From this structure, using the chain rule, we derive the following relation satisfied by $J_A^{(n)}$, which generalizes Eq. (2.33) to $J_A^{(n)}$ with arbitrary number of external gluons,

$$p_A^+ \frac{\partial J_A^{(n)}}{\partial p_A^+} = -\tilde{\eta}^\alpha \frac{\partial J_A^{(n)}}{\partial \eta^\alpha} + \sum_{i=1}^{n-1} k_i^- \frac{\partial J_A^{(n)}}{\partial k_i^-} + \zeta_B \frac{\partial J_A^{(n)}}{\partial \zeta_B}. \quad (2.49)$$

Now, we integrate both sides of Eq. (2.49) over $\prod_{j=1}^{n-1} \left(\int_{-M}^M dk_j^- \right)$ and set all $k_j^+ = 0$. Then, using the definition for $\Gamma_A^{(n)}$, Eq. (2.41), the left hand side is nothing else but $p_A^+ \partial \Gamma_A^{(n)} / \partial p_A^+$. The first term on the right hand side of Eq. (2.49) is simply $-\tilde{\eta}^\alpha \partial \Gamma_A^{(n)} / \partial \eta^\alpha$. Noting that $\zeta_B \partial J_A^{(n)} / \partial \zeta_B = n J_A^{(n)}$, the last term gives simply $n \Gamma_A^{(n)}$. For the middle term, we use integration by parts

$$\begin{aligned} & \prod_{j=1}^{n-1} \left(\int_{-M}^M dk_j^- \right) \sum_{i=1}^{n-1} k_i^- \frac{\partial J_A^{(n)}}{\partial k_i^-} = \prod_{j=1}^{n-1} \left(\int_{-M}^M dk_j^- \right) \sum_{i=1}^{n-1} \left[\frac{\partial}{\partial k_i^-} (k_i^- J_A^{(n)}) - J_A^{(n)} \right] = \\ & \sum_{i=1}^{n-1} \int_{-M}^M \left(\prod_{j \neq i}^{n-1} dk_j^- \right) M \left[J_A^{(n)}(k_i^- = +M, \dots) + J_A^{(n)}(k_i^- = -M, \dots) \right] \\ & - (n-1) \Gamma_A^{(n)}. \end{aligned} \quad (2.50)$$

Combining the partial results, Eqs. (2.49) and (2.50), we obtain the following evolution equation

$$\begin{aligned} p_A^+ \frac{\partial \Gamma_A^{(n)}}{\partial p_A^+} &= \sum_{i=1}^{n-1} \int_{-M}^M \left(\prod_{j \neq i}^{n-1} dk_j^- \right) M \left[J_A^{(n)}(k_i^- = +M, \dots) + J_A^{(n)}(k_i^- = -M, \dots) \right] \\ &+ \Gamma_A^{(n)} - \tilde{\eta}^\alpha \frac{\partial \Gamma_A^{(n)}}{\partial \eta^\alpha}. \end{aligned} \quad (2.51)$$

The jet function $J_A^{(n)}$ in the first term of Eq. (2.51) is evaluated at $\{k_i^+ = 0\}_{i=1}^n$ and the k_j^- s are integrated over for $j = 1, \dots, n-1$ and $j \neq i$. The first term in Eq. (2.51) can be analyzed using the K - G decomposition for gluon i since the k_i^- is evaluated at the scale $M \sim \sqrt{|t|}$. The outcome of the last term in Eq. (2.51) has been determined in Sec. 2.4.2, Fig. 2.4⁴. As a result we have all the tools necessary to determine the asymptotic behavior of the high energy amplitude for process (2.1). To demonstrate this, we will rewrite Eq. (2.51) into the form where on the right hand side there will be a sum of terms involving $\Gamma_A^{(n')}$ s convoluted with functions which do not depend on p_A^+ . Let us proceed term by term.

Again, the K - G decomposition applies to the first term in Eq. (2.51) because the external momenta are fixed with $k_i^- = \pm M$. Using the factorization of a K gluon given in Eq. (2.30) it is clear that the contributions from the K gluons cancel for $J_A^{(n)}$ s evaluated at $k_i^- = +M$ and $k_i^- = -M$. Hence only the G gluon contribution survives in this term. Its most general form is shown in Fig. 2.3b. Before writing it down let us introduce the following notation. For a set of indices $\{1, 2, \dots, n\} \setminus \{i\}$ consider all the possible subsets of this set, with $1, 2, \dots, (n-1)$ number of elements. Let us denote a given subset by π , its complementary subset $\bar{\pi}$, the number of elements in this subset as n_π and in its complementary as $n_{\bar{\pi}} \equiv (n-1) - n_\pi$. With this notation, we can write

⁴Strictly speaking we have analyzed $\tilde{\eta}^\alpha \partial J_A^{(n)} / \partial \eta^\alpha$, but because of the relationship between $J_A^{(n)}$ and $\Gamma_A^{(n)}$ given by Eq. (2.41), once we know $\tilde{\eta}^\alpha \partial J_A^{(n)} / \partial \eta^\alpha$ we also know $\tilde{\eta}^\alpha \partial \Gamma_A^{(n)} / \partial \eta^\alpha$.

the i th contribution to the first term in Eq. (2.51) in the form

$$\begin{aligned}
& J_A^{(n) a_1 \dots a_n} (k_i^- = +M, \dots) + J_A^{(n) a_1 \dots a_n} (k_i^- = -M, \dots) = \sum_{\pi} \int \prod_{j=1}^{N-1} \frac{d^D l_j}{(2\pi)^D} \\
& S_{a_i a_{i_1} \dots a_{i_{n_\pi}} b_1 \dots b_N}^{\mu_1 \dots \mu_N} \left(k_i^- = +M, k_{i_1}^-, \dots, k_{i_{n_\pi}}^-; k_i^+ = 0, k_{i_1}^+ = 0, \dots, k_{i_{n_\pi}}^+ = 0; \right. \\
& \left. k_{i_\perp}, k_{i_1 \perp}, \dots, k_{i_{n_\pi \perp}}; l_1, \dots, l_N; q, \eta \right) \\
\times & J_A^{(n_{\bar{\pi}}+N) a_{\bar{i}_1} \dots a_{\bar{i}_{n_{\bar{\pi}}}} b_1 \dots b_N}^{\mu_1 \dots \mu_N} \left(k_{i_1}^-, \dots, k_{i_{n_{\bar{\pi}}}}^-; k_{i_1}^+ = 0, \dots, k_{i_{n_{\bar{\pi}}}}^+ = 0; \right. \\
& \left. k_{i_1 \perp}, \dots, k_{i_{n_{\bar{\pi}} \perp}}; l_1, \dots, l_N; p_A, q, \eta \right) + (k_i^- \rightarrow -M). \tag{2.52}
\end{aligned}$$

In Eq. (2.52), the summation over repeated indices is understood. We sum over all possible subsets π . In other words, we sum over all possible attachments of external gluons to jet function J_A and to the soft function S . The elements of a given set π are denoted $i_1, i_2, \dots, i_{n_\pi}$. The elements of a complementary set $\bar{\pi}$ are labeled $\bar{i}_1, \bar{i}_2, \dots, \bar{i}_{n_{\bar{\pi}}}$. The number of gluons connecting S and $J_A^{(n_{\bar{\pi}}+N)}$ is N .

Following the procedure described in Sec. 2.5.1 with R_A in Eq. (2.42) replaced by S in Eq. (2.52), we can express the contribution from a G gluon in the first term of Eq. (2.51) in a form

$$\begin{aligned}
& \sum_{i=1}^{n-1} \int_{-M}^M \left(\prod_{j \neq i}^{n-1} dk_j^- \right) M \left[J_A^{(n) a_1 \dots a_n} (k_i^- = +M, \dots) + J_A^{(n) a_1 \dots a_n} (k_i^- = -M, \dots) \right] \\
& = \sum_m \int \prod_{j=1}^m d^{D-2} l_{j\perp} \mathcal{K}_{a_1 \dots a_n; b_1 \dots b_m}^{(n,m)} (k_{1\perp}, \dots, k_{n\perp}, l_{1\perp}, \dots, l_{m\perp}; q, \eta; M) \\
& \times \Gamma_A^{(m) b_1 \dots b_m} (p_A, q, \eta; l_{1\perp}, \dots, l_{m\perp}; M). \tag{2.53}
\end{aligned}$$

The function $\mathcal{K}^{(n,m)}$ does not contain any dependence on p_A . It can contain

delta functions setting some of the color indices b_i , as well as transverse momenta $l_{i\perp}$ of $\Gamma_A^{(m)}$ equal to color indices a_i and transverse momenta $k_{i\perp}$ of $\Gamma_A^{(n)}$.

Next we turn our attention to the last term appearing in Eq. (2.51). The contribution to this term has been depicted graphically in Fig. 2.4. Consider the term in Fig. 2.4a. It can be written in a form

$$\begin{aligned}
& \int_{-M}^M \left(\prod_{j=1}^{n-1} d k_j^- \right) \text{ (Fig. 2.4a)} = \int_{-M}^M \left(\prod_{j=1}^{n-1} d k_j^- \right) \\
& \times \sum_{\pi} S'_{a_i a_{i_1} \dots a_{i_{n\pi}}} b(k_i^-, k_{i_1}^-, \dots, k_{i_{n\pi}}^-; k_i^+ = 0, k_{i_1}^+ = 0, \dots, k_{i_{n\pi}}^+ = 0; \\
& \quad k_{i\perp}, k_{i_1\perp}, \dots, k_{i_{n\pi}\perp}; l = k_i + k_{i_1} + \dots + k_{i_{n\pi}}; q, \eta) \\
& \times J_A^{(n_{\bar{\pi}}+1) a_{\bar{i}_1} \dots a_{\bar{i}_{n_{\bar{\pi}}}}} b(k_{\bar{i}_1}^-, \dots, k_{\bar{i}_{n_{\bar{\pi}}}}^-; k_{\bar{i}_1}^+ = 0, \dots, k_{\bar{i}_{n_{\bar{\pi}}}}^+ = 0; k_{\bar{i}_1\perp}, \dots, k_{\bar{i}_{n_{\bar{\pi}}}\perp}; \\
& \quad l = k_i + k_{i_1} + \dots + k_{i_{n\pi}}; p_A, q, \eta). \tag{2.54}
\end{aligned}$$

In Eq. (2.54), we have used the same notation as in Eq. (2.52). Momentum l connects S' with $J_A^{(n_{\bar{\pi}}+1)}$. Following the same procedure as in Sec. 2.5.1 with R_A appearing in Eq. (2.42) replaced by S' introduced in Eq. (2.54), we can express this contribution in a form given by Eq. (2.53) with a different kernel $\mathcal{K}^{(n,m)}$.

The contribution from Fig. 2.4b can be written

$$\begin{aligned}
& \int_{-M}^M \left(\prod_{j=1}^{n-1} d k_j^- \right) \text{ (Fig. 2.4b)} = \int_{-M}^M \left(\prod_{j=1}^{n-1} d k_j^- \right) \sum_{\pi} \int \frac{d^D k}{(2\pi)^D} \\
& \times S''_{a_i a_{i_1} \dots a_{i_{n\pi}} b c} (k_i^-, k_{i_1}^-, \dots, k_{i_{n\pi}}^-; k_i^+ = 0, k_{i_1}^+ = 0, \dots, k_{i_{n\pi}}^+ = 0; \\
& \quad k_{i\perp}, k_{i_1\perp}, \dots, k_{i_{n\pi}\perp}; k, l; q, \eta) \\
& \times J_A^{(n\bar{\pi}+2) a_{\bar{i}_1} \dots a_{\bar{i}_{n\bar{\pi}}} b c} \left(k_{\bar{i}_1}^-, \dots, k_{\bar{i}_{n\bar{\pi}}}^-; k_{\bar{i}_1}^+ = 0, \dots, k_{\bar{i}_{n\bar{\pi}}}^+ = 0; \right. \\
& \quad \left. k_{\bar{i}_1\perp}, \dots, k_{\bar{i}_{n\bar{\pi}}\perp}; k, l; p_A, q, \eta \right).
\end{aligned} \tag{2.55}$$

The flow of momenta k and l is exhibited in Fig. 2.4b. The momentum k flows through the boxed vertex and the ghost line shown in Fig. 2.4b which forces this momentum to be soft, so that lines k and l are part of the function S'' . Since the line with momentum k is soft, then all gluons attaching to $J_A^{(n\bar{\pi}+2)}$ in Eq. (2.55) are soft and we can again apply the procedure described in Sec. 2.5.1 to bring the contribution in Fig. 2.4b into the form given by Eq. (2.53) with a different kernel, of course.

In summary, we have demonstrated that all the terms on the right hand side of Eq. (2.51) can be put into the form given by Eq. (2.53). This indicates that Eq. (2.51), indeed, describes the evolution of $\Gamma_A^{(n)}$ in $\ln p_A^+$ since it can be written as

$$\begin{aligned}
& \left(p_A^+ \frac{\partial}{\partial p_A^+} - 1 \right) \Gamma_A^{(n) a_1 \dots a_n} (p_A, q, \eta; k_{1\perp}, \dots, k_{n\perp}) = \\
& \sum_m \int \prod_{j=1}^m d^{D-2} l_{j\perp} \mathcal{K}_{a_1 \dots a_n; b_1 \dots b_m}^{(n,m)} (k_{1\perp}, \dots, k_{n\perp}, l_{1\perp}, \dots, l_{m\perp}; q, \eta) \\
& \times \Gamma_A^{(m) b_1 \dots b_m} (p_A, q, \eta; l_{1\perp}, \dots, l_{m\perp}).
\end{aligned} \tag{2.56}$$

The kernels $\mathcal{K}^{(n,m)}$ do not depend on p_A^+ . As indicated above, they can contain delta functions setting some of the color indices b_i , as well as transverse momenta $l_{i\perp}$ of $\Gamma_A^{(m)}$ equal to color indices a_i and transverse momenta $k_{i\perp}$ of $\Gamma_A^{(n)}$. The systematic use of this evolution equation enables us to resum large logarithms $\ln(p_A^+)$ at arbitrary level of logarithmic accuracy. Analogous equation is satisfied by Γ_B . It resums logarithms of $\ln(p_B^-)$.

2.5.3 Counting the number of logarithms

Having derived the evolution equations for $\Gamma_A^{(n)}$, Eqs. (2.51) and (2.56), it does not take too much effort to show that at r -loop order the amplitude contains at most r powers of $\ln(s/|t|)$. We follow the method of Ref. [16]. We have argued in Sec. 2.5.1 that the power of $\ln(s/|t|)$ in the overall amplitude corresponds to the power of $\ln(p_A^+)$ in $\Gamma_A^{(n)}$. So we have to demonstrate that at r -loop order $\Gamma_A^{(n,r)}$, where $\Gamma_A^{(n,r)}$ represents a contribution to $\Gamma_A^{(n)}$ at r -loop level, does not contain more than r logarithms of $\ln(p_A^+)$. We prove this statement by induction. First of all, the tree level contribution to $\Gamma_A^{(n,0)}$ is proportional to the expression

$$\int_{-M}^M \left(\prod_{i=1}^{n-1} dk_{i\perp}^- \right) \sum_{\{i_1, \dots, i_n\}} \prod_{j=1}^{n-1} \frac{1}{(p_A - \sum_{l=1}^j k_{i_l})^2 + i\epsilon} \left(\prod_{j=n}^1 t^{a_{i_j}} \right)_{r_1, r_A}, \quad (2.57)$$

where $t^{a_{i_j}}$ s are the generators of the $SU(3)$ algebra in the fundamental representation. The sum over $\{i_1, \dots, i_n\}$ indicates that we sum over all possible insertions of the external soft gluons. Eq. (2.57) is evaluated at $\{k_i^+ = 0\}_{i=1}^n$. Expanding the denominators in Eq. (2.57) we obtain the expression $-2p_A^+(k_{i_1}^- + \dots + k_{i_j}^-) - (k_{i_1} + \dots + k_{i_j})_{\perp}^2 + i\epsilon$. We see that the poles in k_i^-

planes are not pinched and therefore the k_i^- integrals cannot produce $\ln(p_A^+)$ enhancements.

Next we assume that the statement is true at r -loop order, and show that it then also holds at $(r + 1)$ -loop level. To this end we consider the evolution equation, Eq. (2.51), and examine $(p_A^+ \partial/\partial p_A^+ - 1) \Gamma_A^{(n,r+1)}$. Its contribution is given by the first and the third term on the right hand side of Eq. (2.51). As already mentioned, the first term in Eq. (2.51) can be analyzed using K - G decomposition. The contributions from the K terms cancel each other while the contribution from the G gluons are given by the kind of diagram shown in Fig. 2.3b. The latter, however, can be written as a sum of soft loop integrals over $J_A^{(n',r')}$ with $r' \leq r$, since we loose at least one loop in the original $J_A^{(n,r+1)}$ due to the soft momentum integration. This is demonstrated in Eq. (2.52). Following the procedure described in Sec. 2.5.1, we may express these contributions as transverse momentum integrals of some $\Gamma_A^{(n',r')}$, see Eq. (2.53). These contain at most $r' \leq r$ logarithms of $\ln(p_A^+)$. The contribution from the third term in the evolution equation, Eq. (2.51), is given by the diagrams depicted in Fig. 2.4. These are again soft loop integrals of some $J_A^{(n',r')}$ with $r' \leq r$, and they can be expressed as transverse momentum integrals of $\Gamma_A^{(n',r')}$, see Eqs. (2.54) and (2.55), which have, therefore, at most r logarithms of $\ln(p_A^+)$. Since both terms on the right hand side of Eq. (2.51) have at most r logarithms of $\ln(p_A^+)$, then also $p_A^+ \partial \Gamma_A^{(n,r+1)} / \partial p_A^+$ has at most r logarithms of $\ln(p_A^+)$ at $(r + 1)$ -loop level. This immediately shows that $\Gamma_A^{(n,r+1)}$ itself cannot have more than $(r + 1)$ logarithms of $\ln(p_A^+)$ at $(r + 1)$ -loop level.

This result enables us to formally classify the types of diagrams which contribute to the amplitude at the k -th nonleading logarithm level. As has been

shown in Sec. 2.5.1, we can write an arbitrary contribution to the amplitude for process (2.1) in the Regge limit in the second factorized form given by Eq. (2.40). Consider an r -loop contribution to the amplitude and let L_A , L_B and L_S be the number of loops contained in Γ_A , Γ_B and S . Since Γ_A (Γ_B) can contain L_A (L_B) number of logarithms of p_A^+ (p_B^-) at most, the maximum number of logarithms, $N_{\max\text{Log}}$, we can get is

$$N_{\max\text{Log}} = r - L_S. \quad (2.58)$$

This indicates that when evaluating the amplitude at the k -th nonleading approximation, we need to consider diagrams where $1, 2, \dots, (k+1)$ soft gluons are exchanged between the jet functions J_A and J_B .

2.5.4 Solution of the evolution equations

Having obtained the evolution equations, Eqs. (2.51) and (2.56), we discuss how to construct their solution. Our starting point is Eq. (2.56). In shorthand notation it reads

$$p_A^+ \frac{\partial}{\partial p_A^+} \Gamma_A^{(n,r)} = \sum_{r'=0}^{r-1} \sum_{n'} \mathcal{K}^{(n,n';r-r')} \otimes \Gamma_A^{(n',r')}, \quad (2.59)$$

at r -loop level. Indices n and n' , besides denoting the number of external gluons of the jet function, also label the transverse momenta and the color indices of these gluons. The symbol \otimes in Eq. (2.59) denotes convolution over the transverse momenta and the color indices. Note that Eq. (2.59) holds for Γ_A with the overall factor p_A^+ divided out ($\Gamma_A \equiv \Gamma_A/p_A^+$). We have proved,

in Sec. 2.5.3, that $\Gamma_A^{(n,r)}$ can contain at most r logarithms of $\ln(p_A^+)$ at r -loop level. Therefore the most general expansion for Γ_A is

$$\Gamma_A^{(n,r)} \equiv \sum_{j=0}^r c_j^{(n,r)} \ln^j(p_A^+). \quad (2.60)$$

If we want to know $\Gamma_A^{(n,r)}$ at $N^k\text{LL}$ accuracy ($k = 0$ is LL, $k = 1$ is NLL, etc.), we need to find all $c_j^{(n,r)}$ such that $r - j \leq k$. The coefficients $c_j^{(n,r)}$ in Eq. (2.60) depend on the transverse momenta and the color indices of the external gluons. Using the expansion for $\Gamma_A^{(n,r)}$ and $\Gamma_A^{(n',r')}$, Eq. (2.60), in Eq. (2.59) and comparing the coefficients with the same power of $\ln(p_A^+)$, we obtain the recursive relation satisfied by the coefficients $c_j^{(n,r)}$

$$j c_j^{(n,r)} = \sum_{r'=j-1}^{r-1} \sum_{n'=1}^{n+r-r'} \mathcal{K}^{(n,n';r-r')} \otimes c_{j-1}^{(n',r')}. \quad (2.61)$$

In Eq. (2.61), we have used that, in general, $1 \leq n' \leq n + r - r'$.

We now show that Eq. (2.61) enables us to determine all the relevant coefficients $c_j^{(r,n)}$ of $\Gamma_A^{(n)}$ order by order in perturbation theory at arbitrary logarithmic accuracy. We start at LL, $k = 0$, and consider $n = 1$. At r -loop level we need to find the coefficient $c_r^{(1,r)}$. It can be expressed in terms of lower loop coefficients using Eq. (2.61) and setting $j = r$ and $n = 1$

$$r c_r^{(1,r)} = \sum_{n'=1}^2 \mathcal{K}^{(1,n';1)} \otimes c_{r-1}^{(n',r-1)}. \quad (2.62)$$

In Sec. 3.1 we will prove that the one loop kernel satisfies $\mathcal{K}^{(1,2;1)} = 0$, Eq. (3.6). This implies that in Eq. (2.62) the coefficient $c_r^{(1,r)}$ is expressed in terms

of lower loop coefficient $c_{r-1}^{(1,r-1)}$ and hence, we can construct the coefficients at arbitrary loop level once we compute $c_0^{(1,0)}$, the coefficient corresponding to the tree level jet function $\Gamma_A^{(1,0)}$.

Next we construct all $\Gamma_A^{(n)}$ for $n > 1$ at LL accuracy. Let us assume that we know all $c_r^{(n',r)}$ for all r and for $n' < n$. We apply Eq. (2.61) for $j = r$

$$r c_r^{(n,r)} = \sum_{n'=1}^{n+1} \mathcal{K}^{(n,n';1)} \otimes c_{r-1}^{(n',r-1)}. \quad (2.63)$$

In Sec. 3.2 we will show that the evolution kernel in Eq. (2.63) obeys $\mathcal{K}^{(n,n';1)} = \theta(n-n') \tilde{\mathcal{K}}^{(n,n';1)}$, Eq. (3.39), where $\theta(n-n')$ is the step function. This implies that the sum over n' in Eq. (2.63) terminates at $n' = n$. Isolating this term in Eq. (2.63), we can write

$$r c_r^{(n,r)} = \mathcal{K}^{(n,n;1)} \otimes c_{r-1}^{(n,r-1)} + \sum_{n'=1}^{n-1} \mathcal{K}^{(n,n';1)} \otimes c_{r-1}^{(n',r-1)}. \quad (2.64)$$

So after we calculate the tree level coefficient $c_0^{(n,0)}$, we can construct all the coefficients $c_r^{(n,r)}$ using Eq. (2.64) order by order in perturbation theory, since according to the assumption we know $c_r^{(n',r)}$ for all r and for $n' < n$. This proves that we can construct the jet functions at LL, $k = 0$, for all n to all loops.

We now assume that we have constructed all the jet functions at the $N^k\text{LL}$ accuracy for a given $k \geq 0$ and we will show that we can determine all the jet functions at the $N^{k+1}\text{LL}$ level. We start with $n = 1$. Using Eq. (2.61) with $n = 1$, $j = r - (k + 1)$, isolating the term with $r' = r - 1$ in the sum over r'

and using $\mathcal{K}^{(1,n';1)} = \delta_{1n'} \mathcal{K}^{(1,1;1)}$, we arrive at

$$(r-k-1) c_{r-k-1}^{(1,r)} = \mathcal{K}^{(1,1;1)} \otimes c_{r-k-2}^{(1,r-1)} + \sum_{r'=r-k-2}^{r-2} \sum_{n'=1}^{1+r-r'} \mathcal{K}^{(1,n';r-r')} \otimes c_{r-k-2}^{(n',r')}. \quad (2.65)$$

After we evaluate the coefficient $c_0^{(1,k+1)}$ (impact factor), Eq. (2.65) implies that we can calculate the coefficients $c_{r-k-1}^{(1,r)}$ order by order in perturbation theory, because, according to the induction assumption, we know all the coefficients $c_{r-k-2}^{(n',r')}$ since they are at most N^k LL. Once the coefficients of $\Gamma_A^{(1)}$ are determined at N^{k+1} LL level, we assume that we know all the coefficients of $\Gamma_A^{(n')}$ s for $n' < n$. We want to show that we can now construct all the coefficients for $\Gamma_A^{(n)}$ at N^{k+1} LL accuracy. First we need to calculate $c_0^{(n,k+1)}$. Then we use Eq. (2.61) to express the coefficient $c_{r-k-1}^{(n,r)}$, isolating the terms with $r' = r-1$ and $n' = n$, as

$$\begin{aligned} (r-k-1) c_{r-k-1}^{(n,r)} &= \mathcal{K}^{(n,n;1)} \otimes c_{r-k-2}^{(n,r-1)} + \sum_{n'=1}^{n-1} \mathcal{K}^{(n,n';1)} \otimes c_{r-k-2}^{(n',r-1)} \\ &+ \sum_{r'=r-k-2}^{r-2} \sum_{n'=1}^{n+r-r'} \mathcal{K}^{(n,n';r-r')} \otimes c_{r-k-2}^{(n',r')}. \end{aligned} \quad (2.66)$$

The terms appearing in the sum over r' in Eq. (2.66) are known according to the assumptions since for them $r' - (r-k-2) \leq k$. We also know, according to the induction assumptions, the contributions to the second term of Eq. (2.66), since they have $n' < n$. Therefore, we can construct $c_{r-k-1}^{(n,r)}$ order by order in perturbation theory. This finishes our proof that we can determine the high energy behavior of $\Gamma_A^{(n)}$ at arbitrary logarithmic accuracy. Note that to any fixed accuracy only a finite number of fixed-order calculations of kernels and

coefficients $c_0^{(n,r)}$ must be carried out. In a similar way we can construct a solution for $\Gamma_B^{(m)}$.

Once we know the high energy behavior for $\Gamma_A^{(n)}$ and $\Gamma_B^{(m)}$, then the second factorized form, Eq. (2.40), implies that we also know the high energy behavior for the overall amplitude. Because a jet function $\Gamma^{(n)}$ is always associated with at least $n - 1$ soft loop momentum integrals in the amplitude, we infer from Eq. (2.58) that if we want to know this amplitude at N^K LL accuracy, it is sufficient to know $\Gamma_A^{(n)}$ ($\Gamma_B^{(m)}$) at N^{K+1-n} LL (N^{K+1-m} LL) level for $n \leq K + 1$ ($m \leq K + 1$). We note, however, that to construct these functions according to the algorithm above, it may be necessary to go to slightly larger, although always finite, values of n and m . Let us describe how this comes about, starting with the basic recursion relations for coefficients, Eq. (2.61).

We assume that for fixed n on the left-hand side of Eq. (2.61), the logarithmic accuracy k is bounded by the value necessary to determine the overall amplitude to K th nonleading logarithm: $k = r - j \leq K + 1 - n$, which we may rewrite as $n + r - (K + 1) \leq j \leq r$. On the right-hand side of Eq. (2.61) we encounter the coefficients of the jet functions with n' external lines, satisfying the inequality $n' \leq n + r - r' \leq n + r - (j - 1)$. Combining these two inequalities, we immediately obtain that $n' \leq K + 2$. Then, for any given number of external gluons n' on the right-hand side, we encounter a level of logarithmic accuracy $k' = r' - (j - 1) \leq n + r - n' - (j - 1) \leq K + 2 - n'$. This reasoning indicates that, in general, we will need all $\Gamma_A^{(n')}$ ($\Gamma_B^{(m')}$) at $N^{K+2-n'}$ LL ($N^{K+2-m'}$ LL) level for $n' \leq K + 2$ ($m' \leq K + 2$), when evaluating the amplitude at N^K LL accuracy. We note that for fermion exchange in QED it was shown in Ref. [16] that only contributions with $n' \leq K + 1$ are nonzero. As we

will witness in Chapter 3, two-loop calculations appear to indicate, Ref. [11], that QCD requires the full range of n' identified above, starting at NLL.

2.6 Conclusions

We have established a systematic method that shows that it is possible to resum the large logarithms appearing in the perturbation series of scattering amplitudes for $2 \rightarrow 2$ partonic processes to arbitrary logarithmic accuracy in the Regge limit. Up to corrections suppressed by powers of $|t|/s$, the amplitude can be expressed as a sum of convolutions in transverse momentum space over soft and jet functions, Eq. (2.40). All the large logarithms are organized in the jet functions, Eq. (2.41). They are resummed using Eqs. (2.51) and/or (2.56). The evolution kernel \mathcal{K} in Eq. (2.56) is a calculable function of its arguments order by order in perturbation theory. This is the central result of our analysis.

The derivation of the evolution equations and the procedure for finding the kernels were given above in Coulomb gauge. Clearly, it will be useful and interesting to reformulate our arguments in covariant gauges. In addition, the connection of our formalism to the effective action approach to small- x and the Regge limit, Refs. [35, 36] should provide further insight.

Chapter 3

The Applications

In the previous chapter, we have developed the general formalism for obtaining the high-energy behavior of the scattering amplitude for process (2.1) at arbitrary logarithmic accuracy. In this chapter, we apply these techniques to study this amplitude at LL and NLL level.

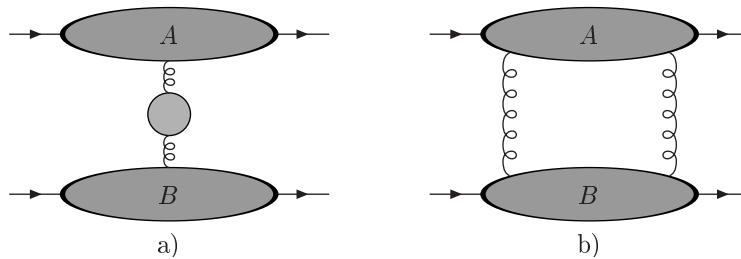


Figure 3.1: Diagrams contributing to the amplitude at NLL approximation: factorized one gluon exchange diagram (a) and non-factorized two gluon exchange diagram (b).

3.1 Amplitude at LL

According to Eq. (2.58), the amplitude at LL comes solely from the factorized diagram shown in Fig. 3.1a, but without any gluon self-energy corrections. The jet A , containing lines moving in the plus direction, and jet B , consisting of lines moving in the minus direction, interact via the exchange of a single soft gluon. This gluon couples to jet A via the $-$ component of its polarization and to jet B via the $+$ component of its polarization. Since $v_A^\alpha N_{\alpha\beta}(q, \eta) v_B^\beta = 1$, we can write at LL

$$A_{\mathbf{8}} b_{\mathbf{8}} = -\frac{1}{t} J_A^{(1)a}(p_A, q, \eta) J_B^{(1)a}(p_B, q, \eta), \quad (3.1)$$

where $b_{\mathbf{8}}$ is the color basis vector corresponding to the octet exchange, defined in Eq. (2.3). Using $s = 2p_A^+ p_B^-$, the logarithmic derivative of the amplitude can be expressed as

$$\frac{\partial A_{\mathbf{8}}}{\partial \ln s} b_{\mathbf{8}} = -\frac{1}{t} \frac{\partial J_A^{(1)a}}{\partial \ln p_A^+} J_B^{(1)a} = -\frac{1}{t} J_A^{(1)a} \frac{\partial J_B^{(1)a}}{\partial \ln p_B^-}. \quad (3.2)$$

In Sec. 2.4.2, Eq. (2.33), we have derived an evolution equation resumming $\ln(p_A^+)$ in $J_A^{(1)}$. We note that $J_A^{(1)} = \Gamma_A^{(1)}$, and that (2.33) is a special case of the evolution equation (2.51). The diagrammatic representation of the first term on the far right hand side of Eq. (2.33), which follows from Fig. 2.4 in the case when we have one external soft gluon attached to a jet function, is given by the diagrams in Fig. 3.2. Diagram in Fig. 3.2a corresponds to Fig. 2.4b and the diagrams in Figs. 3.2b and 3.2c correspond to Fig. 2.4a for $n = 1$. The diagrams in Figs. 3.2b and 3.2c are in the factorized form, while the one

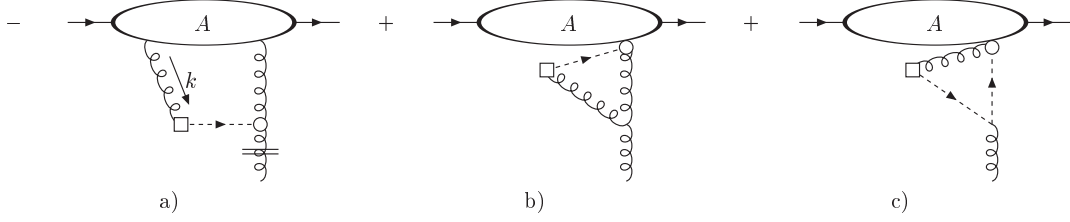


Figure 3.2: Diagrammatic representation of the evolution equation for jet $J_A^{(1)}$ at LL.

in Fig. 3.2a is not.

As discussed in Sec. 2.4.2, power counting shows that the loop momentum k in Fig. 3.2a must be soft. This implies that we can make the following approximations. First, since at LL all internal lines of the jet A are collinear to the $+$ direction, we can neglect the k^+ dependence of $J_A^{(2)}$, i.e. we may set $k^+ = 0$ inside $J_A^{(2)}$. Also, we can pick the plus components of the vertices where the soft gluons attach to the jet $J_A^{(2)}$. A short calculation, which uses the Feynman rules for special lines and vertices listed in Appendix A.4, gives the contribution to Fig. 3.2a in a form

$$\begin{aligned}
 \text{Fig. 3.2a} &= -\bar{g}_s t f_{acb} \int \frac{d^D k}{(2\pi)^D} \frac{1}{k^2(k-q)^2 k \cdot \bar{k}} v_A^\rho N_{\rho\mu}(k) S^\mu(k) \\
 &\times v_B^\alpha N_{\alpha\nu}(q-k) v_A^\nu v_B^\beta v_B^\gamma J_{(A)\beta\gamma}^{(2)bc}(p_A, q, \eta; k^+ = 0, k^-, k_\perp),
 \end{aligned} \tag{3.3}$$

where we have defined $\bar{g}_s \equiv g_s \mu^\epsilon$. Using Eqs. (2.11) and (2.36) for the components of the gluon propagator and the boxed vertex, respectively, it is easy to see that in the Coulomb (Glauber) region, $k^- \ll k^+ \sim k_\perp$, the integrand in Eq. (3.3) becomes an antisymmetric function of k^+ and that

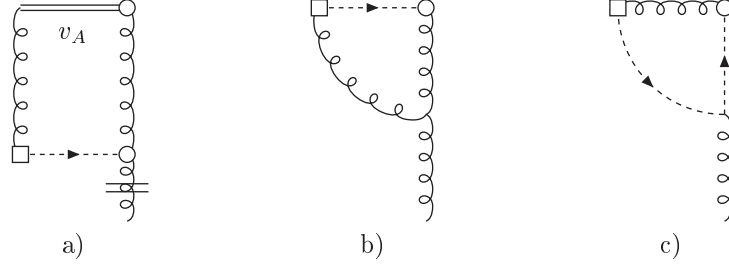


Figure 3.3: Diagrams determining the contributions to the gluon trajectory at the order α_s .

therefore the integration over k^+ vanishes in this region.

In the soft region, where all the components of soft momenta are of the same size $\sqrt{-t}$, we can use the K - G decomposition for the soft gluon with momentum k attached to $J_A^{(2)}$. At LL, however, there cannot be any soft internal lines in $J_A^{(2)}$ in Eq. (3.3), since, as discussed in Sec. 2.5.3, only integrals over collinear momenta can produce powers of $\ln p_A^+$. Therefore, at LL, only the K gluon contributes, because the G gluon must be attached to a soft line. The K gluon can be decoupled from the rest of the jet $J_A^{(2)}$ using the Ward identities, Eq. (2.30). Their application in Eq. (3.3) gives

$$\begin{aligned}
 \text{Fig. 3.2a} &= -i\bar{g}_s^2 C_A t \int \frac{d^D k}{(2\pi)^D} \frac{1}{k^2(k-q)^2 k \cdot \bar{k} v_A \cdot k} v_A^\rho N_{\rho\mu}(k) S^\mu(k) \\
 &\times v_B^\alpha N_{\alpha\nu}(q-k) v_A^\nu J_A^{(1)a}(p_A, q, \eta).
 \end{aligned} \tag{3.4}$$

We have used the identity $f_{acb} f_{dcb} = N_c \delta_{ad} \equiv C_A \delta_{ad}$ in Eq. (3.4). Eq. (3.4) now gives a factorized form for Fig. 3.2a. Since the contributions in Figs. 3.2b and 3.2c are already in the factorized form, we can immediately infer that the gluon reggeizes at LL. Combining the terms from Fig. 3.2 in Eq. (2.33), we

obtain the evolution equation at leading logarithm

$$p_A^+ \frac{\partial}{\partial p_A^+} J_A^{(1)a}(p_A, q, \eta) = \alpha(t) J_A^{(1)a}(p_A, q, \eta). \quad (3.5)$$

Using the notation for evolution kernels introduced in Sec. 2.5.4, Eq. (3.5) implies that

$$\mathcal{K}^{(1,2;1)} = 0. \quad (3.6)$$

In Eq. (3.5)

$$\alpha(t) \equiv 1 + \alpha_a^{(1)}(t) + \alpha_b^{(1)}(t) + \alpha_c^{(1)}(t), \quad (3.7)$$

is the gluon trajectory up to the order α_s , and $\alpha_a^{(1)}(t)$, $\alpha_b^{(1)}(t)$ and $\alpha_c^{(1)}(t)$ are its contributions given in Figs. 3.3a - 3.3c, respectively,

$$\begin{aligned} \alpha_a^{(1)}(t) &\equiv -i\bar{g}_s^2 C_A t \int \frac{d^D k}{(2\pi)^D} \frac{1}{k^2(k-q)^2 k \cdot \bar{k} v_A \cdot k} v_A^\rho N_{\rho\mu}(k) S^\mu(k) \\ &\quad \times v_B^\beta N_{\beta\nu}(q-k) v_A^\nu, \\ \alpha_b^{(1)}(t) &\equiv i\bar{g}_s^2 C_A \int \frac{d^D k}{(2\pi)^D} \frac{1}{k^2(k-q)^2 k \cdot \bar{k}} S_\alpha(k) N^{\alpha\mu}(k) v_A^\rho N_\rho^\nu(q-k) \\ &\quad \times V_{\mu\beta\nu}(k, -q, q-k) v_B^\beta, \\ \alpha_c^{(1)}(t) &\equiv -i\bar{g}_s^2 C_A \int \frac{d^D k}{(2\pi)^D} \frac{1}{k^2 k \cdot \bar{k} (q-k) \cdot (\bar{q}-\bar{k})} v_A^\rho N_{\rho\mu}(k) S^\mu(k) (v_B \cdot \bar{k}). \end{aligned} \quad (3.8)$$

In Eq. (3.8), $V_{\mu\beta\nu}(k, -q, q-k)$ stands for the momentum part of the three-point gluon vertex. After contracting the tensor structures in Eq. (3.8), using the explicit form for $V_{\mu\beta\nu}$, v_A , v_B , S^μ (Eq. (2.34)) and for the components of

the gluon propagator, Eq. (2.11), we obtain for $\alpha_{a,b,c}^{(1)}(t)$,

$$\begin{aligned}
\alpha_a^{(1)}(t) &= -i\bar{g}_s^2 C_A \frac{t}{2} \int \frac{d^D k}{(2\pi)^D} \frac{[k_\perp^2 k_0 + k^2 k_3][(k-q)^2 - (k-q)_\perp^2]}{(k_0 + \bar{k}_3) k^2 (k-q)^2 (k \cdot \bar{k})^2 (k-q) \cdot (\bar{k} - \bar{q})}, \\
\alpha_b^{(1)}(t) &= i\bar{g}_s^2 C_A \frac{1}{2} \int \frac{d^D k}{(2\pi)^D} \frac{1}{k^2 (k-q)^2 (k \cdot \bar{k})^2 (k-q) \cdot (\bar{k} - \bar{q})} \\
&\quad \times [k_\perp^2 \bar{k}^2 (k-q)^2 + 2k^2 k_3^2 (k-q)_\perp \cdot q_\perp + 2k_0^2 k_3^2 k_\perp \cdot (k-q)_\perp + 2k_0^2 k_\perp^2 (k-q)_\perp^2], \\
\alpha_c^{(1)}(t) &= i\bar{g}_s^2 C_A \frac{1}{2} \int \frac{d^D k}{(2\pi)^D} \frac{k_3^2}{(k \cdot \bar{k})^2 (k-q) \cdot (\bar{k} - \bar{q})}. \tag{3.9}
\end{aligned}$$

Next, we perform the k^0 and k^3 integrals in Eq. (3.9). For $\alpha_a^{(1)}(t)$, these integrals are UV/IR finite. However in the case of $\alpha_{b,c}^{(1)}(t)$, the k^0 integral is linearly UV divergent. In order to regularize this energy integral, we invoke split dimensional regularization introduced in Ref. [49]. The idea is to regularize separately the energy and the spatial momentum integrals, i.e. to write $d^4 k_E \rightarrow d^{D_1} k_4 d^{D_2} \vec{k}$ for Euclidean loop momenta k_E . The dimensions D_1 and D_2 are given by $D_1 = 1 - 2\varepsilon_1$ and $D_2 = 3 - 2\varepsilon_2$, with $\varepsilon_j \rightarrow 0+$ for $j = 1, 2$. Since the energy integral for $\alpha_c^{(1)}(t)$ is scaleless, it vanishes in this split dimensional regularization. The energy integrals in $\alpha_{a,b}^{(1)}(t)$ are straightforward.

All the k^3 integrals can be expressed as derivatives with respect to k_\perp^2 and/or $(k-q)_\perp^2$ of a single integral

$$I(a, b) \equiv \int_0^\infty dk^3 \frac{1}{\sqrt{k_3^2 + a^2} (k_3^2 + b^2)} = \frac{1}{b\sqrt{b^2 - a^2}} \ln \left(\frac{b + \sqrt{b^2 - a^2}}{a} \right). \tag{3.10}$$

The result of these integrations over k^3 is

$$\begin{aligned}
\alpha_a^{(1)}(t) &= \alpha_s \mu^{2\epsilon} C_A t \int \frac{d^{D-2}k_\perp}{(2\pi)^{D-2}} \\
&\times \left(I(|k_\perp|, |k_\perp - q_\perp|) \frac{k_\perp^2}{[(k - q)_\perp^2 - k_\perp^2]^2} + \frac{2(k - q)_\perp^2 - 3k_\perp^2}{k_\perp^2 [(k - q)_\perp^2 - k_\perp^2]^2} \right), \\
\alpha_b^{(1)}(t) &= -\alpha_s \mu^{2\epsilon} C_A t \int \frac{d^{D-2}k_\perp}{(2\pi)^{D-2}} \\
&\times \left(I(|k_\perp|, |k_\perp - q_\perp|) \frac{k_\perp^2}{[(k - q)_\perp^2 - k_\perp^2]^2} - \frac{1}{[(k - q)_\perp^2 - k_\perp^2]^2} \right), \\
\alpha_c^{(1)}(t) &= 0.
\end{aligned} \tag{3.11}$$

Combining the results of Eq. (3.11) and Eq. (3.7), we obtain the standard expression for the gluon trajectory at LL

$$\alpha(t) = 1 + C_A \alpha_s \mu^{2\epsilon} \int \frac{d^{D-2}k_\perp}{(2\pi)^{D-2}} \frac{t}{k_\perp^2 (k - q)_\perp^2}. \tag{3.12}$$

We can now simply solve the evolution equation (3.2), to derive the factorized (reggeized) form for the amplitude in the color octet

$$A_{\mathbf{8}}(s, t, \alpha_s) = s^{\alpha(t)} \tilde{A}_{\mathbf{8}}(t, \alpha_s). \tag{3.13}$$

The amplitude factorizes into the universal factor $s^{\alpha(t)}$, which is common for all processes involving two partons in the initial and final state and dominated by the gluon exchange, and the part $\tilde{A}_{\mathbf{8}}$, the so-called impact factor, which is specific to the process under consideration.

3.2 Amplitude at NLL

At NLL level the contribution to the amplitude comes from both the one gluon exchange diagram, Fig. 3.1a, and from the two gluon exchange diagram, Fig. 3.1b. At this level, both singlet and octet color exchange are possible in the latter. Including the self-energy corrections to the propagator of the exchanged gluon (taking into account the corresponding counter-terms), we can write the contribution from the diagram in Fig. 3.1a as follows,

$$A^{(1)} \equiv -\frac{1}{t} J_{(A)\alpha}^{(1)a}(p_A, q, \eta) \left(N^{\alpha\beta}(q, \eta) + \frac{1}{t} v_B^\alpha v_A^\mu \Pi_{\mu\nu}(q, \eta) v_B^\nu v_A^\beta \right) J_{(B)\beta}^{(1)a}(p_B, q, \eta), \quad (3.14)$$

where $\Pi_{\mu\nu}(q, \eta)$ stands for the one loop gluon self-energy. We now put this contribution into the first factorized form, Eq. (2.27), isolating the plus polarization for jet A, and the minus polarization for jet B. At NLL in the amplitude, we need the soft function $S^{(1,1)}$, Eq. (2.27) with $n = m = 1$, to accuracy $\mathcal{O}(\alpha_s)$. Using the tulip-garden formalism described in Appendix A.3, the contribution to the first term on the right hand side of Eq. (3.14) is given by the subtractions shown in Fig. 3.4. In accordance with the notation adopted in Appendix A.3, the dashed lines indicate that we have made soft approximations on gluons that are cut by them. A dashed line cutting a gluon attached to jet $A(B)$ means that the gluon is attached to the corresponding jet through minus(plus) component of its polarization. Since $q^\pm = 0$ in the Regge limit, Eq. (2.2), we have $N^{\mu\pm}(q) = g^{\mu\pm}$. This implies that the contributions between the diagrams in Fig. 3.4c and in Fig. 3.4d as well as between the diagrams in Fig. 3.4e and in Fig. 3.4f cancel each other. Therefore only the

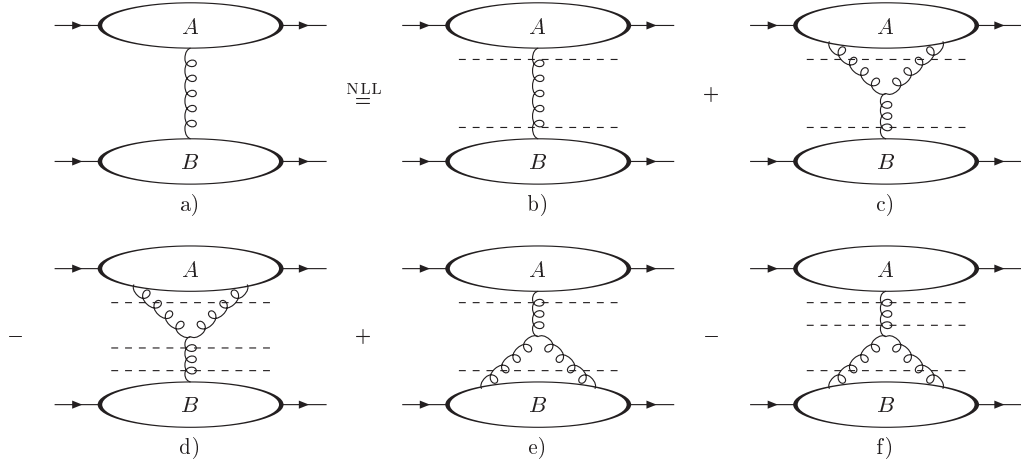


Figure 3.4: Expansion of the one gluon exchange amplitude at NLL using the tulip garden formalism.

zeroth-order soft function diagram in Fig. 3.4b survives in the factorized form, Eq. (2.27).

For the two gluon exchange, Fig. 3.1b, we only need the lowest order soft function at NLL in the amplitude (and LL in singlet exchange). The expression for the two gluon exchange diagram in Fig. 3.1b takes the form, Eq. (2.27),

$$A^{(2)} = \int \frac{d^D k}{(2\pi)^D} J_A^{(2)ab}(k^+ = 0, k^-, k_\perp) S(k^+, k^-, k_\perp) J_B^{(2)ab}(k^- = 0, k^+, k_\perp), \quad (3.15)$$

where $S(k)$ is given by

$$S(k) \equiv \frac{i}{2!} \frac{N^{-+}(k)}{k^2 + i\epsilon} \frac{N^{-+}(q-k)}{(q-k)^2 + i\epsilon}. \quad (3.16)$$

We have suppressed the dependence of the functions appearing in Eq. (3.44) on other arguments for brevity. At NLL accuracy we are entitled to pick the plus Lorentz indices for jet function J_A and the minus indices for jet function

J_B only. We can also set $k^+ = 0$ in J_A and $k^- = 0$ in J_B since all the loop momenta inside the jets are collinear. Eq. (3.44) represents the first factorized form, Eq. (2.27), for the amplitude $A^{(2)}$.

Next, we follow the procedure described in Sec. 2.5.1 to bring the amplitude into the second factorized form, Eq. (2.40). We employ an identity based on Eq. (2.44), for the function $S(k)$ defined in Eq. (3.16)

$$\begin{aligned}
S(k^+, k^-) &= S(k^+ = 0, k^- = 0) \theta(M - |k^+|) \theta(M - |k^-|) \\
&+ [S(k^+, k^- = 0) - S(k^+ = 0, k^- = 0) \theta(M - |k^+|)] \theta(M - |k^-|) \\
&+ [S(k^+ = 0, k^-) - S(k^+ = 0, k^- = 0) \theta(M - |k^-|)] \theta(M - |k^+|) \\
&+ [\{S(k^+, k^-) - S(k^+, k^- = 0) \theta(M - |k^-|)\} - \\
&\quad \{S(k^+ = 0, k^-) - S(k^+ = 0, k^- = 0) \theta(M - |k^-|)\} \theta(M - |k^+|)].
\end{aligned} \tag{3.17}$$

The contribution from the first term in Eq. (3.17) gives immediately the second factorized form with $\Gamma_A^{(2)}$ and $\Gamma_B^{(2)}$ defined in Eq. (2.41) for $n = m = 2$.

We now discuss the rest of the terms in Eq. (3.17), which can be analyzed using the K - G decomposition, since, by construction, there is no contribution from the Glauber region. At the current accuracy only the K -gluon contributes. After substituting the second term of Eq. (3.17) into Eq. (3.44), we can factor the gluon with momentum k from jet $J_B^{(2)}$. However, it is easy to verify, using the definitions for K and G gluons, Eq. (2.29), the Ward identities, Eq. (2.30), and the explicit components of the gluon propagator, Eq. (2.11), that the k^+ integral is over an antisymmetric function. As a re-

sult, this contribution vanishes. In a similar fashion, the contribution from the third term in Eq. (3.17), after used in Eq. (3.44), vanishes, since now we can factor the soft gluon with momentum k from jet $J_A^{(2)}$ and the k^- integral is over an antisymmetric function.

In the case of the last term in Eq. (3.17), after used in Eq. (3.44), we can factor the soft gluon with momentum k from both jets $J_A^{(2)}$ and $J_B^{(2)}$. The integrals of the soft function $S(k)$ over k^+ and k^- are then

$$\tilde{S}(k_\perp, q; M) \equiv C_A \frac{g_s^2}{(2\pi)^2} \int_{-M}^M \frac{dk^+}{k^+} \frac{dk^-}{k^-} S(k^+, k^-, k_\perp, q). \quad (3.18)$$

As usually, we leave the transverse momentum integral undone. The $1/k^+$ and $1/k^-$ in the integral above are given by the Principal Value prescription because there is no contribution from the Glauber region. Since the amplitude is independent on the choice of scale M , we can evaluate it at arbitrary scale. We choose to work in the limit $M \rightarrow 0$. In this limit the contribution to the integral comes from the imaginary parts of the gluon propagators in Eq. (3.16), $-i\pi\delta(k^2)$ and $-i\pi\delta((k-q)^2)$. The integration is then trivial and Eq. (3.18) becomes

$$\tilde{S}(k_\perp, q) \equiv \lim_{M \rightarrow 0} \tilde{S}(k_\perp, q; M) \equiv -C_A \frac{ig_s^2}{8} \frac{1}{k_\perp^2 (k-q)_\perp^2}. \quad (3.19)$$

Combining the partial results of the analysis described above in Eq. (3.44), we arrive at the second factorized form for the double gluon exchange amplitude,

Fig. 3.1b,

$$\begin{aligned}
A^{(2)} &= \int \frac{d^{D-2}k_{\perp}}{(2\pi)^{D-2}} \Gamma_A^{(2)ab}(k_{\perp}) \frac{1}{(2\pi)^2} S(k^+ = 0, k^- = 0, k_{\perp}) \Gamma_B^{(2)ab}(k_{\perp}) \\
&+ \int \frac{d^{D-2}k_{\perp}}{(2\pi)^{D-2}} \Gamma_A^{(1)a}(p_A, q) \tilde{S}(k_{\perp}, q) \Gamma_B^{(1)a}(p_A, q). \tag{3.20}
\end{aligned}$$

Using Eq. (3.14) for $A^{(1)}$ and Eq. (3.20) for $A^{(2)}$, we obtain the amplitude for the process (2.1) at NLL accuracy

$$\begin{aligned}
A^{(\text{NLL})} &= -\frac{1}{t} \Gamma_A^{(1)a}(p_A, q, \eta) \left(1 + \frac{1}{t} \Pi_{+-}(q, \eta) + \frac{i\pi}{2} \alpha^{(1)}(t) \right) \Gamma_B^{(1)a}(p_B, q, \eta) \\
&+ \int \frac{d^{D-2}k_{\perp}}{(2\pi)^{D-2}} \Gamma_A^{(2)ab}(k_{\perp}) \frac{i}{8\pi^2} \frac{1}{k_{\perp}^2 (k-q)_{\perp}^2} \Gamma_B^{(2)ab}(k_{\perp}). \tag{3.21}
\end{aligned}$$

In Eq. (3.21), we have used the explicit form for $S(k^+ = 0, k^- = 0, k_{\perp})$, which can be easily identified from Eq. (3.16). We have also used the integral representation of the gluon trajectory given in Eq. (3.12).

In order to determine the high energy behavior of the amplitude in Eq. (3.21), we need to examine the high energy behavior of $\Gamma_A^{(1)}$ or $\Gamma_B^{(1)}$ at NLL and the evolution of $\Gamma_A^{(2)}$ or $\Gamma_B^{(2)}$ at LL. In this section, we restrict the discussion of evolution equations to LL level, and hence we analyze the behavior of $\Gamma_A^{(2)}$ only. We will address the study of NLL jet evolution, and gluon reggeization at this level in the next section.

We use the evolution equation given by Eq. (2.51) in order to determine the LL dependence of $\Gamma_A^{(2)}$ on $\ln(p_A^+)$. In our special case of the two gluon

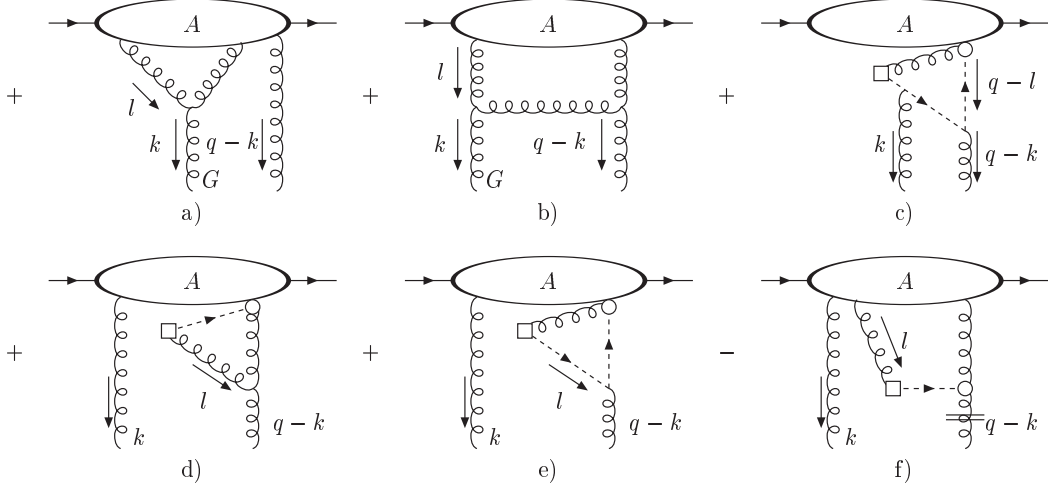


Figure 3.5: Diagrams determining the evolution of $\Gamma_A^{(2)}$.

exchange amplitude, it reads

$$\begin{aligned}
\left(p_A^+ \frac{\partial}{\partial p_A^+} - 1\right) \Gamma_A^{(2)ab} &= M \left[J_A^{(2)ab}(k^- = +M, k^+ = 0, k_\perp) \right. \\
&\quad \left. + J_A^{(2)ab}(k^- = -M, k^+ = 0, k_\perp) \right] - \tilde{\eta}^\alpha \frac{\partial}{\partial \eta^\alpha} \Gamma_A^{(2)ab}.
\end{aligned} \tag{3.22}$$

The first term in Eq. (3.22) can be analyzed using the K - G decomposition. The contributions from the K -gluon cancel between the $J_A^{(2)}(k^- = +M)$ and $J_A^{(2)}(k^- = -M)$. The contributions from the G gluon, which we now discuss, are shown in Figs. 3.5a and 3.5b.

Since the gluon with momentum $q-k$ in Fig. 3.5a cannot be in the Glauber region, we can use K - G decomposition on it. The K part factors from $J_A^{(3)}$, while the G part does not contribute at LL. After factoring out the gluon with momentum $q-k$ and performing the approximations on the jet function $J_A^{(2)}$,

the contribution to Fig. 3.5a for $k^- = +M$ is

$$\begin{aligned} \text{Fig. 3.5a} &= -ig_s^2 f_{aec} f_{deb} \frac{1}{M} \int \frac{d^D l}{(2\pi)^D} S_1(k^+ = 0, k^- = +M, k_\perp, l) \\ &\times J_A^{(2)cd}(l^+ = 0, l^-, l_\perp), \end{aligned} \quad (3.23)$$

where we have defined

$$S_1(k, l) \equiv \frac{N^{-\mu}(l)}{l^2} \frac{N^{-\nu}(k-l)}{(k-l)^2} V_{\mu\rho\nu}(l, -k, k-l) \left(g^{\rho+} - \frac{k^\rho}{M} \right). \quad (3.24)$$

Next we follow the established procedure. First, we write

$$S_1(k, l) = S_1(k, l^- = 0) \theta(M - |l^-|) + [S_1(k, l) - S_1(k, l^- = 0) \theta(M - |l^-|)]. \quad (3.25)$$

When we use the second term of Eq. (3.25) in Eq. (3.23), we can factor the gluon with momentum l from $J_A^{(2)}$. Since the resulting integrand is an antisymmetric function under the simultaneous transformation $M \rightarrow -M$, $l^\pm \rightarrow -l^\pm$, the contributions on the right hand side of Eq. (3.22) evaluated for $k^- = +M$ and $k^- = -M$ cancel each other. Therefore we can write, using Eq. (3.25) in Eq. (3.23),

$$\begin{aligned} \text{Fig. 3.5a} &= -ig_s^2 f_{aec} f_{deb} \frac{1}{M} \int \frac{d^{D-2} l_\perp}{(2\pi)^D} \int dl^+ \\ &\times S_1(k^+ = 0, k^- = +M, k_\perp, l^- = 0, l^+, l_\perp) \Gamma_A^{(2)cd}(l_\perp) + \dots, \end{aligned} \quad (3.26)$$

where by dots we mean the term which is canceled after we take into account

the contributions to both $J_A^{(2)}(k^- = +M)$ and $J_A^{(2)}(k^- = -M)$ on the right hand side of Eq. (3.22).

Next, we perform the l^+ integral in Eq. (3.26). As we have already mentioned above, since the final result does not depend on the scale M , we can choose arbitrary value of M . We have chosen to perform the calculation in the limit $M \rightarrow 0$. Then the only non-vanishing contribution comes from the imaginary part of the propagator $1/[(l-k)^2 + i\epsilon]$, $-i\pi \delta(2Ml^+ + (l-k)_\perp^2)$. For this term the l^+ integration is trivial and we obtain

$$M \text{ (Fig. 3.5a)} = -\alpha_s f_{aec} f_{deb} \int \frac{d^{D-2}l_\perp}{(2\pi)^{D-2}} \frac{2k_\perp \cdot l_\perp}{l_\perp^2 (k-l)_\perp^2} \Gamma_A^{(2)cd}(l_\perp) + \dots, \quad (3.27)$$

which gives an M -independent contribution to the right hand side of Eq. (3.23).

We follow the same steps when dealing with the diagram in Fig. 3.5b, whose soft sub-diagram is given by

$$\begin{aligned} S_2(k, l) &\equiv \frac{N^{-\mu}(l)}{l^2} \frac{N^{-\nu}(q-l)}{(q-l)^2} V_{\mu\rho\gamma}(l, -k, k-l) \left(g^{\rho+} - \frac{k^\rho}{M} \right) \frac{N^{\gamma\delta}(l-k)}{(l-k)^2} \\ &\times V_{\nu\delta-}(q-l, l-k, k-q). \end{aligned} \quad (3.28)$$

First we use the identity (3.25) for S_2 . The contribution due to the second term in Eq. (3.25) vanishes, after the gluon with momentum l has been factored from $J_A^{(2)}$, due to the antisymmetry of the integrand. Hence again, as in the case discussed above, only the term given by $S_2(l^- = 0, l^+, l_\perp, k)$ contributes. In the limit $M \rightarrow 0$, the contribution comes from the imaginary part of the

same denominator as in the case of Fig. 3.5a. The result is

$$\begin{aligned}
M(\text{Fig. 3.5b}) = & - \alpha_s f_{aec} f_{deb} \int \frac{d^{D-2} l_\perp}{(2\pi)^{D-2}} \frac{2}{l_\perp^2 (l-q)_\perp^2 (k-l)_\perp^2} \\
& \times (k_\perp^2 l_\perp^2 - k_\perp \cdot l_\perp l_\perp^2 - k_\perp \cdot q_\perp l_\perp^2 - k_\perp^2 l_\perp \cdot q_\perp + 2k_\perp \cdot l_\perp l_\perp \cdot q_\perp) \\
& \times \Gamma_A^{(2)cd}(l_\perp) + \dots
\end{aligned} \tag{3.29}$$

Combining the results of Eqs. (3.27) and (3.29), we obtain the expression for the surface term in Eq. (3.22)

$$\begin{aligned}
& M [J_A^{(2)ab}(k^- = +M, k^+ = 0, k_\perp) + J_A^{(2)ab}(k^- = -M, k^+ = 0, k_\perp)] \\
& = 2\alpha_s f_{aec} f_{bed} \int \frac{d^{D-2} l_\perp}{(2\pi)^{D-2}} \left(\frac{k_\perp^2}{l_\perp^2 (k-l)_\perp^2} + \frac{(k-q)_\perp^2}{(l-q)_\perp^2 (k-l)_\perp^2} - \frac{q_\perp^2}{l_\perp^2 (q-l)_\perp^2} \right) \\
& \times \Gamma_A^{(2)cd}(l_\perp).
\end{aligned} \tag{3.30}$$

Next, we analyze the contributions to the term $\tilde{\eta}^\alpha \partial / \partial \eta^\alpha \Gamma_A^{(2)}$ in the evolution equation (3.22). The contributing diagrams are shown in Figs. 3.5c - 3.5f. Note that for every diagram in Figs. 3.5c - 3.5f, we have also diagrams when a loop containing the boxed vertex is attached to the external gluon with momentum k , instead of to the external gluon with momentum $q - k$.

In Fig. 3.5c, we have to consider all the possible insertions of external gluons with momenta k and $q - k$. We have six possibilities. The contribution shown in Fig. 3.5c is proportional to (omitting the color factor)

$$\int_{-M}^M dk^- (\text{Fig. 3.5c}) \propto \int_{-M}^M dk^- \int \frac{d^D l}{(2\pi)^D} \frac{N^{-\mu}(l) S_\mu(l)}{l^2} \frac{(\bar{l} - \bar{k})^+}{(\bar{l} - \bar{k})^2} \frac{(\bar{q} - \bar{l})^+}{(\bar{q} - \bar{l})^2} (k^+ = 0). \tag{3.31}$$

Since the integrand is an antisymmetric function under $k^- \rightarrow -k^-$ and $l^\pm \rightarrow$

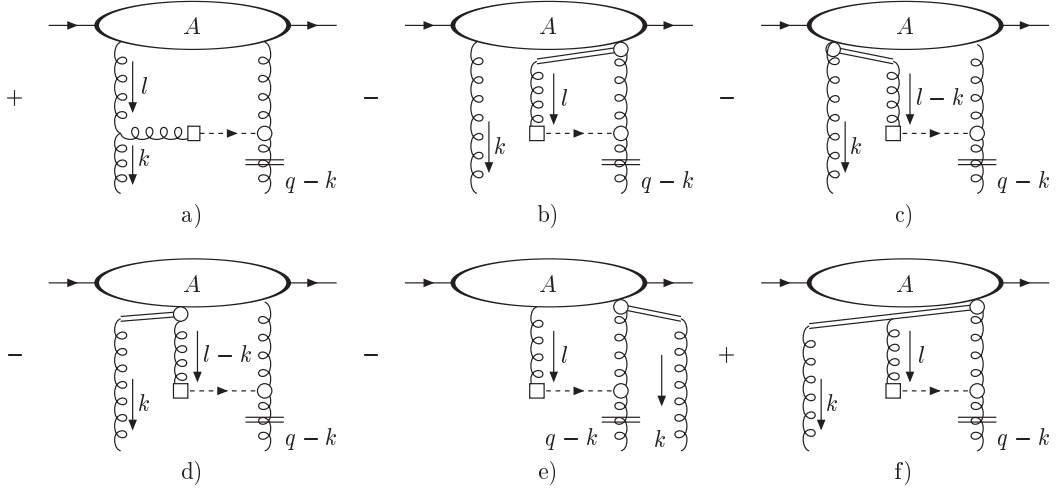


Figure 3.6: Contributions to the diagram in Fig. 3.5f when the gluon coming out of the boxed vertex is attached to the soft line (a) and when either or both gluons with momenta k and l are K gluons and they are factored from the jet (b - f).

$-l^\pm$, the integral in Eq. (3.31) vanishes. The same antisymmetry property holds for the remaining five diagrams and therefore, there is no contribution from them.

Let us next focus on the diagram in Fig. 3.5f. When the gluon with momentum l attaches to a soft line inside of the jet $J_A^{(3)}$, the contribution takes the form shown in Fig. 3.6a. If it attaches to a jet line, its contribution can be written as

$$\begin{aligned}
 \text{Fig. 3.5f} &= -g_s f_{bcd} \int \frac{d^D l}{(2\pi)^D} S_3(k^+ = 0, k^-, k_\perp, l) \\
 &\times J_A^{(3)acd}(k^+ = 0, k^-, k_\perp, l^+ = 0, l^-, l_\perp), \quad (3.32)
 \end{aligned}$$

with the soft function

$$S_3(k, l) \equiv (q - k)^2 \frac{N^{-\mu}(l)}{l^2} \frac{S_\mu(l)}{l \cdot \bar{l}} \frac{N^{-+}(q - k - l)}{(q - k - l)^2}. \quad (3.33)$$

We use the identity for this soft function S_3 , obtained from Eq. (3.17) by the replacement $k^+ \rightarrow l^-$,

$$\begin{aligned} S_3(l^-, k^-) &= S_3(l^- = 0, k^- = 0) \theta(M - |l^-|) \theta(M - |k^-|) \\ &+ [S_3(l^-, k^- = 0) - S_3(l^- = 0, k^- = 0) \theta(M - |l^-|)] \theta(M - |k^-|) \\ &+ [S_3(l^- = 0, k^-) - S_3(l^- = 0, k^- = 0) \theta(M - |k^-|)] \theta(M - |l^-|) \\ &+ [\{S_3(l^-, k^-) - S_3(l^-, k^- = 0) \theta(M - |k^-|)\} \\ &- \{S_3(l^- = 0, k^-) - S_3(l^- = 0, k^- = 0) \theta(M - |k^-|)\} \theta(M - |l^-|)], \end{aligned} \quad (3.34)$$

to treat the soft gluons with momenta k and l attached to jet $J_A^{(3)}$. The contribution from the first term in Eq. (3.34), when used in Eq. (3.32), vanishes since the integrand $S_3(k^+ = k^- = 0, k_\perp, l^- = 0, l^+, l_\perp)$ is an antisymmetric function of l^+ , as can be easily checked using Eqs. (2.11), (2.36) and (B.35). We can apply the K - G decomposition on the gluon with momentum l when treating the second term in Eq. (3.34) used in Eq. (3.32). At LL only the K gluon contributes. It can be factored from the jet function $J_A^{(3)}$ with the result shown in Figs. 3.6b and 3.6c. In a similar way we can treat the gluon with momentum k in the third term of Eq. (3.34). After we factor this gluon from the jet $J_A^{(3)}$, we obtain the contributions shown in Figs. 3.6d and 3.6e. In the case of the last term in Eq. (3.34), we can factor out both soft gluons

with momenta k and l from jet $J_A^{(3)}$. The result of this factorization is shown in Fig. 3.6f.

Next, we note that the combination of the diagrams in Figs. 3.5d, 3.5e and 3.6b is the same as the result encountered in the analysis of the LL amplitude, Fig. 3.3. We write

$$\int_{-M}^M dk^- (\text{Fig. 3.5d} + \text{Fig. 3.5e} + \text{Fig. 3.6b}) = \alpha^{(1)}(q_\perp - k_\perp) \Gamma_A^{(2)ab}(p_A, q, k_\perp). \quad (3.35)$$

where $\alpha^{(1)}(q - k)$ in Eq. (3.35) is given by the diagrams in Fig. 3.3 with an external momentum $q - k = (0^+, 0^-, q_\perp - k_\perp)$. In the case when the gluon coming out of the boxed vertex attaches to an external gluon with momentum k , we evaluate the one loop trajectory $\alpha^{(1)}(k_\perp)$ in Eq. (3.35).

To complete the analysis, we have to discuss the diagrams in Figs. 3.6a and 3.6c - 3.6f. In the region $l^\pm \sim l_\perp$, we can factor the gluon with momentum l from the jet function $J_A^{(2)}(l^+ = 0, l^-, l_\perp)$ in the case of the diagram in Fig. 3.6a. The resulting k^- and l^\pm integral is over an antisymmetric function of k^- and l^\pm , and therefore it vanishes. So the only contribution comes from the Glauber region, where we can set $l^- = 0$ outside $J_A^{(2)}(l^+ = 0, l^-, l_\perp)$. As above, we perform the l^+ and k^- integrals in the limit $M \rightarrow 0$. The integrand does not develop a singularity in k^- and/or l^+ strong enough to compensate for the shrinkage of the integration region $\int_{-M}^M dk^-$ when $M \rightarrow 0$. Hence the diagram in Fig. 3.6a does not contribute in the limit $M \rightarrow 0$. In a similar way as for the diagram in Fig. 3.6a, none of the diagrams in Figs. 3.6c - 3.6f contribute. The diagrams in Figs. 3.6c - 3.6e vanish in the $M \rightarrow 0$ limit, while in the case of the diagram in Fig. 3.6f the k^- and l^\pm integral is over an antisymmetric

function of k^- and l^\pm .

At this point we have discussed all the contributions appearing on the right hand side of the evolution equation (3.22). Combining the partial results given by Eqs. (3.35) and (3.30) in Eq. (3.22), we arrive at the evolution equation governing the high energy behavior of $\Gamma_A^{(2)}$

$$\begin{aligned}
\left(p_A^+ \frac{\partial}{\partial p_A^+} - 1\right) \Gamma_A^{(2)ab}(p_A^+, q, k_\perp) &= 2\alpha_s f_{aec} f_{bed} \int \frac{d^{D-2}l_\perp}{(2\pi)^{D-2}} \Gamma_A^{(2)cd}(p_A^+, q, l_\perp) \\
&\times \left(\frac{k_\perp^2}{l_\perp^2 (k-l)_\perp^2} + \frac{(k-q)_\perp^2}{(l-q)_\perp^2 (k-l)_\perp^2} - \frac{q_\perp^2}{l_\perp^2 (q-l)_\perp^2} \right) \\
&+ (\alpha^{(1)}(k_\perp) + \alpha^{(1)}(q_\perp - k_\perp)) \times \Gamma_A^{(2)ab}(p_A^+, q, k_\perp).
\end{aligned} \tag{3.36}$$

Projecting out onto the color singlet in Eq. (3.36), we immediately recover the celebrated BFKL equation [21].

3.2.1 Evolution of $\Gamma^{(n)}$ at LL

We can now generalize Eq. (3.36) to the case of $\Gamma_A^{(n)}$. The evolution kernel in this case contains, besides a piece diagonal in the number of external gluons, also contributions which relate jet functions with different number of external

gluons

$$\begin{aligned}
& \left(p_A^+ \frac{\partial}{\partial p_A^+} - 1 \right) \Gamma_A^{(n) a_1 \dots a_n} (p_A^+, q, k_{1\perp}, \dots, k_{n\perp}) = \\
& 2\alpha_s \sum_{i < j}^n f_{a_i e b_i} f_{a_j e b_j} \int \frac{d^{D-2} l_{i\perp}}{(2\pi)^{D-2}} \frac{d^{D-2} l_{j\perp}}{(2\pi)^{D-2}} \delta^{(2)}(l_{i\perp} + l_{j\perp} - k_{i\perp} - k_{j\perp}) \\
& \times \left(\frac{k_{i\perp}^2}{l_{i\perp}^2 (k_i - l_i)_\perp^2} + \frac{k_{j\perp}^2}{l_{j\perp}^2 (k_j - l_j)_\perp^2} - \frac{(k_i + k_j)_\perp^2}{l_{i\perp}^2 l_{j\perp}^2} \right) \\
& \times \Gamma_A^{(n) a_1 \dots b_i \dots b_j \dots a_n} (p_A^+, q, k_{1\perp}, \dots, l_{i\perp}, \dots, l_{j\perp}, \dots, k_{n\perp}) \\
& + \sum_{i=1}^n (\alpha^{(1)}(k_{i\perp})) \times \Gamma_A^{(n) a_1 \dots a_n} (p_A^+, q, k_{1\perp}, \dots, k_{n\perp}) \\
& + \sum_{n'=1}^{n-1} \mathcal{K}_{a_1 \dots a_n; b_1 \dots b_{n'}}^{(n, n')} \otimes_\perp \Gamma_A^{(n') b_1 \dots b_{n'}}, \tag{3.37}
\end{aligned}$$

where \otimes_\perp denotes a convolution in transverse momentum space. The last term in Eq. (3.37) corresponds to the configurations when one or more external gluons attach to a gluon or a ghost lines forming the one loop kernel derived for $\Gamma_A^{(2)}$. Using the notation of Sec. 2.5.4, we can write Eq. (3.37) at r -loop order in a form

$$\left(p_A^+ \frac{\partial}{\partial p_A^+} - 1 \right) \Gamma_A^{(n, r)} = \sum_{n'=1}^n \mathcal{K}^{(n, n'; 1)} \otimes \Gamma_A^{(n', r-1)}. \tag{3.38}$$

It corresponds to Eq. (2.64) of Sec. 2.5.4 when written in terms of the coefficients $c_r^{(n, r)}$ introduced in Eq. (2.60). From Eq. (3.38) we immediately see that the following property of the one loop kernel

$$\mathcal{K}^{(n, n'; 1)} = \theta(n - n') \tilde{\mathcal{K}}^{(n, n'; 1)}, \tag{3.39}$$

is satisfied. We recall that this step was essential in demonstrating that the set of evolution equations, Eq. (2.51), forms a consistent system, refer to the paragraph above Eq. (2.64).

The term diagonal in the number of external gluons in Eq. (3.37) coincides with the evolution equation derived in Ref. [17]. Our formalism, besides enabling us to go systematically beyond LL accuracy, indicates that even at LL, in addition to the kernels found in Ref. [17], the kernel has contributions which relate jet functions with different number of external gluons.

3.3 Gluon reggeization at NLL

In this section, we study the NLL evolution equation and the gluon reggeization. In Sec. 3.3.1, we identify the contributions to the amplitude at NLL and negative signature channel. Sec. 3.3.2 gives a detailed derivation of the relevant evolution equation.

3.3.1 Color octet and negative signature amplitude

The statement of gluon reggeization means that the scattering amplitude in the Regge limit, dominated by the gluon exchange (color octet) in the t -channel, and antisymmetric under $s \leftrightarrow u$ (negative signature), takes the form

$$A_{\mathbf{8}}^{(-)}(s, t)_{r_A r_B, r_1 r_2} = F_A^a(t)_{r_1 r_A} \left[\left(\frac{s}{-t} \right)^{\alpha(t)} - \left(\frac{-s}{-t} \right)^{\alpha(t)} \right] F_B^a(t)_{r_2 r_B}, \quad (3.40)$$

where $F_A^a(t)$ and $F_B^a(t)$ are the impact factors, which depend on the properties of the scattered particles. The Regge trajectory $\alpha(t)$ determines the depen-

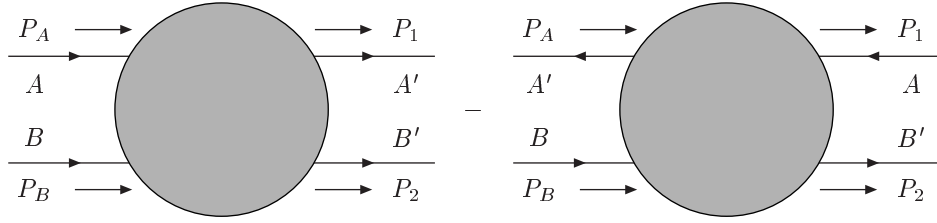


Figure 3.7: Projection of the amplitude onto the negative signature channel.

dence on the energy \sqrt{s} . It is a universal function of t meaning that it does not depend on the particles involved in the scattering. In order to project onto the negative signature channel, besides the amplitude for $qq' \rightarrow qq'$ scattering, Eq. (2.1), we consider the amplitude for the process

$$\bar{q}(p_A, r_1, \lambda_A) + q'(p_B, r_B, \lambda_B) \rightarrow \bar{q}(p_A - q, r_A, \lambda_1) + q'(p_B + q, r_2, \lambda_2). \quad (3.41)$$

The amplitude for scattering (3.41), $\tilde{A}(s, t)$, can be obtained from the amplitude for the process (2.1), $A(s, t)$, by the crossing symmetry $s \leftrightarrow u$. This means that $\tilde{A}(s, t) = A(u, t) \simeq A(-s, t)$. Hence, if we define

$$A^{(-)}(s, t) \equiv \frac{1}{2} \left(A(s, t) - \tilde{A}(s, t) \right), \quad (3.42)$$

as indicated in Fig. 3.7, the amplitude $A^{(-)}$ will have a negative signature by construction. Since $s \sim -u$ in the Regge limit, the logarithmic derivative of this amplitude is:

$$\frac{\partial A^{(-)}}{\partial \ln s}(s, t) = \frac{1}{2} \left(s \frac{\partial A}{\partial s}(s, t) - u \frac{\partial \tilde{A}}{\partial u}(s, t) \right), \quad (3.43)$$

We now isolate the negative signature contribution to the amplitude for

process (2.1) at NLL. The projection of the set of two gluon exchange diagrams, Fig. 3.1b, onto the negative signature takes the form:

$$\begin{aligned}
A_2^{(-)} &= \int \frac{d^D k}{(2\pi)^D} \left[J_A^{(2)ab}(k^+ = 0, k^-, k_\perp) - \tilde{J}_A^{(2)ab}(k^+ = 0, k^-, k_\perp) \right] \\
&\times S(k^+, k^-, k_\perp) \times J_B^{(2)ab}(k^- = 0, k^+, k_\perp), \tag{3.44}
\end{aligned}$$

where $S(k)$ has been defined in Eq. (3.16) and $\tilde{J}_A^{(2)}$ is the jet function corresponding to the anti-quark in the process (3.41) moving in the plus direction. In Appendix B.1 we show that the jet functions $J_A^{(n)}$ and $\tilde{J}_A^{(n)}$ are related by the symmetry:

$$J_A^{(n)}(k_i^+ \rightarrow -k_i^+, k_i^- \rightarrow -k_i^-, k_{i\perp} \rightarrow k_{i\perp}) = (-1)^{n-1} (-1)^{\lambda_A + \lambda_1} \tilde{J}_A^{(n)}(k_i^+, k_i^-, k_{i\perp}), \tag{3.45}$$

in the Regge limit. Applying this identity to the jet function with two external gluons ($n = 2$), the helicity conserving part of the jet function ($\lambda_A + \lambda_1 = 2\lambda_A = \pm 1$) obeys:

$$\tilde{J}_A^{(2)}(k^+ = 0, -k^-, k_\perp) = J_A^{(2)}(k^+ = 0, k^-, k_\perp). \tag{3.46}$$

We apply this result to analyze Eq. (3.44). Using Eqs. (3.16) and (3.46), we easily see that in the Glauber region $k^- \ll k^+ \sim k_\perp$ the integrand in Eq. (3.44) is over an antisymmetric function of k^- and therefore the k^- integral vanishes. This indicates that there is no contribution from the Glauber region when analyzing a soft gluon with momentum k in Fig. 3.2b and therefore this gluon can be factored from the jet functions $J_A^{(2)}$ and $J_B^{(2)}$. As a consequence,

the high-energy behavior of the amplitude for the process (2.1), projected onto the negative signature channel, is determined by the jet functions with one external gluon only, $J_A^{(1)}$ and $J_B^{(1)}$. It also means that $A_2^{(-)}$ is automatically in the color octet channel.

Combining the contributions from the one and the two gluon exchange diagrams shown in Fig. 3.1, the negative signature amplitude $A_{\mathbf{8}}^{(-)}$ takes the form:

$$A_{\mathbf{8}}^{(-)} = -\frac{1}{t} \left(J_A^{(1)a}(p_A, q, \eta) - \tilde{J}_A^{(1)a}(p_A, q, \eta) \right) \left(1 + \frac{1}{t} \Pi_{+-}(q, \eta) + \frac{i\pi}{2} \alpha^{(1)}(t) \right) \times J_B^{(1)a}(p_A, q, \eta), \quad (3.47)$$

where $\Pi_{+-}(q, \eta)$ is the one-loop gluon self-energy and $\alpha^{(1)}(t)$ is the one-loop contribution to the gluon trajectory given in Eq. (3.12). Eq. (3.47) indicates that in order to determine the high energy behavior of the scattering amplitude, we need to determine the high-energy behavior of $J_A^{(1)}$ and $\tilde{J}_A^{(1)}$. If we show that $J_A^{(1)}$ and $\tilde{J}_A^{(1)}$ satisfy:

$$\begin{aligned} p_A^+ \frac{\partial J_A^{(1)}}{\partial p_A^+} &= \alpha(t) J_A^{(1)}, \\ p_A^+ \frac{\partial \tilde{J}_A^{(1)}}{\partial p_A^+} &= \alpha(t) \tilde{J}_A^{(1)}, \end{aligned} \quad (3.48)$$

at NLL, then the solution to the evolution equation (3.48) used in Eqs. (3.43) and (3.47) implies the Regge ansatz, Eq. (3.40). This would provide a proof of gluon reggeization at NLL to all orders in perturbation theory in QCD, Ref. [28]. We study the evolution equation (3.48) in the next section.

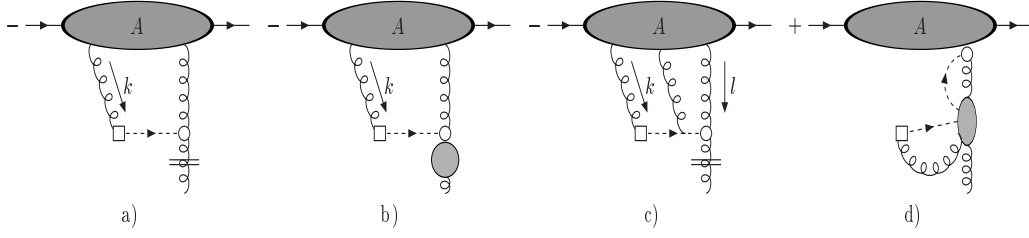


Figure 3.8: Diagrammatic representation of the evolution equation for jet $J_A^{(1)}$ at NLL.

3.3.2 NLL evolution equation for $J_A^{(1)}$

We now derive the evolution equation for jet function $J_A^{(1)a}$ at NLL. We restrict ourselves to $J_A^{(1)}$ since $\tilde{J}_A^{(1)}$ can be analyzed in the same way. Applying the general evolution equation, Eq. (2.51), for $n = 1$ and using the results in Fig. 2.4, we arrive at the contributions to $(\partial/\partial \ln p_A^+ - 1)J_A^{(1)a}$ shown in Fig. 3.8. The diagram in Fig. 3.8d, is already in a factorized form so it does not need to be analyzed further. The blob in the bottom part of this diagram represents all possible two loop corrections.

In Fig. 3.8b, the bottom dark blob denotes the one loop gluon-self energy. The gluon with momentum k can be analyzed the same way as in the case of LL, Sec. 3.1, with a result in a factorized form.

In order to prove reggeization of a gluon at NLL, we need to show that the soft gluon with momentum k in Fig. 3.8a and the soft gluons with momenta k and l in Fig. 3.8c can be factored from the jet functions $J_A^{(2)}$ and $J_A^{(3)}$, respectively. Let us now analyze these particular diagrams. The contribution to Fig. 3.8a can be written

$$\text{Fig. 3.8a} = -ig_s f_{abc} \int \frac{d^D k}{(2\pi)^D} S_{\mu\nu}(k, q) J_{(A)bc}^{(2)\mu\nu}(p_A, q; k). \quad (3.49)$$

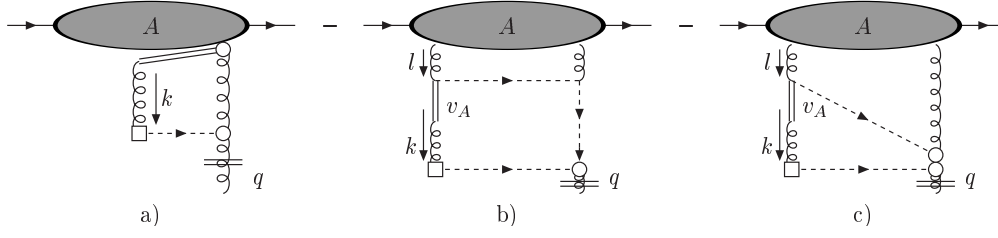


Figure 3.9: Contributions to Fig. 3.8a from the K gluon at NLL.

Next, we use the following identity for the integrand in Eq. (3.49)

$$\begin{aligned}
S_{\mu\nu}(k) J_{(A)bc}^{(2)\mu\nu}(k) &= S_{++}(k) J_{(A)bc}^{(2)++}(k^+ = 0, k^-, k_\perp) \\
&+ \left[S_{++}(k) J_{(A)bc}^{(2)++}(k) - S_{++}(k) J_{(A)bc}^{(2)++}(k^+ = 0, k^-, k_\perp) \right] \\
&+ \left[S_{\mu\nu}(k) J_{(A)bc}^{(2)\mu\nu}(k) - S_{++}(k) J_{(A)bc}^{(2)++}(k) \right]. \quad (3.50)
\end{aligned}$$

The first term in Eq. (3.50), after being inserted into Eq. (3.49), can be analyzed using the K - G decomposition, since there is no contribution from the Glauber region due to the antisymmetry of $S_{++}(k^+, k^- = 0, k_\perp)$ under the transformation $k^+ \rightarrow -k^+$. The contributions from the K gluon, after applying the Ward identities, can be expressed in a form shown in Fig. 3.9. The diagram in Fig. 3.9a is the same as in the case of LL. At NLL, we also have to insert the gluon and ghost self-energies where appropriate. This diagram is in a factorized form and therefore consistent with a gluon reggeization at NLL.

As for diagrams in Figs. 3.9b and 3.9c, the gluon with momentum l can be factored from the jet function $J_A^{(2)}$ as shown in Appendix B.2. Thus the contributions from the K gluon in Figs. 3.9a - 3.9c can be written in a factorized form and they are in an agreement with the gluon reggeization at NLL.

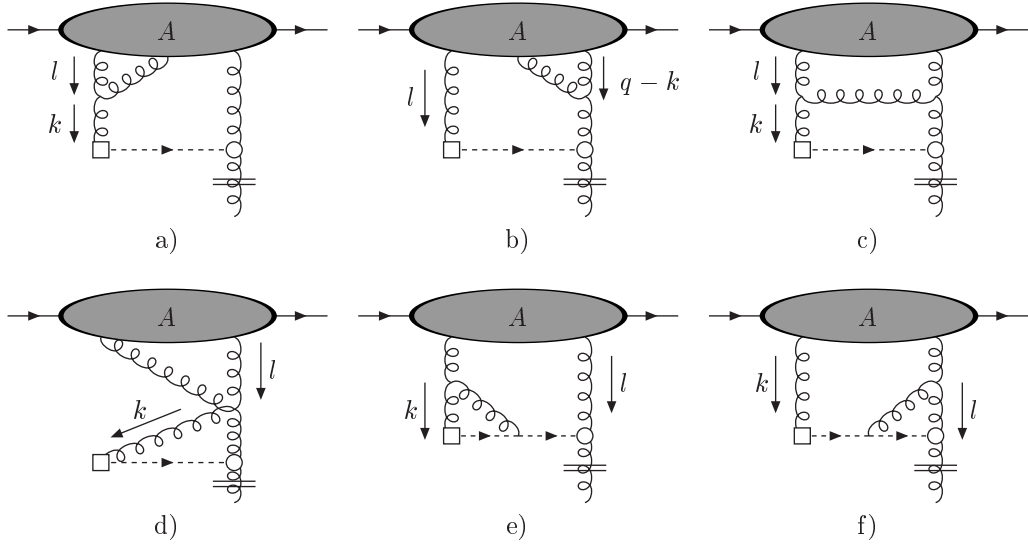


Figure 3.10: Soft contributions to Figs. 3.8a and 3.8c.

Next, we analyze the contributions from the G gluon with momentum k corresponding to the first term in Eq. (3.50) and to Fig. 3.8a. They come from the diagrams shown in Figs. 3.10a, 3.10c and 3.10d since the G gluon must be attached to a soft line. In Appendix B.2, we show that the soft gluons with momenta l and $k - l$ can be factored from the jet function $J_A^{(3)}$ in Fig. 3.10a, the soft gluons with momenta l can be factored from the jet functions $J_A^{(2)}$ in Figs. 3.10c and 3.10d and therefore the contribution from the G gluon corresponding to Fig. 3.8a is in a factorized form.

Now, we examine the gluons with momenta k and/or $q - k$ in the second and the third terms of Eq. (3.50), after used in Eq. (3.49). They must attach to soft lines and therefore the typical contributions to these terms come from diagrams shown in Figs. 3.10a - 3.10d. First we analyze the contributions to the second term in Eq. (3.50). As shown in Appendix B.2, the contribution to the diagram in Fig. 3.10c is in a factorized form. However, there are

contributions to the diagrams in Fig. 3.10a and Fig. 3.10b, coming from the region when all soft gluons external to $J_A^{(3)}$ are Glauber, which cannot be written in a simple factorized form. These contributions, Eq. (B.20) and Eq. (B.24), are rather in a form of a convolution in transverse momentum space.

As far as the last term in Eq. (3.50) is concerned, its contributions come from the diagrams in Figs. 3.10a - 3.10d. As we demonstrate in Appendix B.2, the soft gluons external to $J_A^{(3)}$ in Figs. 3.10a and 3.10b, as well as the soft gluons external to $J_A^{(2)}$ in Figs. 3.10c and 3.10d can be factored from the jet functions.

Finally, we need to examine the diagram in Fig. 3.8c which can be written as

$$\begin{aligned}
\text{Fig. 3.8c} &\equiv \int \frac{d^D k}{(2\pi)^D} \frac{d^D l}{(2\pi)^D} S_{bcd}(k, l, q) \\
&\times J_A^{(3) bcd}(p_A, q; k^+ = 0, k^-, k_\perp, l^+ = 0, l^-, l_\perp) \\
&+ \int \frac{d^D l}{(2\pi)^D} S_{bc}(l, q) J_A^{(2) bc}(p_A, q; l^+ = 0, l^-, l_\perp) \\
&+ \int \frac{d^D k}{(2\pi)^D} S_{bc}(k, q) J_A^{(2) bc}(p_A, q; k^+ = 0, k^-, k_\perp). \quad (3.51)
\end{aligned}$$

The contribution to the first term in Eq. (3.51) comes from a diagram shown in Fig. 3.8c where the soft gluons with momenta k , l and $q - k - l$ attach to jet lines inside the jet function $J_A^{(3)}$. At NLL we can set $k^+ = l^+ = 0$ inside $J_A^{(3)}$ and also the soft gluons attach to the plus components of the jet's vertices. As shown in Appendix B.2, in the region when both gluons with momenta k and l are Glauber, we cannot factor out these gluons and the contribution from this double Glauber region is not in a factorized form.

The contribution to the last two terms in Eq. (3.51) comes from the graphs shown in Figs. 3.10e and 3.10f, respectively. The gluon with momentum $q - k - l$ attaches to soft gluons with momenta k , Fig. 3.10e, and l , Fig. 3.10f, respectively. In Appendix B.2 we demonstrate that the gluons external to $J_A^{(2)}$, can be factored from the jet functions $J_A^{(2)}$.

As a result of the previous reasoning, we arrive at a conclusion that the evolution equation for the jet function $J_A^{(1)}$ at NLL takes the form:

$$\begin{aligned}
p_A^+ \frac{\partial J_A^{(1)a}}{\partial p_A^+}(p_A, q) &= \mathcal{K}^{(1,1)}(t) J_A^{(1)a}(p_A, q) + \int \frac{d^{D-2}k_\perp}{(2\pi)^{D-2}} \frac{d^{D-2}l_\perp}{(2\pi)^{D-2}} \mathcal{K}_{abcd}^{(1,3)}(q, k_\perp, l_\perp) \\
&\times \Gamma_A^{(3)bcd}(p_A, q; k_\perp, l_\perp). \tag{3.52}
\end{aligned}$$

The kernel $\mathcal{K}^{(1,1)}$ is given by all the diagrams where it was possible to factor the soft gluons from the jet functions. This piece is in an agreement with gluon reggeization at NLL according to Eq. (3.48). Besides this term, there is a contribution in Eq. (3.52) corresponding to the configurations when all soft gluons external to the jet function $J_A^{(3)}$ are Glauber. Combining the results of Eqs. (B.20), (B.24) and (B.39) in Appendix B.2, we can find out the explicit form of the kernel $\mathcal{K}^{(1,3)}$. The presence of this term in Eq. (3.52) suggests the breakdown of gluon reggeization at NLL level. We have to note the following, however. At two loop level, these non-factorizing terms vanish. The non-factorizing piece in every diagram comes from the double pinched region, corresponding to the two delta function terms originating from the two denominators on the fermion line present in the tree-level jet function. They, however, do not produce any dependence on transverse momenta and therefore this term is symmetric in external momenta. Hence if we inter-

change the two external momenta flowing out of $J_A^{(3)}$ and into the three point gluon-gluon-gluon or ghost-gluon-ghost vertex, Figs. 3.10a, 3.10b and 3.8c, the integrand becomes an antisymmetric function under this exchange and the integral vanishes. However, when the jet function contains loop corrections, it will, in general, not be symmetric under the interchange of external momenta only. In order to get the symmetry, we need to interchange the colors as well. Nevertheless, the above argument shows that the standard analysis and the calculations which have been performed at the two loop level, Refs. [26] - [33], are not in a contradiction with our results.

3.4 Conclusions

As an illustration of the general algorithm we have demonstrated it in an action at NLL in both the amplitude and the evolution equations. First, in Sec. 3.1, we have performed the resummation of the amplitude at LL. We have found the standard expression for the gluon Regge trajectory, Eq. (3.12). Then, in Sec. 3.2, we have identified the class of diagrams contributing to the amplitude at NLL level. They involved one and two gluon exchange diagrams, Fig. 3.1. The resummation of the two gluon exchange diagram in Sec. 3.2, needed to be performed at LL. It has lead to the celebrated BFKL equation, Eq. (3.36). The one gluon exchange contribution had to be resummed at NLL. Together with this resummation, we have addressed the question of gluon reggeization at NLL in Sec. 3.3. We have found that the majority of the terms in the evolution kernel are in an agreement with this conjecture to all orders in perturbation theory. However, we have also identified contributions

violating the Regge ansatz starting at the three loop level and calculated the corresponding evolution kernels, Eqs. (B.20), (B.24), (B.39). We have not been able to prove that these contributions decouple from the jets. A further study of symmetries involving jets with three external gluons should shed more light on the presence or absence of the non-factorized terms, Ref. [11].

Part II

Resummation in Dijet Events

Chapter 4

Event Shape / Energy Flow Correlations

4.1 Introduction

The agreement of theoretical predictions with experiment for jet cross sections is often impressive. This is especially so for inclusive jet cross sections at high p_T , using fixed-order factorized perturbation theory and parton distribution functions [52]. A good deal is also known about the substructure of jets, through the theoretical and experimental study of multiplicity distributions and fragmentation functions [53], and of event shapes [54–56]. Event shape distributions [57–59] in particular offer a bridge between the perturbative, short-distance and the nonperturbative, long-distance dynamics of QCD [60].

Energy flow [61] into angular regions between energetic jets gives information that is in some ways complementary to what we learn from event shapes. In perturbation theory, the distribution of particles in the final state reflects

interference between radiation from different jets [53], and there is ample evidence for perturbative antenna patterns in interjet radiation at both e^+e^- [62] and hadron colliders [63, 64]. Energy flow between jets must also encode the mechanisms that neutralize color in the hadronization process, and the transition of QCD from weak to strong coupling. Knowledge of the interplay between energy and color flows [65, 66] may help identify the underlying event in hadron collisions [67], to distinguish QCD bremsstrahlung from signals of new physics. Nevertheless, the systematic computation of energy flow into interjet regions has turned out to be subtle [68] for reasons that we will review below, and requires a careful construction of the class of jet events. It is the purpose of this work to provide such a construction, using event shapes as a tool.

In this paper, we introduce correlations between event shapes and energy flow, “shape/flow correlations”, that are sensitive primarily to radiation from the highest-energy jets. So long as the observed energy is not too small, in a manner to be quantified below, we may control logarithms of the ratio of energy flow to jet energy [66, 69].

The energy flow observables that we discuss below are distributions associated with radiation into a chosen interjet angular region, Ω . Within Ω we identify a kinematic quantity $Q_\Omega \equiv \varepsilon Q$, at c.m. energy Q , with $\varepsilon \ll 1$. Q_Ω may be the sum of energies, transverse energies or related observables for the particles emitted into Ω . Let us denote by $\bar{\Omega}$ the complement of Ω . We are interested in the distribution of Q_Ω for events with a fixed number of jets in

$\bar{\Omega}$. This set of events may be represented schematically as

$$A + B \rightarrow \text{Jets} + X_{\bar{\Omega}} + R_{\Omega}(Q_{\Omega}). \quad (4.1)$$

Here $X_{\bar{\Omega}}$ stands for radiation into the regions between Ω and the jet axes, and R_{Ω} for radiation into Ω .

The subtlety associated with the computation of energy flow concerns the origin of logarithms, and is illustrated by Fig. 4.1. Gluon 1 in Fig. 4.1 is an example of a primary gluon, emitted directly from the hard partons near a jet axes. Phase space integrals for primary emissions contribute single logarithms per loop: $(1/Q_{\Omega})\alpha_s^n \ln^{n-1}(Q/Q_{\Omega}) = (1/\varepsilon Q)\alpha_s^n \ln^{n-1}(1/\varepsilon)$, $n \geq 1$, and these logarithms exponentiate in a straightforward fashion [66]. At fixed Q_{Ω} for Eq. (4.1), however, there is another source of potentially large logarithmic corrections in Q_{Ω} . These are illustrated by gluon 2 in the figure, an example of secondary radiation in Ω , originating a parton emitted by one of the leading jets that define the event into intermediate region $\bar{\Omega}$. As observed by Dasgupta and Salam [68], emissions into Ω from such secondary partons can also result in logarithmic corrections, of the form $(1/Q_{\Omega})\alpha_s^n \ln^{n-1}(\bar{Q}_{\bar{\Omega}}/Q_{\Omega})$, $n \geq 2$, where $\bar{Q}_{\bar{\Omega}}$ is the maximum energy emitted into $\bar{\Omega}$. These logarithms arise from strong ordering in the energies of the primary and secondary radiation because real and virtual enhancements associated with secondary emissions do not cancel each other fully at fixed Q_{Ω} .

If the cross section is fully inclusive outside of Ω , so that no restriction is placed on the radiation into $\bar{\Omega}$, $\bar{Q}_{\bar{\Omega}}$ can approach Q , and the secondary logarithms can become as important as the primary logarithms. Such a cross

section, in which only radiation into a fixed portion of phase space (Ω) is specified, was termed “non-global” by Dasgupta and Salam, and the associated logarithms are also called non-global [68, 70, 71].

In effect, a non-global definition of energy flow is not restrictive enough to limit final states to a specific set of jets, and non-global logarithms are produced by jets of intermediate energy, emitted in directions between region Ω and the leading jets. Thus, interjet energy flow does not always originate directly from the leading jets, in the absence of a systematic criterion for suppressing intermediate radiation. Correspondingly, non-global logarithms reflect color flow at all scales, and do not exponentiate in a simple manner. Our aim in this paper is to formulate a set of observables for interjet radiation in which non-global logarithms are replaced by calculable corrections, and which reflect the flow of color at short distances. By restricting the sizes of event shapes, we will limit radiation in region $\bar{\Omega}$, while retaining the chosen jet structure.

An important observation that we will employ below is that non-global logarithms are not produced by secondary emissions that are very close to a jet direction, because a jet of parallel-moving particles emits soft radiation coherently. By fixing the value of an event shape near the limit of narrow jets, we avoid final states with large energies in $\bar{\Omega}$ away from the jet axes. At the same time, we will identify limits in which non-global logarithms reemerge as leading corrections, and where the methods introduced to study nonglobal effects in Refs. [68, 70, 71] provide important insights.

To formalize these observations, we study below correlated observables for e^+e^- annihilation into two jets. (In Eq. (4.1) A and B denote positron and

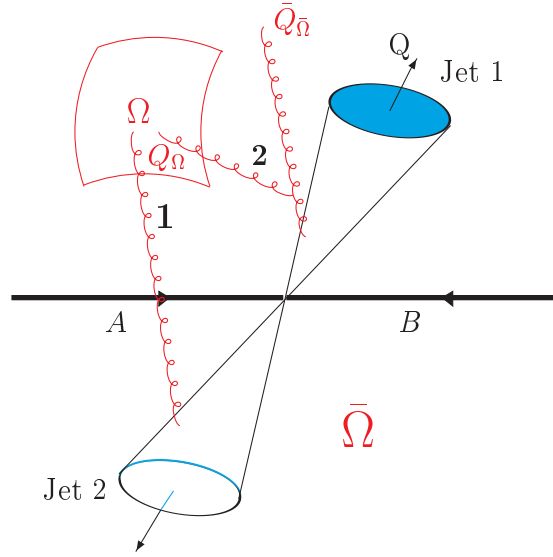


Figure 4.1: Sources of global and non-global logarithms in dijet events. Configuration 1, a primary emission, is the source of global logarithms. Configuration 2 can give non-global logarithms.

electron.) In e^+e^- annihilation dijet events, the underlying color flow pattern is simple, which enables us to concentrate on the energy flow within the event. We will introduce a class of event shapes, $\bar{f}(a)$ suitable for measuring energy flow into only part of phase space, with a an adjustable parameter. To avoid large non-global logarithmic corrections we weight events by $\exp[-\nu\bar{f}]$, with ν the Laplace transform conjugate variable.

For the restricted set of events with narrow jets, energy flow is proportional to the lowest-order cross section for gluon radiation into the selected region. The resummed cross section, however, remains sensitive to color flow at short distances through anomalous dimensions associated with coherent interjet soft emission. In a sense, our results show that an appropriate selection of jet events

automatically suppresses nonglobal logarithms, and confirms the observation of coherence in interjet radiation [53, 63].

In the next section, we introduce the event shapes that we will correlate with energy flow, and describe their relation to the thrust and jet broadening. Section 3 contains the details of the factorization procedure that characterizes the cross section in the two-jet limit. This is followed in Sec. 4 by a derivation of the resummation of logarithms of the event shape and energy flow, following the method introduced by Collins and Soper [72]. We then go on in Sec. 5 to exhibit analytic results at leading logarithmic accuracy in Q_Ω/Q and next-to-leading logarithm in the event shape. Section 6 contains representative numerical results. We conclude with a summary and a brief outlook on further applications.

4.2 Shape/Flow Correlations

4.2.1 Weights and energy flow in dijet events

In the notation of Eq. (4.1), we will study an event shape distribution for the process

$$e^+ + e^- \rightarrow J_1(p_{J_1}) + J_2(p_{J_2}) + X_{\bar{\Omega}}(\bar{f}) + R_\Omega(Q_\Omega), \quad (4.2)$$

at c.m. energy $Q \gg Q_\Omega \gg \Lambda_{\text{QCD}}$. Two jets with momenta p_{J_c} , $c = 1, 2$ emit soft radiation (only) at wide angles. Again, Ω is a region between the jets to be specified below, where the total energy or the transverse energy Q_Ω of the soft radiation is measured, and $\bar{\Omega}$ denotes the remaining phase space (see Fig. 4.1). Radiation into $\bar{\Omega}$ is constrained by event shape \bar{f} . We refer to cross

sections at fixed values (or transforms) of \bar{f} and Q_Ω as shape/flow correlations.

To impose the two-jet condition on the states of Eq. (4.2) we choose weights that suppress states with substantial radiation into $\bar{\Omega}$ away from the jet axes. We now introduce a class of event shapes \bar{f} , related to the thrust, that enforce the two-jet condition in a natural way.

These event shapes interpolate between and extend the familiar thrust [55] and jet broadening [58,59], through an adjustable parameter a . For each state N that defines process (4.2), we separate $\bar{\Omega}$ into two regions, $\bar{\Omega}_c$, $c = 1, 2$, containing jet axes, $\hat{n}_c(N)$. To be specific, we let $\bar{\Omega}_1$ and $\bar{\Omega}_2$ be two hemispheres that cover the entire space except for their intersections with region Ω . Region $\bar{\Omega}_1$ is centered on \hat{n}_1 , and $\bar{\Omega}_2$ is the opposite hemisphere. We will specify the method that determines the jet axes \hat{n}_1 and \hat{n}_2 momentarily. To identify a meaningful jet, of course, the total energy within $\bar{\Omega}_1$ should be a large fraction of the available energy, of the order of $Q/2$ in dijet events. In e^+e^- annihilation, if there is a well-collimated jet in $\bar{\Omega}_1$ with nearly half the total energy, there will automatically be one in $\bar{\Omega}_2$.

We are now ready to define the contribution from particles in region $\bar{\Omega}_c$ to the a -dependent event shape,

$$\bar{f}_{\bar{\Omega}_c}(N, a) = \frac{1}{\sqrt{s}} \sum_{\hat{n}_i \in \bar{\Omega}_c} k_{i,\perp}^a \omega_i^{1-a} (1 - \hat{n}_i \cdot \hat{n}_c)^{1-a}, \quad (4.3)$$

where a is any real number less than two, and where $\sqrt{s} = Q$ is the c.m. energy. The sum is over those particles of state N with direction \hat{n}_i that flow into $\bar{\Omega}_c$, and their transverse momenta $k_{i,\perp}$ are measured relative to \hat{n}_c . The jet axis \hat{n}_1 for jet 1 is identified as that axis that minimizes the specific thrust-

related quantity $\bar{f}_{\bar{\Omega}_1}(N, a = 0)$. When $\bar{\Omega}_c$ in Eq. (4.3) is extended to all of phase space, the case $a = 0$ is then essentially $1 - T$, with T the thrust, while $a = 1$ is related to the jet broadening.

Any choice $a < 2$ in (4.3) specifies an infrared safe event shape variable, because the contribution of any particle i to the event shape behaves as θ_i^{2-a} in the collinear limit, $\theta_i = \cos^{-1}(\hat{n}_i \cdot \hat{n}_c) \rightarrow 0$. Negative values of a are clearly permissible, and the limit $a \rightarrow -\infty$ corresponds to the total cross section. At the other limit, the factorization and resummation techniques that we discuss below will apply only to $a < 1$. For $a > 1$, contributions to the event shape (4.3) from energetic particles near the jet axis are generically larger than contributions from soft, wide-angle radiation, or equal for $a = 1$. When this is the case, the analysis that we present below must be modified, at least beyond the level of leading logarithm [59].

In summary, once \hat{n}_1 is fixed, we have divided the phase space into three regions:

- Region Ω , in which we measure, for example, the energy flow,
- Region $\bar{\Omega}_1$, the entire hemisphere centered on \hat{n}_1 , that is, around jet 1, except its intersection with Ω ,
- Region $\bar{\Omega}_2$, the complementary hemisphere, except its intersection with Ω .

In these terms, we define the complete event shape variable $\bar{f}(N, a)$ by

$$\bar{f}(N, a) = \bar{f}_{\bar{\Omega}_1}(N, a) + \bar{f}_{\bar{\Omega}_2}(N, a), \quad (4.4)$$

with \bar{f}_{Ω_c} , $c = 1, 2$ given by (4.3) in terms of the axes \hat{n}_1 of jet 1 and \hat{n}_2 of jet 2. We will study the correlations of this set of event shapes with the energy flow into Ω , denoted as

$$f(N) = \frac{1}{\sqrt{s}} \sum_{\hat{n}_i \in \Omega} \omega_i. \quad (4.5)$$

The differential cross section for such dijet events at fixed values of \bar{f} and f is now

$$\begin{aligned} \frac{d\bar{\sigma}(\varepsilon, \bar{\varepsilon}, s, a)}{d\varepsilon d\bar{\varepsilon} d\hat{n}_1} &= \frac{1}{2s} \sum_N |M(N)|^2 (2\pi)^4 \delta^4(p_I - p_N) \\ &\quad \times \delta(\varepsilon - f(N)) \delta(\bar{\varepsilon} - \bar{f}(N, a)) \delta^2(\hat{n}_1 - \hat{n}(N)), \end{aligned} \quad (4.6)$$

where we sum over all final states N that contribute to the weighted event, and where $M(N)$ denotes the corresponding amplitude for $e^+e^- \rightarrow N$. The total momentum is p_I , with $p_I^2 = s \equiv Q^2$. As mentioned in the introduction, for much of our analysis, we will work with the Laplace transform of (4.6),

$$\begin{aligned} \frac{d\sigma(\varepsilon, \nu, s, a)}{d\varepsilon d\hat{n}_1} &= \int_0^\infty d\bar{\varepsilon} e^{-\nu\bar{\varepsilon}} \frac{d\bar{\sigma}(\varepsilon, \bar{\varepsilon}, s, a)}{d\varepsilon d\bar{\varepsilon} d\hat{n}_1} \\ &= \frac{1}{2s} \sum_N |M(N)|^2 e^{-\nu\bar{f}(N, a)} (2\pi)^4 \delta^4(p_I - p_N) \\ &\quad \times \delta(\varepsilon - f(N)) \delta^2(\hat{n}_1 - \hat{n}(N)). \end{aligned} \quad (4.7)$$

Singularities of the form $(1/\bar{\varepsilon}) \ln^n(1/\bar{\varepsilon})$ in the cross section (4.6) give rise to logarithms $\ln^{n+1} \nu$ in the transform (4.7).

Since we are investigating energy flow in two-jet cross sections, we fix the

constants ε and $\bar{\varepsilon}$ to be both much less than unity:

$$0 < \varepsilon, \bar{\varepsilon} \ll 1. \quad (4.8)$$

We refer to this as the elastic limit for the two jets. In the elastic limit, the dependence of the directions of the jet axes on soft radiation is weak. We will return to this dependence below. Independent of soft radiation, we can always choose our coordinate system such that the transverse momentum of jet 1 is zero,

$$p_{J_1, \perp} = 0, \quad (4.9)$$

with \vec{p}_{J_1} in the x_3 direction. In the limit $\bar{\varepsilon}, \varepsilon \rightarrow 0$, and in the overall c.m., p_{J_1} and p_{J_2} then approach light-like vectors in the plus and minus directions:

$$\begin{aligned} p_{J_1}^\mu &\rightarrow \left(\sqrt{\frac{s}{2}}, 0^-, 0_\perp \right) \\ p_{J_2}^\mu &\rightarrow \left(0^+, \sqrt{\frac{s}{2}}, 0_\perp \right). \end{aligned} \quad (4.10)$$

As usual, it is convenient to work in light-cone coordinates, $p^\mu = (p^+, p^-, p_\perp)$, which we normalize as $p^\pm = (1/\sqrt{2})(p^0 \pm p^3)$. For small ε and $\bar{\varepsilon}$, the cross section (4.6) has corrections in $\ln(1/\varepsilon)$ and $\ln(1/\bar{\varepsilon})$, which we will organize in the following.

4.2.2 Weight functions and jet shapes

In Eq. (4.3), a is a parameter that allows us to study various event shapes within the same formalism; it helps to control the approach to the two-jet

limit. As noted above, $a < 2$ for infrared safety, although the factorization that we will discuss below applies beyond leading logarithm only to $1 > a > -\infty$. A similar weight function with a non-integer power has been discussed in a related context for $2 > a > 1$ in [73]. To see how the parameter a affects the shape of the jets, let us reexpress the weight function for jet 1 as

$$\bar{f}_{\bar{\Omega}_1}(N, a) = \frac{1}{\sqrt{s}} \sum_{\hat{n}_i \in \bar{\Omega}_1} \omega_i \sin^a \theta_i (1 - \cos \theta_i)^{1-a}, \quad (4.11)$$

where θ_i is the angle of the momentum of final state particle i with respect to jet axis \hat{n}_1 . As $a \rightarrow 2$ the weight vanishes only very slowly for $\theta_i \rightarrow 0$, and at fixed $\bar{f}_{\bar{\Omega}_1}$, the jet becomes very narrow. On the other hand, as $a \rightarrow -\infty$, the event shape vanishes more and more rapidly in the forward direction, and the cross section at fixed $\bar{f}_{\bar{\Omega}_1}$ becomes more and more inclusive in the radiation into $\bar{\Omega}_1$.

In this paper, as in Ref. [66], we seek to control corrections in the single-logarithmic variable $\alpha_s(Q) \ln(1/\varepsilon)$, with $\varepsilon = Q_\Omega/Q$. Such a resummation is most relevant when

$$\alpha_s(Q) \ln \left(\frac{1}{\varepsilon} \right) \geq 1 \rightarrow \varepsilon \leq \exp \left(\frac{-1}{\alpha_s(Q)} \right). \quad (4.12)$$

Let us compare these logarithms to non-global effects in shape/flow correlations. At $\nu = 0$ and for $a \rightarrow -\infty$, the cross section becomes inclusive outside Ω . As we show below, the non-global logarithms discussed in Refs. [66, 68] appear in shape/flow correlations as logarithms of the form $\alpha_s(Q) \ln(1/(\varepsilon\nu))$, with ν the moment variable conjugate to the event shape. To treat these

logarithms as subleading for small ε and (relatively) large ν , we require that

$$\alpha_s(Q) \ln \left(\frac{1}{\varepsilon\nu} \right) < 1 \rightarrow \varepsilon > \frac{1}{\nu} \exp \left(\frac{-1}{\alpha_s(Q)} \right). \quad (4.13)$$

For large ν , there is a substantial range of ε in which both (4.12) and (4.13) can hold. When ν is large, moments of the correlation are dominated precisely by events with strongly two-jet energy flows, which is the natural set of events in which to study the influence of color flow on interjet radiation. (The peak of the thrust cross section is at $(1 - T)$ of order one-tenth at LEP energies, corresponding to ν of order ten, so the requirement of large ν is not overly restrictive.) In the next subsection, we show how the logarithms of $(\varepsilon\nu)^{-1}$ emerge in a low order example. This analysis also assumes that a is not large in absolute value. The event shape at fixed angle decreases exponentially with a , and we shall see that higher-order corrections can be proportional to a . We always treat $\ln \nu$ as much larger than $|a|$.

4.2.3 Low order example

In this section, we check the general ideas developed above with the concrete example of a two-loop cross section for the process (4.2). This is the lowest order in which a non-global logarithm occurs, as observed in [68]. We normalize this cross section to the Born cross section for inclusive dijet production. A similar analysis for the same geometry has been carried out in [68] and [74].

The kinematic configuration we consider is shown in Fig. 4.2. Two fast partons, of velocities $\vec{\beta}_1$ and $\vec{\beta}_2$, are treated in eikonal approximation. In addition, gluons are emitted into the final state. A soft gluon with momentum

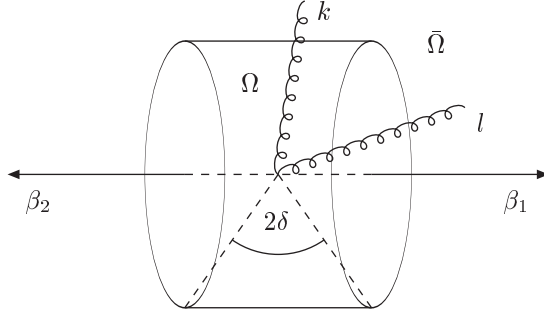


Figure 4.2: A kinematic configuration that gives rise to the non-global logarithms. A soft gluon with momentum k is radiated into the region Ω , and an energetic gluon with momentum l is radiated into $\bar{\Omega}$. Four-vectors β_1 and β_2 , define the directions of jet 1 and jet 2, respectively.

k is radiated into region Ω and an energetic gluon with momentum l is emitted into the region $\bar{\Omega}$. We consider the cross section at fixed energy, $\omega_k \equiv \varepsilon\sqrt{s}$. As indicated above, non-global logarithms arise from strong ordering of the energies of the gluons, which we choose as $\omega_l \gg \omega_k$. In this region, the gluon l plays the role of a “primary” emission, while k is a “secondary” emission.

For our calculation, we take the angular region Ω to be a “slice” or “ring” in polar angle of width 2δ , or equivalently, (pseudo) rapidity interval $(-\eta, \eta)$, with

$$\Delta\eta = 2\eta = \ln\left(\frac{1 + \sin\delta}{1 - \sin\delta}\right), \quad (4.14)$$

The lowest-order diagrams for this process are those shown in Fig. 4.3, including distinguishable diagrams in which the momenta k and l are interchanged.

The diagrams of Fig. 4.3 give rise to color structures C_F^2 and $C_F C_A$, but terms proportional to C_F^2 may be associated with a factorized contribution to the cross section, in which the gluon k is emitted coherently by the combina-

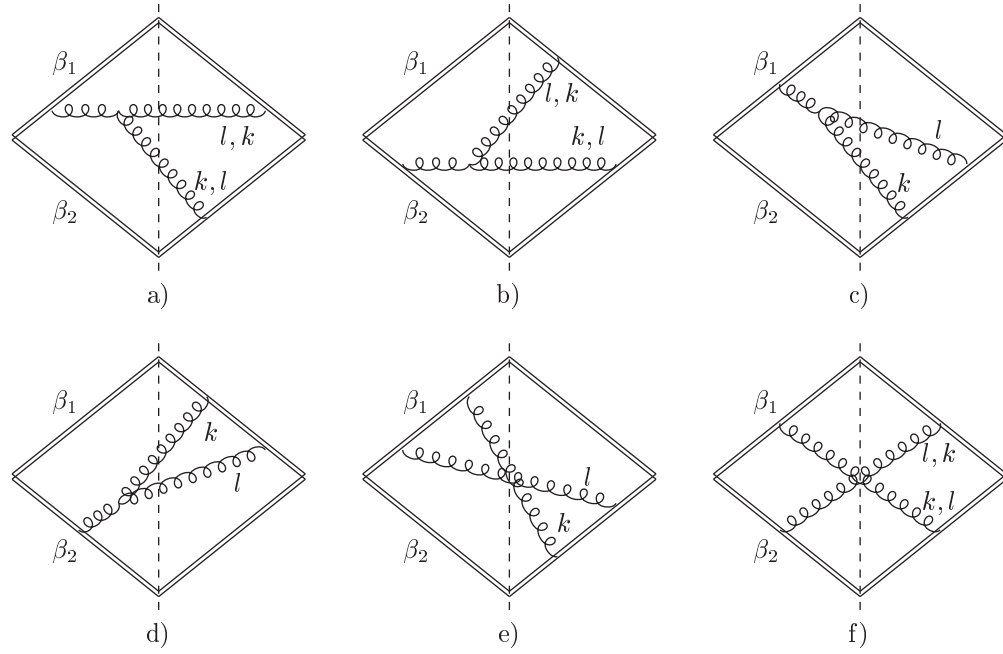


Figure 4.3: The relevant two-loop cut diagrams corresponding to the emission of two real gluons in the final state contributing to the eikonal cross section. The dashed line represents the final state, with contributions to the amplitude to the left, and to the complex conjugate amplitude to the right.

tions of the gluon l and the eikonals. To generate the $C_F C_A$ part, on the other hand, gluon k must “resolve” gluon l from the eikonal lines, giving a result that depends on the angles between \vec{l} and the eikonal directions.

The computation of the diagrams is outlined in Appendix C.1; here we quote the results. We adopt the notation $c_l \equiv \cos \theta_l$, $s_l \equiv \sin \theta_l$, with θ_l the angle of momentum \vec{l} measured relative to $\vec{\beta}_1$, and similarly for k . We take, as indicated above, a Laplace transform with respect to the shape variable, and identify the logarithm in the conjugate variable ν . We find that the logarithmic $C_F C_A$ -dependence of Fig. 4.3 may be written as a dimensionless eikonal cross section in terms of one energy and two polar angular integrals as

$$\begin{aligned} \frac{d\sigma_{\text{eik}}}{d\varepsilon} &= C_F C_A \left(\frac{\alpha_s}{\pi}\right)^2 \frac{1}{\varepsilon} \int_{-\sin \delta}^{\sin \delta} dc_k \int_{\sin \delta}^1 dc_l \int_{\varepsilon\sqrt{s}}^{\sqrt{s}} \frac{d\omega_l}{\omega_l} e^{-\nu \omega_l (1-c_l)^{1-a} s_l^a / Q} \\ &\times \left[\frac{1}{c_k + c_l} \frac{1}{1 + c_k} \left(\frac{1}{1 + c_l} + \frac{1}{1 - c_k} \right) - \frac{1}{s_k^2} \frac{1}{1 + c_l} \right]. \end{aligned} \quad (4.15)$$

In this form, the absence of collinear singularities in the $C_F C_A$ term at $\cos \theta_l = +1$ is manifest, independent of ν . Collinear singularities in the l integral completely factorize from the k integral, and are proportional to C_F^2 . The logarithmic dependence on ε for $\nu > 1$ is readily found to be

$$\frac{d\sigma_{\text{eik}}}{d\varepsilon} = C_F C_A \left(\frac{\alpha_s}{\pi}\right)^2 \frac{1}{\varepsilon} \ln \left(\frac{1}{\varepsilon\nu} \right) C(\Delta\eta), \quad (4.16)$$

where $C(\Delta\eta)$ is a finite function of the angle δ , given explicitly in Appendix C.1.

We can contrast this result to what happens when $\nu = 0$, that is, for an inclusive, non-global cross section. In this case, recalling that $\varepsilon = Q_\Omega/Q$, we

find in place of Eq. (4.16) the non-global logarithm

$$\frac{d\sigma_{\text{eik}}}{d\varepsilon} = C_F C_A \left(\frac{\alpha_s}{\pi}\right)^2 \frac{1}{\varepsilon} \ln\left(\frac{Q}{Q_\Omega}\right) C(\Delta\eta). \quad (4.17)$$

As anticipated, the effect of the transform is to replace the non-global logarithm in Q/Q_Ω , by a logarithm of $1/(\varepsilon\nu)$. We are now ready to generalize this result, starting from the factorization properties of the cross section near the two-jet limit.

4.3 Factorization of the Cross Section

In this section we study the factorization of the correlations (4.6). The analysis is based on a general approach that begins with the all-orders treatment of singularities in perturbative cross sections [75, 76], and derives factorization from the analyticity and gauge properties of high energy Green functions and cross sections [8]. The functions that appear in factorized cross sections are expressible in terms of QCD matrix elements [77], and the matrix elements that we will encounter are familiar from related analyses for heavy quark and jet production [78]. We refer in several places below to standard arguments discussed in more detail in [76, 8]. The aim of this section, and the reason why a careful analysis is necessary, is to identify the specific dimensionless combinations of kinematic variables on which the factorized matrix elements may depend. We will use these dependences in the following section, when we discuss the resummation properties of our correlations.

4.3.1 Leading regions near the two-jet limit

In order to resum logarithms of ε and $\bar{\varepsilon}$ (or equivalently ν , the Laplace conjugate of $\bar{\varepsilon}$) we have first to identify their origin in momentum space when $\varepsilon, \bar{\varepsilon} \rightarrow 0$. Following the procedure and terminology of [75], we identify “leading regions” in the momentum integrals of cut diagrams, which can give rise to logarithmic enhancements of the cross section associated with lines approaching the mass shell. Within these regions, the lines of a cut diagram fall into the following subdiagrams:

- A hard-scattering, or “short-distance” subdiagram H , where all components of line momenta are far off-shell, by order Q .
- Jet subdiagrams, J_1 and J_2 , where energies are fixed and momenta are collinear to the outgoing primary partons and the jet directions that emerge from the hard scattering. (For $\varepsilon = \bar{\varepsilon} = 0$, the sum of all energies in each jet is one-half the total energy.) To characterize the momenta of the lines within the jets, we introduce a scaling variable, $\lambda \ll 1$. Within jet 1, momenta ℓ scale as $(\ell^+ \sim Q, \ell^- \sim \lambda Q, \ell_\perp \sim \lambda^{1/2} Q)$.
- A soft subdiagram, S connecting the jet functions J_1 and J_2 , in which the components of momenta k are small compared to Q in all components, scaling as $(k^\pm \sim \lambda Q, k_\perp \sim \lambda Q)$.

An arbitrary final state N is the union of substates associated with these subdiagrams:

$$N = N_s \oplus N_{J_1} \oplus N_{J_2}. \quad (4.18)$$

As a result, the event shape \bar{f} can also be written as a sum of contributions from the soft and jet subdiagrams:

$$\bar{f}(N, a) = \bar{f}^N(N_s, a) + \bar{f}_{\Omega_1}^N(N_{J_1}, a) + \bar{f}_{\Omega_2}^N(N_{J_2}, a). \quad (4.19)$$

The superscript N reminds us that the contributions of final-state particles associated with the soft and jet functions depend implicitly on the full final state, through the determination of the jet axes, as discussed in Sec. 2. In contrast, the energy flow weight, $f(N)$, depends only on particles emitted at wide angles, and is hence insensitive to collinear radiation:

$$f(N) = f(N_s). \quad (4.20)$$

When we sum over all diagrams that have a fixed final state, the contributions from these leading regions may be factorized into a set of functions, each of which corresponds to one of the generic hard, soft and jet subdiagrams. The arguments for this factorization at leading power have been discussed extensively [72, 8, 79]. The cross section becomes a convolution in $\bar{\epsilon}$, with the sums over states linked by the delta function which fixes \hat{n}_1 , and by momentum

conservation,

$$\begin{aligned}
\frac{d\bar{\sigma}(\varepsilon, \bar{\varepsilon}, s, a)}{d\varepsilon d\bar{\varepsilon} d\hat{n}_1} &= \frac{d\sigma_0}{d\hat{n}_1} H(s, \hat{n}_1) \sum_{N_s, N_{J_c}} \int d\bar{\varepsilon}_s \mathcal{S}(N_s) \delta(\varepsilon - f(N_s)) \\
&\quad \times \delta(\bar{\varepsilon}_s - \bar{f}^N(N_s, a)) \\
&\quad \times \prod_{c=1}^2 \int d\bar{\varepsilon}_{J_c} \mathcal{J}_c(N_{J_c}) \delta(\bar{\varepsilon}_{J_c} - \bar{f}_{\Omega_c}^N(N_{J_c}, a)) \\
&\quad \times (2\pi)^4 \delta^4(p_I - p(N_{J_2}) - p(N_{J_1}) - p(N_s)) \\
&\quad \times \delta^2(\hat{n}_1 - \hat{n}(N)) \delta(\bar{\varepsilon} - \bar{\varepsilon}_{J_1} - \bar{\varepsilon}_{J_2} - \bar{\varepsilon}_s) \\
&= \frac{d\sigma_0}{d\hat{n}_1} \delta(\varepsilon) \delta(\bar{\varepsilon}) + \mathcal{O}(\alpha_s). \tag{4.21}
\end{aligned}$$

Here $d\sigma_0/d\hat{n}_1$ is the Born cross section for the production of a single particle (quark or antiquark) in direction \hat{n}_1 , while the short-distance function $H(s, \hat{n}_1) = 1 + \mathcal{O}(\alpha_s)$, which describes corrections to the hard scattering, is an expansion in α_s with finite coefficients. The functions $\mathcal{J}_c(N_{J_c})$, $\mathcal{S}(N_s)$ describe the internal dynamics of the jets and wide-angle soft radiation, respectively. We will specify these functions below. We have suppressed their dependence on a factorization scale. Radiation at wide angles from the jets will be well-described by our soft functions $\mathcal{S}(N_s)$, while we will construct the jet functions $\mathcal{J}_c(N_{J_c})$ to be independent of ε , as in Eq. (4.21).

So far, we have specified our sums over states in Eq. (4.21) only when all lines in N_s are soft, and all lines in N_{J_c} have momenta that are collinear, or nearly collinear to p_{J_c} . As ε and $\bar{\varepsilon}$ vanish, these are the only final-state momenta that are kinematically possible. Were we to restrict ourselves to these configurations only, however, it would not be straightforward to make the individual sums over N_s and N_{J_c} infrared safe. Thus, it is necessary

to include soft partons in N_s that are emitted near the jet directions, and soft partons in the N_{J_c} at wide angles. We will show below how to define the functions $\mathcal{J}_c(N_{J_c})$, $\mathcal{S}(N_s)$ so that they generate factoring, infrared safe functions that avoid double counting. We know on the basis of the arguments of Refs. [72,8,79] that corrections to the factorization of soft from jet functions are suppressed by powers of the weight functions ε and/or $\bar{\varepsilon}$.

4.3.2 The factorization in convolution form

Although formally factorized, the jet and soft functions in Eq. (4.21) are still linked in a potentially complicated way through their dependence on the jet axes. Our strategy is to simplify this complex dependence to a simple convolution in contributions to $\bar{\varepsilon}$, accurate to leading power in ε and $\bar{\varepsilon}$.

First, we note that the cross section of Eq. (4.21) is singular for vanishing ε and $\bar{\varepsilon}$, but is a smooth function of s and \hat{n}_1 . We may therefore make any approximation that changes s and/or \hat{n}_1 by an amount that vanishes as a power of ε and $\bar{\varepsilon}$ in the leading regions.

Correspondingly, the amplitudes for jet c are singular in $\bar{\varepsilon}_{J_c}$, but depend smoothly on the jet energy and direction, while the soft function is singular in both ε and $\bar{\varepsilon}_s$, but depends smoothly on the jet directions. As a result, at fixed values of ε and $\bar{\varepsilon}$ we may approximate the jet directions and energies by their values at $\varepsilon = \bar{\varepsilon} = 0$ in the soft and jet functions.

Finally, we may make any approximation that affects the value of ε and/or $\bar{\varepsilon}_{J_c}$ by amounts that vanish faster than linearly for $\bar{\varepsilon} \rightarrow 0$. It is at this stage that we will require that $a < 1$.

With these observations in mind, we enumerate the replacements and approximations by which we reduce Eq. (4.21), while retaining leading-power accuracy.

1. To simplify the definitions of the jets in Eq. (4.21), we make the replacements $\bar{f}_{\bar{\Omega}_c}^N(N_{J_c}, a) \rightarrow \bar{f}_c(N_{J_c}, a)$ with

$$\bar{f}_c(N_{J_c}, a) \equiv \frac{1}{\sqrt{s}} \sum_{\text{all } \hat{n}_i \in N_{J_c}} k_{i,\perp}^a \omega_i^{1-a} (1 - \hat{n}_i \cdot \hat{n}_c)^{1-a} . \quad (4.22)$$

The jet weight function $\bar{f}_c(N_{J_c}, a)$ now depends only on particles associated with N_{J_c} . The contribution to $\bar{f}_c(N_{J_c}, a)$ from particles within region $\bar{\Omega}_c$, is exactly the same here as in the weight (4.3), but we now include particles in all other directions. In this way, the independent sums over final states of the jet amplitudes will be naturally infrared safe. The value of $\bar{f}_c(N_{J_c}, a)$ differs from the value of $\bar{f}_{\bar{\Omega}_c}^N(N_{J_c}, a)$, however, due to radiation outside $\bar{\Omega}_c$, as indicated by the new subscript. This radiation is hence at wide angles to the jet axis. In the elastic limit (4.8), it is also constrained to be soft. Double counting in contributions to the total event shape, $\bar{f}(N, a)$, will be avoided by an appropriate definition of the soft function below. The sums over states are still not yet fully independent, however, because the jet directions \hat{n}_c still depend on the full final state N .

2. Next, we turn our attention to the condition that fixes the jet direction \hat{n}_1 . Up to corrections in the orientation of \hat{n}_1 that vanish as powers of ε

and $\bar{\varepsilon}$, we may neglect the dependence of \hat{n}_1 on N_s and N_{J_2} :

$$\delta(\hat{n}_1 - \hat{n}(N)) \rightarrow \delta(\hat{n}_1 - \hat{n}(N_{J_1})). \quad (4.23)$$

In Appendix C.2, we show that this replacement also leaves the value of $\bar{\varepsilon}$ unchanged, up to corrections that vanish as $\bar{\varepsilon}^{2-a}$. Thus, for $a < 1$, (4.23) is acceptable to leading power. For $a < 1$, we can therefore identify the direction of jet 1 with \hat{n}_1 . These approximations simplify Eq. (4.21) by eliminating the implicit dependence of the jet and soft weights on the full final state. We may now treat \hat{n}_1 as an independent vector.

3. In the leading regions, particles that make up each final-state jet are associated with states N_{J_c} , while N_s consists of soft particles only. In the momentum conservation delta function, we can neglect the four-momenta of lines in N_s , whose energies all vanish as $\varepsilon, \bar{\varepsilon} \rightarrow 0$:

$$\delta^4(p_I - p(N_{J_2}) - p(N_{J_1}) - p(N_s)) \rightarrow \delta^4(p_I - p_{J_2} - p_{J_1}). \quad (4.24)$$

4. Because the cross section is a smooth function of the jet energies and directions, we may also neglect the masses of the jets within the momentum conservation delta function, as in Eq. (4.10). In this approximation,

we derive in the c.m.,

$$\begin{aligned}
\delta^4(p_I - p_{J_2} - p_{J_1}) &\rightarrow \delta(\sqrt{s} - \omega(N_{J_1}) - \omega(N_{J_2})) \delta(|\vec{p}_{J_1}| - |\vec{p}_{J_2}|) \frac{1}{|\vec{p}_{J_1}|^2} \\
&\quad \times \delta^2(\hat{n}_1 + \hat{n}_2) \\
&\rightarrow \frac{2}{s} \delta\left(\frac{\sqrt{s}}{2} - \omega(N_{J_1})\right) \delta\left(\frac{\sqrt{s}}{2} - \omega(N_{J_2})\right) \\
&\quad \times \delta^2(\hat{n}_1 + \hat{n}_2). \tag{4.25}
\end{aligned}$$

Our jets are now back-to-back:

$$\hat{n}_2 \rightarrow -\hat{n}_1. \tag{4.26}$$

Implementing these replacements and approximations for $a < 1$, we rewrite the cross section Eq. (4.21) as

$$\begin{aligned}
\frac{d\bar{\sigma}(\varepsilon, \bar{\varepsilon}, s, a)}{d\varepsilon d\bar{\varepsilon} d\hat{n}_1} &= \frac{d\sigma_0}{d\hat{n}_1} H(s, \hat{n}_1, \mu) \int d\bar{\varepsilon}_s \bar{S}(\varepsilon, \bar{\varepsilon}_s, a, \mu) \\
&\quad \times \prod_{c=1}^2 \int d\bar{\varepsilon}_{J_c} \bar{J}_c(\bar{\varepsilon}_{J_c}, a, \mu) \delta(\bar{\varepsilon} - \bar{\varepsilon}_{J_1} - \bar{\varepsilon}_{J_2} - \bar{\varepsilon}_s), \tag{4.27}
\end{aligned}$$

with (as above) $H = 1 + \mathcal{O}(\alpha_s)$. Referring to the notation of Eqs. (4.21) and (4.22), the functions \bar{S} and \bar{J}_c are:

$$\bar{S}(\varepsilon, \bar{\varepsilon}_s, a, \mu) = \sum_{N_s} \mathcal{S}(N_s, \mu) \delta(\varepsilon - f(N_s)) \delta(\bar{\varepsilon}_s - \bar{f}(N_s, a)) \tag{4.28}$$

$$\begin{aligned}
\bar{J}_c(\bar{\varepsilon}_{J_c}, a, \mu) &= \frac{2}{s} (2\pi)^6 \sum_{N_{J_c}} \mathcal{J}_c(N_{J_c}, \mu) \delta(\bar{\varepsilon}_{J_c} - \bar{f}_c(N_{J_c}, a)) \delta\left(\frac{\sqrt{s}}{2} - \omega(N_{J_c})\right) \\
&\quad \times \delta^2(\hat{n}_1 \pm \hat{n}(N_{J_c})), \tag{4.29}
\end{aligned}$$

with the plus sign in the angular delta function for jet 2, and the minus for jet 1. The weight functions for the jets are given by Eq. (4.22) and induce dependence on the parameter a . We have introduced the factorization scale μ , which we set equal to the renormalization scale.

We note that we must construct the soft functions $\bar{S}(N_s, \mu)$ to cancel the contributions of final-state particles from each of the $\bar{J}_c(N_{J_c}, \mu)$ to the weight ε , as well as the contributions of the jet functions to $\bar{\varepsilon}$ from soft radiation outside their respective regions $\bar{\Omega}_c$. Similarly, the jet amplitudes must be constructed to include collinear enhancements only in their respective jet directions. Explicit constructions that satisfy these requirements will be specified in the following subsections.

To disentangle the convolution in (4.27), we take Laplace moments with respect to $\bar{\varepsilon}$:

$$\begin{aligned} \frac{d\sigma(\varepsilon, \nu, s, a)}{d\varepsilon d\hat{n}_1} &= \int_0^\infty d\bar{\varepsilon} e^{-\nu\bar{\varepsilon}} \frac{d\bar{\sigma}(\varepsilon, \bar{\varepsilon}, a)}{d\varepsilon d\bar{\varepsilon} d\hat{n}_1} \\ &= \frac{d\sigma_0}{d\hat{n}_1} H(s, \hat{n}_1, \mu) S(\varepsilon, \nu, a, \mu) \prod_{c=1}^2 J_c(\nu, a, \mu). \end{aligned} \quad (4.30)$$

Here and below unbarred quantities are the transforms in $\bar{\varepsilon}$, and barred quantities denote untransformed functions.

$$S(\varepsilon, \nu, a, \mu) = \int_0^\infty d\bar{\varepsilon}_s e^{-\nu\bar{\varepsilon}_s} \bar{S}(\varepsilon, \bar{\varepsilon}_s, a, \mu), \quad (4.31)$$

and similarly for the jet functions.

In the following subsections, we give explicit constructions for the functions participating in the factorization formula (4.27), which satisfy the requirement

of infrared safety, and avoid double counting. An illustration of the cross section factorized into these functions is shown in Fig. 4.4. As discussed above, non-global logarithms will emerge when $\varepsilon\nu$ becomes small enough.

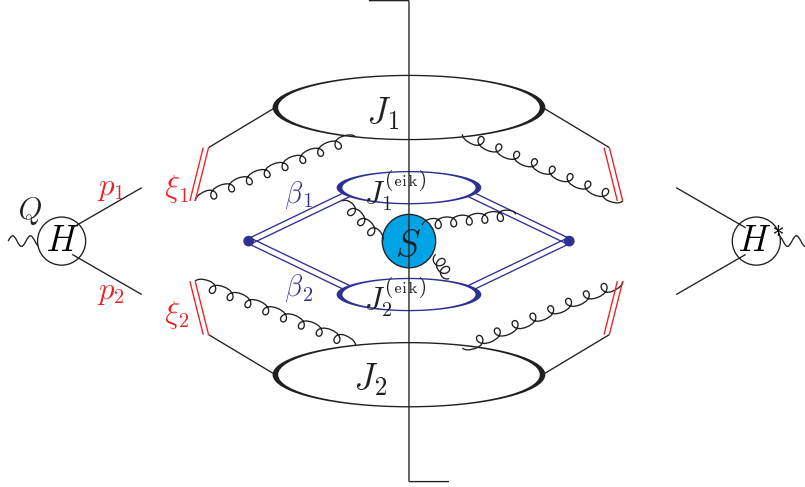


Figure 4.4: Factorized cross section (4.27) after the application of Ward identities. The vertical line denotes the final state cut.

4.3.3 The short-distance function

The power counting described in [75] shows that in Feynman gauge the subdiagrams of Fig. 4.4 that contribute to H in Eq. (4.27) at leading power in ε and $\bar{\varepsilon}$ are connected to each of the two jet subdiagrams by a single on-shell quark line, along with a possible set of on-shell, collinear gluon lines that carry scalar polarizations. The hard subdiagram is not connected directly to the soft subdiagram in any leading region.

The couplings of the scalar-polarized gluons that connect the jets with short-distance subdiagrams may be simplified with the help of Ward identities

(see, e. g. [8]). At each order of perturbation theory, the coupling of scalar-polarized gluons from either jet to the short-distance function is equivalent to their coupling to a path-ordered exponential of the gauge field, oriented in any direction that is not collinear to the jet. Corrections are infrared safe, and can be absorbed into the short-distance function. Let $h(p_{J_c}, \hat{n}_1, \mathcal{A})$ represent the set of all short-distance contributions to diagrams that couple any number of scalar-polarized gluons to the jets, in the amplitude for the production of any final state. The argument \mathcal{A} stands for the fields that create the scalar-polarized gluons linking the short-distance function to the jets. On a diagram-by-diagram basis, h depends on the momentum of each of the scalar-polarized gluons. After the sum over all diagrams, however, we can make the replacement:

$$h(p_{J_c}, \hat{n}_1, \mathcal{A}^{(q,\bar{q})}) \rightarrow \Phi_{\xi_2}^{(\bar{q})}(0, -\infty; 0) h_2(p_{J_c}, \hat{n}_1, \xi_c) \Phi_{\xi_1}^{(q)}(0, -\infty; 0), \quad (4.32)$$

where h_2 is a short-distance function that depends only on the total momenta p_{J_1} and p_{J_2} . It also depends on vectors ξ_c that characterize the path-ordered exponentials $\Phi(0, -\infty; 0)$:

$$\Phi_{\xi_c}^{(f)}(0, -\infty; 0) = P e^{-ig \int_{-\infty}^0 d\lambda \xi_c \cdot \mathcal{A}^{(f)}(\lambda \xi_c)}, \quad (4.33)$$

where the superscript (f) indicates that the vector potential takes values in representation f, in our case the representation of a quark or antiquark. These operators will be associated with gauge-invariant definitions of the jet functions below. To avoid spurious collinear singularities, we choose the vectors ξ_c ,

$c = 1, 2$, off the light cone. In the full cross section (4.30) the ξ_c -dependence cancels, of course.

The dimensionless short-distance function $H = |h_2|^2$ in Eq. (4.27) depends on \sqrt{s} and $p_{J_c} \cdot \xi_c$, but not on any variable that vanishes with ε and $\bar{\varepsilon}$:

$$H(p_{J_c}, \xi_c, \hat{n}_1, \mu) = H \left(\frac{\sqrt{s}}{\mu}, \frac{p_{J_c} \cdot \hat{\xi}_c}{\mu}, \hat{n}_1, \alpha_s(\mu) \right), \quad (4.34)$$

where

$$\hat{\xi}_c \equiv \xi_c / \sqrt{|\xi_c^2|}. \quad (4.35)$$

Here we have observed that each diagram is independent of the overall scale of the eikonal vector ξ_c^μ .

4.3.4 The jet functions

The jet functions and the soft functions in Eq. (4.27) can be defined in terms of specific matrix elements, which absorb the relevant contributions to leading regions in the cross section, and which are infrared safe. Their perturbative expansions specify the functions \mathcal{S} and \mathcal{J}_c of Eq. (4.29). We begin with our definition of the jet functions.

The jet functions, which absorb enhancements collinear to the two outgoing particles produced in the primary hard scattering, can be defined in terms of matrix elements in a manner reminiscent of parton distribution or decay

functions [77]. To be specific, we consider the quark jet function:

$$\begin{aligned}
\bar{J}_c^\mu(\bar{\varepsilon}_{J_c}, a, \mu) &= \frac{2}{s} \frac{(2\pi)^6}{\mathcal{N}_C} \sum_{N_{J_c}} \text{Tr} \left[\gamma^\mu \left\langle 0 \left| \Phi_{\xi_c}^{(q)\dagger}(0, -\infty; 0) q(0) \right| N_{J_c} \right\rangle \right. \\
&\quad \times \left. \left\langle N_{J_c} \left| \bar{q}(0) \Phi_{\xi_c}^{(q)}(0, -\infty; 0) \right| 0 \right\rangle \right] \\
&\quad \times \delta(\bar{\varepsilon}_{J_c} - \bar{f}_c(N_{J_c}, a)) \delta\left(\frac{\sqrt{s}}{2} - \omega(N_{J_c})\right) \\
&\quad \times \delta^2(\hat{n}_c - \hat{n}(N_{J_c})), \tag{4.36}
\end{aligned}$$

where \mathcal{N}_C is the number of colors, and where \hat{n}_c denotes the direction of the momentum of jet c , Eq. (4.29), with $\hat{n}_2 = -\hat{n}_1$. q is the quark field, $\Phi_{\xi_c}^{(q)}(0, -\infty; 0)$ a path-ordered exponential in the notation of (4.33), and the trace is taken over color and Dirac indices. We have chosen the normalization so that the jet functions \bar{J}^μ in (4.36) are dimensionless and begin at lowest order with

$$\bar{J}_c^{\mu(0)}(\bar{\varepsilon}_{J_c}, a, \mu) = \beta_c^\mu \delta(\bar{\varepsilon}_{J_c}), \tag{4.37}$$

with β_c^μ the lightlike velocities corresponding to the jet momenta in Eq. (4.10):

$$\beta_1^\mu = \delta_{\mu+}, \quad \beta_2^\mu = \delta_{\mu-}. \tag{4.38}$$

The scalar jet functions of Eq. (4.29) are now obtained by projecting out the component of J_c^μ in the jet direction:

$$\bar{J}_c(\bar{\varepsilon}_{J_c}, a, \mu) = \bar{\beta}_c \cdot \bar{J}'_c(\bar{\varepsilon}_{J_c}, a, \mu) = \delta(\bar{\varepsilon}_{J_c}) + \mathcal{O}(\alpha_s), \tag{4.39}$$

where $\bar{\beta}_1 = \beta_2$, $\bar{\beta}_2 = \beta_1$ are the lightlike vectors in the directions opposite to β_1 and β_2 , respectively. By construction, the \bar{J}_c are linear in $\bar{\beta}_c$.

To resum the jet functions in the variables $\bar{\varepsilon}_{J_c}$, it is convenient to reexpress the weight functions (4.22) in combinations of light-cone momentum components that are invariant under boosts in the x_3 direction,

$$\begin{aligned}\bar{f}_1(N_{J_1}, a) &= \frac{1}{s^{1-a/2}} \sum_{\hat{n}_i \in N_{J_1}} k_{i,\perp}^a (2p_{J_1}^+ k_i^-)^{1-a}, \\ \bar{f}_2(N_{J_2}, a) &= \frac{1}{s^{1-a/2}} \sum_{\hat{n}_i \in N_{J_2}} k_{i,\perp}^a (2p_{J_2}^- k_i^+)^{1-a}.\end{aligned}\quad (4.40)$$

Here we have used the relation $\sqrt{s}/2 = \omega_{J_c}$, valid for both jets in the c.m. At the same time, we make the identification,

$$\frac{1}{s} \delta\left(\frac{\sqrt{s}}{2} - \omega(N_{J_c})\right) \delta^2(\hat{n}_c - \hat{n}(N_{J_c})) = \frac{1}{4} \delta^3(\vec{p}_{J_c} - \vec{p}(N_{J_c})), \quad (4.41)$$

which again holds in the c.m. frame. The spatial components of each p_{J_c} are thus fixed. Given that we are at small $\bar{\varepsilon}_{J_c}$, the jet functions may be thought of as functions of the light-like jet momenta $p_{J_c}^\mu$ of Eq. (4.10) and of $\bar{\varepsilon}_{J_c}$. Because the vector jet function is constructed to be dimensionless, \bar{J}_c^μ in Eq. (4.36) is proportional to β_c rather than p_{J_c} . Otherwise, it is free of explicit β_c -dependence.

The jet functions can now be written in terms of boost-invariant arguments,

homogeneous of degree zero in ξ_c :

$$\begin{aligned} \bar{J}_c(\bar{\varepsilon}_{J_c}, a, \mu) = & \bar{\beta}_{c\mu} \left[\beta_c^\mu \bar{J}_c^{(1)} \left(\frac{p_{J_c} \cdot \hat{\xi}_c}{\mu}, \bar{\varepsilon}_{J_c} \frac{\sqrt{s}}{\mu} \left(\frac{\sqrt{s}}{2p_{J_c} \cdot \hat{\xi}_c} \right)^{1-a}, a, \alpha_s(\mu) \right) \right. \\ & \left. + \frac{2\xi_c^\mu \beta_c \cdot \xi_c}{|\xi_c|^2} \bar{J}_c^{(2)} \left(\frac{p_{J_c} \cdot \hat{\xi}_c}{\mu}, \bar{\varepsilon}_{J_c} \frac{\sqrt{s}}{\mu} \left(\frac{\sqrt{s}}{2p_{J_c} \cdot \hat{\xi}_c} \right)^{1-a}, a, \alpha_s(\mu) \right) \right], \end{aligned} \quad (4.42)$$

where $\bar{J}^{(1)}$ and $\bar{J}^{(2)}$ are independent functions, and where we have suppressed possible dependence on $\hat{\xi}_{c,\perp}$. For jet c , the weight $\bar{\varepsilon}_{J_c}$ is fixed by $\delta(\bar{\varepsilon}_{J_c} - \bar{f}_c(N_{J_c}, a))$, where on the right-hand side of the expression for the weight (4.40), the sum over each particle's momentum involves the overall factor $(2p_{J_c}^\pm/\sqrt{s})^{1-a}$. After integration over final states at fixed $\bar{\varepsilon}_{J_c}$, the jet can thus depend on the vector $p_{J_c}^\mu$. At the same time, it is easy to see from the definition of the weight that $p_{J_c}^\mu$ can only appear in the combination $(1/\bar{\varepsilon}_{J_c}\sqrt{s})^{1/(1-a)} (2p_{J_c}^\mu/\sqrt{s})$. This vector can combine with ξ_c to form an invariant, and all ξ_c -dependence comes about in this way.

Expression (4.42) can be further simplified by noting that

$$2\bar{\beta}_c \cdot \xi_c \beta_c \cdot \xi_c = \xi_c^2 + \xi_{c,\perp}^2. \quad (4.43)$$

Choosing $\xi_{c,\perp} = 0$, we find a single combination,

$$\bar{J}_c(\bar{\varepsilon}_{J_c}, a, \mu) = \bar{J}_c \left(\frac{p_{J_c} \cdot \hat{\xi}_c}{\mu}, \bar{\varepsilon}_{J_c} \frac{\sqrt{s}}{\mu} (\zeta_c)^{1-a}, a, \alpha_s(\mu) \right), \quad (4.44)$$

where, in the notation of Eq. (4.42), $\bar{J}_c = \bar{J}_c^{(1)} + \bar{J}_c^{(2)}$, and we have defined

$$\zeta_c \equiv \frac{\sqrt{s}}{2p_{J_c} \cdot \hat{\xi}_c}. \quad (4.45)$$

In these terms, the Laplace moments of the jet function inherit dependence on the moment variable ν through

$$\begin{aligned} J_c(\nu, a, \mu) &= \int_0^\infty d\bar{\varepsilon}_{J_c} e^{-\nu \bar{\varepsilon}_{J_c}} \bar{J}_c(\bar{\varepsilon}_{J_c}, a, \mu) \\ &\equiv J_c\left(\frac{p_{J_c} \cdot \hat{\xi}_c}{\mu}, \frac{\sqrt{s}}{\mu\nu} (\zeta_c)^{1-a}, a, \alpha_s(\mu)\right), \end{aligned} \quad (4.46)$$

where the unbarred and barred quantities denote transformed and untransformed functions, respectively. We have constructed the jet functions to be independent of ε , since the radiation into Ω is at wide angles from the jet axes and can therefore be completely factored from the collinear radiation. This radiation at wide angles is contained in the soft function, which will be defined below in a manner that avoids double counting in the cross section.

4.3.5 The soft function

Given the definitions for the jet functions in the previous subsection, and the factorization (4.27), we may in principle calculate the soft function S order by order in perturbation theory. We can derive a more explicit definition of the soft function, however, by relating it to an eikonal analog of Eq. (4.27).

As reviewed in Refs. [66, 8], soft radiation at wide angles from the jets decouples from the collinear lines within the jet. As a result, to compute amplitudes for wide-angle radiation, the jets may be replaced by nonabelian

phases, or Wilson lines. We therefore construct a dimensionless quantity, $\sigma^{(\text{eik})}$, in which gluons are radiated by path-ordered exponentials Φ , which mimic the color flow of outgoing quarks,

$$\Phi_{\beta_c}^{(f)}(\infty, 0; x) = P e^{-ig \int_0^\infty d\lambda \beta_c \cdot \mathcal{A}^{(f)}(\lambda \beta_c + x)}, \quad (4.47)$$

with β_c a light-like velocity in either of the jet directions. For the two-jet cross section at measured ε and $\bar{\varepsilon}_{\text{eik}}$, we define

$$\begin{aligned} \bar{\sigma}^{(\text{eik})}(\varepsilon, \bar{\varepsilon}_{\text{eik}}, a, \mu) &\equiv \frac{1}{\mathcal{N}_C} \sum_{N_{\text{eik}}} \left\langle 0 \left| \Phi_{\beta_2}^{(\bar{q})\dagger}(\infty, 0; 0) \Phi_{\beta_1}^{(q)\dagger}(\infty, 0; 0) \right| N_{\text{eik}} \right\rangle \\ &\quad \times \left\langle N_{\text{eik}} \left| \Phi_{\beta_1}^{(q)}(\infty, 0; 0) \Phi_{\beta_2}^{(\bar{q})}(\infty, 0; 0) \right| 0 \right\rangle \\ &\quad \times \delta(\varepsilon - f(N_{\text{eik}})) \delta(\bar{\varepsilon}_{\text{eik}} - \bar{f}(N_{\text{eik}}, a)) \\ &= \delta(\varepsilon) \delta(\bar{\varepsilon}_{\text{eik}}) + \mathcal{O}(\alpha_s). \end{aligned} \quad (4.48)$$

The sum is over all final states N_{eik} in the eikonal cross section. The renormalization scale in this cross section, which will also serve as a factorization scale, is denoted μ . Here the event shape function $\bar{\varepsilon}_{\text{eik}}$ is defined by $\bar{f}(N_{\text{eik}}, a)$ as in Eqs. (4.3) and (4.4), distinguishing between the hemispheres around the jets. As usual, \mathcal{N}_C is the number of colors, and a trace over color is understood.

The eikonal cross section (4.48) models the soft radiation away from the jets, including the radiation into Ω , accurately. It also contains enhancements for configurations collinear to the jets, which, however, are already taken into account by the partonic jet functions in (4.27). Indeed, (4.48) does not reproduce the partonic cross section accurately for collinear radiation. It is also easy to verify at lowest order that even at fixed $\bar{\varepsilon}_{\text{eik}}$ the eikonal cross section (4.48)

is ultraviolet divergent in dimensional regularization, unless we also impose a cutoff on the energy of real gluon emission collinear to β_1 or β_2 .

The construction of the soft function S from $\bar{\sigma}^{(\text{eik})}$ is nevertheless possible because the eikonal cross section (4.48) factorizes in the same manner as the cross section itself, into eikonal jet functions and a soft function. The essential point [65] is that the soft function in the factorized eikonal cross section is the same as in the original cross section (4.27). The eikonal jets organize all collinear enhancements in (4.48), including the spurious ultraviolet divergences. These eikonal jet functions are defined analogously to their partonic counterparts, Eq. (4.36), but now with ordered exponentials replacing the quark fields,

$$\begin{aligned}
\bar{J}_c^{(\text{eik})}(\bar{\varepsilon}_c, a, \mu) &\equiv \frac{1}{\mathcal{N}_C} \sum_{N_c^{(\text{eik})}} \left\langle 0 \left| \Phi_{\xi_c}^{(f_c)\dagger}(0, -\infty; 0) \Phi_{\beta_c}^{(f_c)\dagger}(\infty, 0; 0) \right| N_c^{(\text{eik})} \right\rangle \\
&\quad \times \left\langle N_c^{(\text{eik})} \left| \Phi_{\beta_c}^{(f_c)}(\infty, 0; 0) \Phi_{\xi_c}^{(f_c)}(0, -\infty; 0) \right| 0 \right\rangle \\
&\quad \times \delta(\bar{\varepsilon}_c - \bar{f}_c(N_c^{(\text{eik})}, a)) \\
&= \delta(\bar{\varepsilon}_c) + \mathcal{O}(\alpha_s), \tag{4.49}
\end{aligned}$$

where f_c is a quark or antiquark, and where the trace over color is understood. The weight functions are given as above, by Eq. (4.22), with the sum over particles in all directions.

In terms of the eikonal jets, the eikonal cross section (4.48) factorizes as

$$\begin{aligned}
\bar{\sigma}^{(\text{eik})}(\varepsilon, \bar{\varepsilon}_{\text{eik}}, a, \mu) &\equiv \int d\bar{\varepsilon}_s \bar{S}(\varepsilon, \bar{\varepsilon}_s, a, \mu) \prod_{c=1}^2 \int d\bar{\varepsilon}_c \bar{J}_c^{(\text{eik})}(\bar{\varepsilon}_c, a, \mu) \\
&\quad \times \delta(\bar{\varepsilon}_{\text{eik}} - \bar{\varepsilon}_s - \bar{\varepsilon}_1 - \bar{\varepsilon}_2), \tag{4.50}
\end{aligned}$$

where we pick the factorization scale equal to the renormalization scale μ . As for the full cross section, the convolution in (4.50) is simplified by a Laplace transformation (4.46) with respect to $\bar{\varepsilon}_{\text{eik}}$, which allows us to solve for the soft function as

$$S(\varepsilon, \nu, a, \mu) = \frac{\sigma^{(\text{eik})}(\varepsilon, \nu, a, \mu)}{\prod_{c=1}^2 J_c^{(\text{eik})}(\nu, a, \mu)} = \delta(\varepsilon) + \mathcal{O}(\alpha_s). \quad (4.51)$$

In this ratio, collinear logarithms in ν and the unphysical ultraviolet divergences and their associated cutoff dependence cancel between the eikonal cross section and the eikonal jets, leaving a soft function that is entirely free of collinear enhancements. The soft function retains ν -dependence through soft emission, which is also restricted by the weight function ε . In addition, because soft radiation within the eikonal jets can be factored from its collinear radiation, just as in the partonic jets, all logarithms in ν associated with wide-angle radiation are identical between the partonic and eikonal jets, and factor from logarithmic corrections associated with collinear radiation in both cases. As a result, the inverse eikonal jet functions cancel contributions from the wide-angle soft radiation of the partonic jets in the transformed cross section (4.30).

Given the definition of the energy flow weight function f , Eq. (4.5), the soft function is not boost invariant. In addition, because it is free of collinear logs, it can have at most a single logarithm per loop. Its dependence on ε is therefore only through ratios of the dimensional quantities $\varepsilon\sqrt{s}$ with the renormalization (factorization) scale.

As in the case of the partonic jets, Eq. (4.46), we need to identify the variable through which ν appears in the soft function. We note that dependence on the velocity vectors β_c and the factorization vectors ξ_c must be scale invariant in each, since they arise only from eikonal lines and vertices. The eikonal jet functions cannot depend explicitly on the scale-less, lightlike eikonal velocities β_c , and $\sigma^{(\text{eik})}$ is independent of the ξ_c . Dependence on the factorization vectors ξ_c enters only through the weight functions, (4.40) for the eikonal jets, in a manner analogous to the case of the partonic jets. This results in a dependence on $(\zeta_c)^{1-a}$, as above, with ζ_c defined in Eq. (4.45). In summary, we may characterize the arguments of the soft function in transform space as

$$S(\varepsilon, \nu, a, \mu) = S\left(\frac{\varepsilon\sqrt{s}}{\mu}, \varepsilon\nu, \frac{\sqrt{s}}{\mu\nu} (\zeta_c)^{1-a}, a, \alpha_s(\mu)\right). \quad (4.52)$$

4.4 Resummation

We may summarize the results of the previous section by rewriting the transform of the factorized cross section (4.30) in terms of the hard, jet and soft functions identified above, which depend on the kinematic variables and the moment ν according to Eqs. (4.34), (4.46) and (4.52) respectively,

$$\begin{aligned} \frac{d\sigma(\varepsilon, \nu, s, a)}{d\varepsilon d\hat{n}_1} &= \frac{d\sigma_0}{d\hat{n}_1} H\left(\frac{\sqrt{s}}{\mu}, \frac{p_{J_c} \cdot \hat{\xi}_c}{\mu}, \hat{n}_1, \alpha_s(\mu)\right) \\ &\quad \times \prod_{c=1}^2 J_c\left(\frac{p_{J_c} \cdot \hat{\xi}_c}{\mu}, \frac{\sqrt{s}}{\mu\nu} (\zeta_c)^{1-a}, a, \alpha_s(\mu)\right) \\ &\quad \times S\left(\frac{\varepsilon\sqrt{s}}{\mu}, \varepsilon\nu, \frac{\sqrt{s}}{\mu\nu} (\zeta_c)^{1-a}, a, \alpha_s(\mu)\right). \end{aligned} \quad (4.53)$$

The natural scale for the strong coupling in the short-distance function H is $\sqrt{s}/2$. Setting $\mu = \sqrt{s}/2$, however, introduces large logarithms of ε in the soft function and large logarithms of ν in both the soft and jet functions. The purpose of this section is to control these logarithms by the identification and solution of renormalization group and evolution equations.

The information necessary to perform the resummations is already present in the factorization (4.53). The cross section itself is independent of the factorization scale

$$\mu \frac{d}{d\mu} \frac{d\sigma(\varepsilon, \nu, s, a)}{d\varepsilon d\hat{n}_1} = 0, \quad (4.54)$$

and of the choice of the eikonal directions, $\hat{\xi}_c$, used in the factorization,

$$\frac{\partial}{\partial \ln(p_{J_c} \cdot \hat{\xi}_c)} \frac{d\sigma(\varepsilon, \nu, s, a)}{d\varepsilon d\hat{n}_1} = 0. \quad (4.55)$$

The arguments of this section closely follow the analysis of Ref. [80]. We will see that the dependence of jet and soft functions on the parameter a that characterizes the event shapes (3) is reflected in the resummed correlations, so that the relationship between correlations with different values of a is both calculable and nontrivial.

4.4.1 Energy flow

As a first step, we use the renormalization group equation (4.54) to organize dependence on the energy flow variable ε . Applying Eq. (4.54) to the factorized correlation (4.53), we derive the following consistency conditions, which are

themselves renormalization group equations:

$$\mu \frac{d}{d\mu} \ln S \left(\frac{\varepsilon \sqrt{s}}{\mu}, \varepsilon \nu, \frac{\sqrt{s}}{\mu \nu} (\zeta_c)^{1-a}, a, \alpha_s(\mu) \right) = -\gamma_s(\alpha_s(\mu)), \quad (4.56)$$

$$\mu \frac{d}{d\mu} \ln J_c \left(\frac{p_{J_c} \cdot \hat{\xi}_c}{\mu}, \frac{\sqrt{s}}{\mu \nu} (\zeta_c)^{1-a}, a, \alpha_s(\mu) \right) = -\gamma_{J_c}(\alpha_s(\mu)), \quad (4.57)$$

$$\mu \frac{d}{d\mu} \ln H \left(\frac{\sqrt{s}}{\mu}, \frac{p_{J_c} \cdot \hat{\xi}_c}{\mu}, \hat{n}_1, \alpha_s(\mu) \right) = \gamma_s(\alpha_s(\mu)) + \sum_{c=1}^2 \gamma_{J_c}(\alpha_s(\mu)). \quad (4.58)$$

The anomalous dimensions γ_d , $d = s, J_c$ can depend only on variables held in common between at least two of the functions. Because each function is infrared safe, while ultraviolet divergences are present only in virtual diagrams, the anomalous dimensions cannot depend on the parameters ν , ε or a . This leaves as arguments of the γ_d only the coupling $\alpha_s(\mu)$, which we exhibit, and ζ_c , which we suppress for now.

Solving Eqs. (4.56) and (4.57) we find

$$S \left(\frac{\varepsilon \sqrt{s}}{\mu}, \varepsilon \nu, \frac{\sqrt{s}}{\mu \nu} (\zeta_c)^{1-a}, a, \alpha_s(\mu) \right) = S \left(\frac{\varepsilon \sqrt{s}}{\mu_0}, \varepsilon \nu, \frac{\sqrt{s}}{\mu_0 \nu} (\zeta_c)^{1-a}, a, \alpha_s(\mu_0) \right) \times e^{-\int_{\mu_0}^{\mu} \frac{d\lambda}{\lambda} \gamma_s(\alpha_s(\lambda))}, \quad (4.59)$$

$$J_c \left(\frac{p_{J_c} \cdot \hat{\xi}_c}{\mu}, \frac{\sqrt{s}}{\mu \nu} (\zeta_c)^{1-a}, a, \alpha_s(\mu) \right) = J_c \left(\frac{p_{J_c} \cdot \hat{\xi}_c}{\tilde{\mu}_0}, \frac{\sqrt{s}}{\tilde{\mu}_0 \nu} (\zeta_c)^{1-a}, a, \alpha_s(\tilde{\mu}_0) \right) \times e^{-\int_{\tilde{\mu}_0}^{\mu} \frac{d\lambda}{\lambda} \gamma_{J_c}(\alpha_s(\lambda))}, \quad (4.60)$$

for the soft and jet functions. As suggested above, we will eventually pick $\mu \sim \sqrt{s}$ to avoid large logs in H . Using these expressions in Eq. (4.53) we

can avoid logarithms of ε or ν in the soft function, by evolving from $\mu_0 = \varepsilon\sqrt{s}$ to the factorization scale $\mu \sim \sqrt{s}$. No choice of $\tilde{\mu}_0$, however, controls all logarithms of ν in the jet functions. Leaving $\tilde{\mu}_0$ free, we find for the cross section (4.53) the intermediate result

$$\begin{aligned} \frac{d\sigma(\varepsilon, \nu, s, a)}{d\varepsilon d\hat{n}_1} &= \frac{d\sigma_0}{d\hat{n}_1} H\left(\frac{\sqrt{s}}{\mu}, \frac{p_{J_c} \cdot \hat{\xi}_c}{\mu}, \hat{n}_1, \alpha_s(\mu)\right) \\ &\times S(1, \varepsilon\nu, (\zeta_c)^{1-a}, a, \alpha_s(\varepsilon\sqrt{s})) \exp\left\{-\int_{\varepsilon\sqrt{s}}^{\mu} \frac{d\lambda}{\lambda} \gamma_s(\alpha_s(\lambda))\right\} \\ &\times J_c\left(\frac{p_{J_c} \cdot \hat{\xi}_c}{\tilde{\mu}_0}, \frac{\sqrt{s}}{\tilde{\mu}_0\nu} (\zeta_c)^{1-a}, a, \alpha_s(\tilde{\mu}_0)\right) \exp\left\{-\int_{\tilde{\mu}_0}^{\mu} \frac{d\lambda}{\lambda} \gamma_{J_c}(\alpha_s(\lambda))\right\}. \end{aligned} \quad (4.61)$$

We have avoided introducing logarithms of ε into the jet functions, which originally only depend on ν , by evolving the soft and the jet functions independently. The choice of $\mu_0 = \varepsilon\sqrt{s}$ or \sqrt{s}/ν for the soft function is to some extent a matter of convenience, since the two choices differ by logarithms of $\varepsilon\nu$. In general, if we choose $\mu_0 = \sqrt{s}/\nu$, logarithms of $\varepsilon\nu$ will appear multiplied by coefficients that reflect the size of region Ω . An example is Eq. (4.15) above. When Ω has a small angular size, $\mu_0 = \sqrt{s}/\nu$ is generally the more natural choice, since then logarithms in $\varepsilon\nu$ will enter with small weights. In contrast, when Ω grows to cover most angular directions, as in the study of rapidity gaps [82], it is more natural to choose $\mu_0 = \varepsilon\sqrt{s}$.

4.4.2 Event shape transform

The remaining unorganized “large” logarithms in (4.61), are in the jet functions, which we will resum by using the consistency equation (4.55). The requirement that the cross section be independent of $p_{J_c} \cdot \hat{\xi}_c$ implies that the jet, soft and hard functions obey equations analogous to (4.56)–(4.58), again in terms of the variables that they hold in common [80]. The same results may be derived following the method of Collins and Soper [72], by defining the jets in an axial gauge, and then studying their variations under boosts.

For our purposes, only the equation satisfied by the jet functions [72, 80] is necessary,

$$\begin{aligned} \frac{\partial}{\partial \ln(p_{J_c} \cdot \hat{\xi}_c)} \ln J_c \left(\frac{p_{J_c} \cdot \hat{\xi}_c}{\mu}, \frac{\sqrt{s}}{\mu\nu} (\zeta_c)^{1-a}, a, \alpha_s(\mu) \right) \\ = K_c \left(\frac{\sqrt{s}}{\mu\nu} (\zeta_c)^{1-a}, a, \alpha_s(\mu) \right) + G_c \left(\frac{p_{J_c} \cdot \hat{\xi}_c}{\mu}, \alpha_s(\mu) \right) \end{aligned} \quad (4.62)$$

The functions K_c and G_c compensate the ξ_c -dependence of the soft and hard functions, respectively, which determines the kinematic variables upon which they may depend. In particular, notice the combination of ν - and ξ_c -dependence required by the arguments of the jet function, Eq. (4.46).

Since the definition of our jet functions (4.36) is gauge invariant, we can derive the kernels K_c and G_c by an explicit computation of $\partial J_c / \partial \ln(p_{J_c} \cdot \hat{\xi}_c)$ in any gauge. The multiplicative renormalizability of the jet function, Eq. (4.57), with an anomalous dimension that is independent of $p_{J_c} \cdot \hat{\xi}_c$ ensures that the right-hand side of Eq. (4.62) is a renormalization-group invariant.

Thus, $K_c + G_c$ are renormalized additively, and satisfy [72]

$$\begin{aligned}\mu \frac{d}{d\mu} K_c \left(\frac{\sqrt{s}}{\mu\nu} (\zeta_c)^{1-a}, a, \alpha_s(\mu) \right) &= -\gamma_{K_c}(\alpha_s(\mu)), \\ \mu \frac{d}{d\mu} G_c \left(\frac{p_{J_c} \cdot \hat{\xi}_c}{\mu}, \alpha_s(\mu) \right) &= \gamma_{K_c}(\alpha_s(\mu)).\end{aligned}\quad (4.63)$$

Since G_c and hence γ_{K_c} , may be computed from virtual diagrams, they do not depend on a , and γ_{K_c} is the universal Sudakov anomalous dimension [72, 83].

With the help of these evolution equations, the terms K_c and G_c in Eq. (4.62) can be reexpressed as [84]

$$\begin{aligned}& K_c \left(\frac{\sqrt{s}}{\mu\nu} (\zeta_c)^{1-a}, a, \alpha_s(\mu) \right) + G_c \left(\frac{p_{J_c} \cdot \hat{\xi}_c}{\mu}, \alpha_s(\mu) \right) \\ &= K_c \left(\frac{1}{c_1}, a, \alpha_s \left(c_1 \frac{\sqrt{s}}{\nu} (\zeta_c)^{1-a} \right) \right) + G_c \left(\frac{1}{c_2}, \alpha_s \left(c_2 p_{J_c} \cdot \hat{\xi}_c \right) \right) \\ &\quad - \int_{c_1 \sqrt{s} (\zeta_c)^{1-a} / \nu}^{c_2 p_{J_c} \cdot \hat{\xi}_c} \frac{d\lambda'}{\lambda'} \gamma_{K_c}(\alpha_s(\lambda')) \\ &= -B'_c \left(c_1, c_2, a, \alpha_s \left(c_2 p_{J_c} \cdot \hat{\xi}_c \right) \right) - 2 \int_{c_1 \sqrt{s} (\zeta_c)^{1-a} / \nu}^{c_2 p_{J_c} \cdot \hat{\xi}_c} \frac{d\lambda'}{\lambda'} A'_c(c_1, a, \alpha_s(\lambda')), \end{aligned}\quad (4.64)$$

where in the second equality we have shifted the argument of the running

coupling in K_c , and have introduced the notation

$$\begin{aligned}
B'_c(c_1, c_2, a, \alpha_s(\mu)) &\equiv -K_c\left(\frac{1}{c_1}, a, \alpha_s(\mu)\right) - G_c\left(\frac{1}{c_2}, \alpha_s(\mu)\right), \\
2A'_c(c_1, a, \alpha_s(\mu)) &\equiv \gamma_{K_c}(\alpha_s(\mu)) + \beta(g(\mu))\frac{\partial}{\partial g(\mu)}K_c\left(\frac{1}{c_1}, a, \alpha_s(\mu)\right).
\end{aligned}
\tag{4.65}$$

The primes on the functions A'_c and B'_c are to distinguish these anomalous dimensions from their somewhat more familiar versions given below.

The solution to Eq. (4.62) with $\mu = \tilde{\mu}_0$ is

$$\begin{aligned}
&J_c\left(\frac{p_{J_c} \cdot \hat{\xi}_c}{\tilde{\mu}_0}, \frac{\sqrt{s}}{\tilde{\mu}_0 \nu} (\zeta_c)^{1-a}, a, \alpha_s(\tilde{\mu}_0)\right) = J_c\left(\frac{\sqrt{s}}{2\zeta_0 \tilde{\mu}_0}, \frac{\sqrt{s}}{\tilde{\mu}_0 \nu} (\zeta_0)^{1-a}, a, \alpha_s(\tilde{\mu}_0)\right) \\
&\times \exp\left\{-\int_{\sqrt{s}/(2\zeta_0)}^{p_{J_c} \cdot \hat{\xi}_c} \frac{d\lambda}{\lambda} \left[B'_c(c_1, c_2, a, \alpha_s(c_2\lambda)) + 2 \int_{c_1 \frac{s^{1-a/2}}{\nu(2\lambda)^{1-a}}}^{c_2 \lambda} \frac{d\lambda'}{\lambda'} A'_c(c_1, a, \alpha_s(\lambda')) \right]\right\},
\end{aligned}
\tag{4.66}$$

where we evolve from $\sqrt{s}/(2\zeta_0)$ to $p_{J_c} \cdot \hat{\xi}_c = \sqrt{s}/(2\zeta_c)$ (see Eq. (4.45)) with

$$\zeta_0 = \left(\frac{\nu}{2}\right)^{1/(2-a)}. \tag{4.67}$$

After combining Eqs. (4.60) and (4.66), the choice $\tilde{\mu}_0 = \sqrt{s}/(2\zeta_0) = \frac{\sqrt{s}}{\nu}(\zeta_0)^{1-a}$

allows us to control all large logarithms in the jet functions simultaneously:

$$\begin{aligned}
& J_c \left(\frac{p_{J_c} \cdot \hat{\xi}_c}{\mu}, \frac{\sqrt{s}}{\mu\nu} (\zeta_c)^{1-a}, a, \alpha_s(\mu) \right) = J_c \left(1, 1, a, \alpha_s \left(\frac{\sqrt{s}}{2\zeta_0} \right) \right) \\
& \times \exp \left\{ - \int_{\sqrt{s}/(2\zeta_0)}^{\mu} \frac{d\lambda}{\lambda} \gamma_{J_c}(\alpha_s(\lambda)) \right\} \\
& \times \exp \left\{ - \int_{\sqrt{s}/(2\zeta_0)}^{p_{J_c} \cdot \hat{\xi}_c} \frac{d\lambda}{\lambda} \left[B'_c(c_1, c_2, a, \alpha_s(c_2\lambda)) + 2 \int_{c_1 \frac{s^{1-a/2}}{\nu(2\lambda)^{1-a}}}^{c_2\lambda} \frac{d\lambda'}{\lambda'} A'_c(c_1, a, \alpha_s(\lambda')) \right] \right\}.
\end{aligned} \tag{4.68}$$

As observed above, we treat a as a fixed parameter, with $|a|$ small compared to $\ln(1/\varepsilon)$ and $\ln\nu$.

4.4.3 The resummed correlation

Using Eq. (4.68) in (4.61), and setting $\mu = \sqrt{s}/2$, we find a fully resummed form for the correlation,

$$\begin{aligned}
\frac{d\sigma(\varepsilon, \nu, s, a)}{d\varepsilon d\hat{n}_1} &= \frac{d\sigma_0}{d\hat{n}_1} H\left(\frac{2p_{J_c} \cdot \hat{\xi}_c}{\sqrt{s}}, \hat{n}_1, \alpha_s\left(\frac{\sqrt{s}}{2}\right)\right) \\
&\times S\left(1, \varepsilon\nu, (\zeta_c)^{1-a}, a, \alpha_s(\varepsilon\sqrt{s})\right) \exp\left\{-\int_{\varepsilon\sqrt{s}}^{\sqrt{s}/2} \frac{d\lambda}{\lambda} \gamma_s(\alpha_s(\lambda))\right\} \\
&\times \prod_{c=1}^2 J_c\left(1, 1, a, \alpha_s\left(\frac{\sqrt{s}}{2\zeta_0}\right)\right) \exp\left\{-\int_{\sqrt{s}/(2\zeta_0)}^{\sqrt{s}/2} \frac{d\lambda}{\lambda} \gamma_{J_c}(\alpha_s(\lambda))\right\} \\
&\times \exp\left\{-\int_{\sqrt{s}/(2\zeta_0)}^{p_{J_c} \cdot \hat{\xi}_c} \frac{d\lambda}{\lambda} \left[B'_c(c_1, c_2, a, \alpha_s(c_2\lambda)) + 2 \int_{c_1 \frac{s^{1-a/2}}{\nu(2\lambda)^{1-a}}}^{c_2\lambda} \frac{d\lambda'}{\lambda'} A'_c(c_1, a, \alpha_s(\lambda')) \right]\right\}.
\end{aligned} \tag{4.69}$$

Alternatively, we can combine all jet-related exponents in Eq. (4.69) in the correlation. As we will verify below in Section 4.5.2, the cross section is independent of the choice of ξ_c . As a result, we can choose

$$p_{J_c} \cdot \hat{\xi}_c = \frac{\sqrt{s}}{2}. \tag{4.70}$$

This choice allows us to combine γ_{J_c} and B'_c in Eq. (4.69),

$$\begin{aligned}
\frac{d\sigma(\varepsilon, \nu, s, a)}{d\varepsilon d\hat{n}_1} &= \frac{d\sigma_0}{d\hat{n}_1} H\left(1, \hat{n}_1, \alpha_s\left(\frac{\sqrt{s}}{2}\right)\right) \\
&\times S(1, \varepsilon\nu, 1, a, \alpha_s(\varepsilon\sqrt{s})) \exp\left\{-\int_{\varepsilon\sqrt{s}}^{\sqrt{s}/2} \frac{d\lambda}{\lambda} \gamma_s(\alpha_s(\lambda))\right\} \prod_{c=1}^2 J_c\left(1, 1, a, \alpha_s\left(\frac{\sqrt{s}}{2\zeta_0}\right)\right) \\
&\times \exp\left\{-\int_{\sqrt{s}/(2\zeta_0)}^{\sqrt{s}/2} \frac{d\lambda}{\lambda} [\gamma_{J_c}(\alpha_s(\lambda)) + B'_c(c_1, c_2, a, \alpha_s(c_2\lambda))\right. \\
&\quad \left.+ 2 \int_{c_1 \frac{s^{1-a/2}}{\nu(2\lambda)^{1-a}}}^{c_2\lambda} \frac{d\lambda'}{\lambda'} A'_c(c_1, a, \alpha_s(\lambda'))]\right\}, \tag{4.71}
\end{aligned}$$

with ζ_0 given by Eq. (4.67).

In Eqs. (4.69) and (4.71), the energy flow ε appears at the level of one logarithm per loop, in S , in the first exponent. Leading logarithms of ε are therefore resummed by knowledge of $\gamma_s^{(1)}$, the one-loop soft anomalous dimension, where we employ the standard notation,

$$\gamma_s(\alpha_s) = \sum_{n=0}^{\infty} \gamma_s^{(n)} \left(\frac{\alpha_s}{\pi}\right)^n \tag{4.72}$$

for any expansion in α_s . At the same time, ν appears in up to two logarithms per loop, characteristic of conventional Sudakov resummation. To control ν -dependence at the same level as ε -dependence, it is natural to work to next-to-leading logarithm in ν , by which we mean the level $\alpha_s^k \ln^k \nu$ in the exponent. As usual, this requires one loop in B'_c and γ_{J_c} , and two loops in the Sudakov

anomalous dimension A'_c , Eq. (4.65). These functions are straightforward to calculate from their definitions given in the previous sections. Only the soft function S in Eqs. (4.69) and (4.71) contains information on the geometry of Ω . The exponents are partially process-dependent, but geometry-independent. In Section 4.5, we will derive explicit expressions for these quantities, suitable for resummation to leading logarithm in ε and next-to-leading logarithm in ν .

4.4.4 The inclusive event shape

It is also of interest to consider the cross section for e^+e^- -annihilation into two jets without fixing the energy of radiation into Ω , but with the final state radiation into all of phase space weighted according to Eq. (4.4), schematically

$$e^+ + e^- \rightarrow J_1(p_{J_1}, \bar{f}_{\bar{\Omega}_1}) + J_2(p_{J_2}, \bar{f}_{\bar{\Omega}_2}), \quad (4.73)$$

where $\bar{\Omega}_1$ and $\bar{\Omega}_2$ cover the entire sphere. This cross section can be factorized and resummed in a completely analogous manner. The final state is a convolution in the contributions of the jet and soft functions to $\bar{\varepsilon}$ as in Eq. (4.27), but with no separate restriction on energy flow into Ω . All particles contribute to the event shape. We obtain an expression very analogous to Eq. (4.69) for this inclusive event shape in transform space, which can be written in terms of the same jet functions as before, and a new function S^{incl} for soft radiation

as:

$$\begin{aligned}
\frac{d\sigma^{\text{incl}}(\nu, s, a)}{d\hat{n}_1} &= \frac{d\sigma_0}{d\hat{n}_1} H\left(\frac{2p_{J_c} \cdot \hat{\xi}_c}{\sqrt{s}}, \hat{n}_1, \alpha_s(\sqrt{s}/2)\right) \\
&\times S^{\text{incl}}\left((\zeta_c)^{1-a}, a, \alpha_s\left(\frac{\sqrt{s}}{\nu}\right)\right) \exp\left\{-\int_{\sqrt{s}/\nu}^{\sqrt{s}/2} \frac{d\lambda}{\lambda} \gamma_s(\alpha_s(\lambda))\right\} \\
&\times \prod_{c=1}^2 J_c\left(1, 1, a, \alpha_s\left(\frac{\sqrt{s}}{2\zeta_0}\right)\right) \exp\left\{-\int_{\sqrt{s}/(2\zeta_0)}^{\sqrt{s}/2} \frac{d\lambda}{\lambda} \gamma_{J_c}(\alpha_s(\lambda))\right\} \\
&\times \exp\left\{-\int_{\sqrt{s}/(2\zeta_0)}^{p_{J_c} \cdot \hat{\xi}_c} \frac{d\lambda}{\lambda} \left[B'_c(c_1, c_2, a, \alpha_s(c_2\lambda)) + 2 \int_{c_1 \frac{s^{1-a/2}}{\nu(2\lambda)^{1-a}}}^{c_2\lambda} \frac{d\lambda'}{\lambda'} A'_c(c_1, a, \alpha_s(\lambda')) \right] \right\}.
\end{aligned} \tag{4.74}$$

Here the soft function $S^{\text{incl}} = 1 + \mathcal{O}(\alpha_s)$. The double-logarithmic dependence of the shape transform is identical to our resummed correlation, Eq. (4.69). We will show below, in Sec. 4.5.3, that Eq. (4.74) coincides at NLL with the known result for the thrust [57] when we choose $a = 0$.

4.5 Results at NLL

4.5.1 Lowest order functions and anomalous dimensions

In this section, we describe the low-order calculations and results that provide explicit expressions for the resummed shape/flow correlations and inclusive event shape distributions at next-to-leading logarithm in ν and leading logarithm in ε (we refer to this level collectively as NLL below). We go on to

verify that for the case $a = 0$ we rederive the known result for the resummed thrust at NLL, and we exhibit the expressions for the correlation that we will evaluate in Sec. 4.6.

The soft function

The one-loop soft anomalous dimension is readily calculated in Feynman gauge from the combination of virtual diagrams in $\sigma^{(\text{eik})}$, Eq. (4.48), and $J^{(\text{eik})}$, Eq. (4.49), in Eq. (4.51). The calculation and the result are equivalent to those of Ref. [65], where the soft function was formulated in axial gauge,

$$\gamma_s^{(1)} = -2 C_F \left[\sum_{c=1}^2 \ln \left(\beta_c \cdot \hat{\xi}_c \right) - \ln \left(\frac{\beta_1 \cdot \beta_2}{2} \right) - 1 \right]. \quad (4.75)$$

The first, ξ_c -dependent logarithmic term is associated with the eikonal jets, while the second is a finite remainder from the combination of $\sigma^{(\text{eik})}$ and $J^{(\text{eik})}$ in (4.51). Whenever $\xi_{c,\perp} = 0$, the logarithmic terms cancel identically, leaving only the final term, which comes from the $\hat{\xi}_c$ eikonal self-energy diagrams in the eikonal jet functions.

The soft function is normalized to $S^{(0)}(\varepsilon) = \delta(\varepsilon)$ as can be seen from (4.51). For non-zero ε , $d\sigma/d\varepsilon$ is given at lowest order by

$$S^{(1)}(\varepsilon \neq 0, \Omega) = C_F \frac{1}{\varepsilon} \int_{\Omega} d\text{PS}_2 \frac{1}{2\pi} \frac{\beta_1 \cdot \beta_2}{\beta_1 \cdot \hat{k} \beta_2 \cdot \hat{k}}, \quad (4.76)$$

where PS_2 denotes the two-dimensional angular phase space to be integrated over region Ω , and $\hat{k} \equiv k/\omega_k$. We emphasize again that the soft function contains the only geometry-dependence of the cross section. Also, $S^{(1)}$ for

$\varepsilon \neq 0$ is independent of ν and a .

As an example, consider a cone with opening angle 2δ , centered at angle α from jet 1. In this case, the lowest-order soft function is given by

$$S^{(1)}(\varepsilon \neq 0, \alpha, \delta) = C_F \frac{1}{\varepsilon} \ln \left(\frac{1 - \cos^2 \alpha}{\cos^2 \alpha - \cos^2 \delta} \right). \quad (4.77)$$

Similarly, we may choose Ω as a ring extending angle δ_1 to the right and δ_2 to the left of the plane perpendicular to the jet directions in the center-of-mass. In this case, we obtain

$$S^{(1)}(\varepsilon \neq 0, \delta_1, \delta_2) = C_F \frac{1}{\varepsilon} \ln \left(\frac{(1 + \sin \delta_1)(1 + \sin \delta_2)}{(1 - \sin \delta_1)(1 - \sin \delta_2)} \right) = C_F \frac{2}{\varepsilon} \Delta\eta, \quad (4.78)$$

with $\Delta\eta$ the rapidity spanned by the ring. For a ring centered around the center-of-mass ($\delta_1 = \delta_2 = \delta$) the angular integral reduces to the form that we encountered in the example of Sec. 4.2.3, and that we will use in our numerical examples of Sec. 4.6, with $\Delta\eta$ given by Eq. (4.14).

The jet functions

Recall from Eq. (4.39) that the lowest-order jet function is given by $J_c^{(0)} = 1$.

The anomalous dimensions of the jet functions are found to be

$$\gamma_{J_c}^{(1)} = -\frac{3}{2} C_F, \quad (4.79)$$

the same for each of the jets. The jet anomalous dimensions are process-independent, but of course flavor-dependent. The same anomalous dimensions for final-state quark jets appear in three- and higher-jet cross sections.

The K - G -decomposition

The anomalous dimension for the K - G -decomposition is, as noted above, the Sudakov anomalous dimension,

$$\gamma_{K_c}^{(1)} = 2C_F, \quad (4.80)$$

$$\gamma_{K_c}^{(2)} = KC_F, \quad (4.81)$$

also independent of the jet-direction. The well-known coefficient K (not to be confused with the functions K_c) is given by [85]

$$K = \left(\frac{67}{18} - \frac{\pi^2}{6} \right) C_A - \frac{10}{9} T_F N_f, \quad (4.82)$$

with the normalization $T_F = 1/2$ and N_f the number of quark flavors.

K_c and G_c , the functions that describe the evolution of the jet functions in Eq. (4.62), are given at one loop by

$$\begin{aligned} K_c^{(1)} \left(\frac{s^{1-a/2}}{\mu\nu} \left(2p_{J_c} \cdot \hat{\xi}_c \right)^{a-1}, a \right) &= -C_F \ln \left(e^{2\gamma_E - (1-a)} \frac{\mu^2 \nu^2}{s^{2-a}} \left(2p_{J_c} \cdot \hat{\xi}_c \right)^{2(1-a)} \right), \\ G_c^{(1)} \left(\frac{p_{J_c} \cdot \hat{\xi}_c}{\mu} \right) &= -C_F \ln \left(e^{-1} \frac{\left(2p_{J_c} \cdot \hat{\xi}_c \right)^2}{\mu^2} \right). \end{aligned} \quad (4.83)$$

Evolving them to the values of μ with which they appear in the functions A'_c and B'_c , Eq. (4.65), they become

$$K_c^{(1)} \left(\frac{1}{c_1}, a \right) = -C_F \ln \left(e^{2\gamma_E - (1-a)} c_1^2 \right), \quad (4.84)$$

$$G_c^{(1)} \left(\frac{1}{c_2} \right) = -C_F \ln \left(e^{-1} \frac{4}{c_2^2} \right). \quad (4.85)$$

Recall that G_c is computed from virtual diagrams only, and thus does not depend on the weight function. It therefore agrees with the result found in [72]. The soft-gluon contribution, K_c , which involves real gluon diagrams, does depend on the cross section being resummed.

With the definitions (4.65) of A'_c and B'_c we obtain

$$A'_c{}^{(1)} = C_F, \quad (4.86)$$

$$A'_c{}^{(2)}(c_1, a) = \frac{1}{2}C_F \left[K + \frac{\beta_0}{2} \ln(e^{2\gamma_E-1+a} c_1^2) \right], \quad (4.87)$$

$$B'_c{}^{(1)}(c_1, c_2, a) = 2C_F \ln \left(e^{\gamma_E-1+a/2} \frac{2c_1}{c_2} \right). \quad (4.88)$$

Here β_0 is the one-loop coefficient of the QCD beta-function, $\beta_0 = \frac{1}{3}(11\mathcal{N}_C - 4T_F N_f)$ ($\beta(g) = -g\frac{\alpha_s}{4\pi}\beta_0 + \mathcal{O}(g^3)$).

The hard scattering, and the Born cross section

At NLL only the lowest-order hard scattering function contributes, which is normalized to

$$H^{(0)}(\alpha_s(\sqrt{s}/2)) = 1. \quad (4.89)$$

At this order the hard function is independent of the eikonal vectors ξ_c , although it acquires ξ_c -dependence at higher order through the factorization described in Sec. 4.3.3. For completeness, we also give the electromagnetic Born cross section $\frac{d\sigma_0}{d\hat{n}_1}$, at fixed polar and azimuthal angle:

$$\frac{d\sigma_0}{d\hat{n}_1} = \mathcal{N}_C \left(\sum_{\mathbf{f}} Q_{\mathbf{f}}^2 \right) \frac{\alpha_{\text{em}}^2}{4s} (1 + \cos^2 \theta), \quad (4.90)$$

where θ is the c.m. polar angle of \hat{n}_1 , $e Q_f$ is the charge of quark flavor f , and $\alpha_{\text{em}} = e^2/(4\pi)$ is the fine structure constant.

4.5.2 Checking the ξ_c -dependence

It is instructive to verify how dependence on the eikonal vectors ξ_c cancels in the exponents of the resummed cross section (4.69) at the accuracy at which we work, single logarithms of ε , and single and double logarithms of ν . In these exponents, ξ_c -dependence enters only through the combinations $(\beta_c \cdot \hat{\xi}_c)$ and $(p_{J_c} \cdot \hat{\xi}_c)$.

Let us introduce the following notation for the exponents in Eq. (4.69), to which we will return below:

$$\begin{aligned}
E_1 &\equiv - \int_{\varepsilon\sqrt{s}}^{\sqrt{s}/2} \frac{d\lambda}{\lambda} \gamma_s(\alpha_s(\lambda)) - \sum_{c=1}^2 \int_{\sqrt{s}/(2\zeta_0)}^{\sqrt{s}/2} \frac{d\lambda}{\lambda} \gamma_{J_c}(\alpha_s(\lambda)), \quad (4.91) \\
E_2 &\equiv - \sum_{c=1}^2 \int_{\sqrt{s}/(2\zeta_0)}^{p_{J_c} \cdot \hat{\xi}_c} \frac{d\lambda}{\lambda} \left[B'_c(c_1, c_2, a, \alpha_s(c_2\lambda)) + 2 \int_{c_1 \frac{s^{1-a/2}}{\nu(2\lambda)^{1-a}}}^{c_2\lambda} \frac{d\lambda'}{\lambda'} A'_c(c_1, a, \alpha_s(\lambda')) \right]. \quad (4.92)
\end{aligned}$$

At NLL, explicit ξ_c dependence is found only in γ_s , Eq. (4.75), for E_1 , and in the upper limit of the λ integral of E_2 . We then find that

$$\frac{\partial}{\partial \ln \beta_c \cdot \hat{\xi}_c} (E_1 + E_2) = 2C_F \int_{\varepsilon\sqrt{s}}^{\sqrt{s}/2} \frac{d\lambda}{\lambda} \frac{\alpha_s(\lambda)}{\pi} - 2C_F \int_{c_1 \frac{s^{1-a/2}}{\nu(2p_{J_c} \cdot \hat{\xi}_c)^{1-a}}}^{c_2 p_{J_c} \cdot \hat{\xi}_c} \frac{d\lambda'}{\lambda'} \frac{\alpha_s(\lambda')}{\pi} + \text{NNLL}. \quad (4.93)$$

Here the second term stems entirely from $A'^{(1)}$, Eq. (4.86); other contributions of E_2 are subleading. The ξ_c -dependence in the exponents begins only at the level that we do not resum, at $\alpha_s \ln(1/\varepsilon\nu)$, which is compensated by corrections in $S(\varepsilon\nu, \alpha_s)$. The remaining contributions are of NNLL order, that is, proportional to $\alpha_s^k(\sqrt{s}) \ln^{k-1}(\nu\beta_c \cdot \hat{\xi}_c)$, as may be verified by expanding the running couplings. Thus, as required by the factorization procedure, the relevant ξ_c -dependence cancels between the resummed soft and jet functions, which give rise to the first and second integrals, respectively, in Eq. (4.93).

4.5.3 The inclusive event shape at NLL

We can simplify the differential event shape, Eq. (4.74), by absorbing the soft anomalous dimension γ_s into the remaining terms. We will find a form that can be compared directly to the classic NLL resummation for the thrust ($a = 0$). This is done by rewriting the integral over the soft anomalous dimension as

$$\begin{aligned}
\int_{\sqrt{s}/\nu}^{\sqrt{s}/2} \frac{d\lambda}{\lambda} \gamma_s(\alpha_s(\lambda)) &= \int_{\sqrt{s}/[2(\nu/2)^{1/(2-a)}]}^{\sqrt{s}/2} \frac{d\lambda}{\lambda} \gamma_s(\alpha_s(\lambda)) \\
&+ \int_{\sqrt{s}/\nu}^{\sqrt{s}/[2(\nu/2)^{1/(2-a)}]} \frac{d\lambda}{\lambda} \gamma_s(\alpha_s(\lambda)) = \int_{\sqrt{s}/[2(\nu/2)^{1/(2-a)}]}^{\sqrt{s}/2} \frac{d\lambda}{\lambda} \gamma_s(\alpha_s(\lambda)) \\
&+ (1-a) \int_{\sqrt{s}/[2(\nu/2)^{1/(2-a)}]}^{\sqrt{s}/2} \frac{d\lambda}{\lambda} \gamma_s\left(\alpha_s\left(\frac{s^{1-a/2}}{\nu(2\lambda)^{1-a}}\right)\right) \\
&= (2-a) \int_{\sqrt{s}/[2(\nu/2)^{1/(2-a)}]}^{\sqrt{s}/2} \frac{d\lambda}{\lambda} \gamma_s(\alpha_s(\lambda)) \\
&- (1-a) \int_{\sqrt{s}/[2(\nu/2)^{1/(2-a)}]}^{\sqrt{s}/2} \frac{d\lambda}{\lambda} \int_{s^{1-a/2}/[\nu(2\lambda)^{1-a}]}^{\lambda} \frac{d\lambda'}{\lambda'} \beta(g(\lambda')) \frac{\partial}{\partial g} \gamma_s(\alpha_s(\lambda')) .
\end{aligned} \tag{4.94}$$

In the first equality we split the λ integral so that the limits of the first term match those of the B'_c integral of Eq. (4.74). In the second equality we have changed variables in the second term according to

$$\lambda \rightarrow \left(\frac{s^{1-\frac{a}{2}}}{2^{1-a}\nu\lambda} \right)^{\frac{1}{1-a}}, \quad (4.95)$$

so that the limits of the second integral also match. In the third equality of Eq. (4.94), we have reexpressed the running coupling at the old scale λ in terms of the new scale. This is a generalization of the procedure of Ref. [86], applied originally to the threshold-resummed Drell-Yan cross section [87].

Using Eq. (4.94), and identifying $p_{J_c} \cdot \hat{\xi}_c$ with $\sqrt{s}/2$ (Eq. (4.70)) in the inclusive event shape distribution, Eq. (4.74), we can rewrite this distribution at NLL as

$$\begin{aligned} \frac{d\sigma^{\text{incl}}(\nu, s, a)}{d\hat{n}_1} &= \frac{d\sigma_0}{d\hat{n}_1} \\ &\times \prod_{c=1}^2 \exp \left\{ - \int_{\sqrt{s}/[2(\nu/2)^{1/(2-a)}]}^{\sqrt{s}/2} \frac{d\lambda}{\lambda} [B_c(c_1, c_2, a, \alpha_s(\lambda))] \right. \\ &\left. + 2 \int_{c_1 \frac{s^{1-a/2}}{\nu(2\lambda)^{1-a}}}^{c_2 \lambda} \frac{d\lambda'}{\lambda'} A_c(c_1, a, \alpha_s(\lambda')) \right\}, \end{aligned} \quad (4.96)$$

where we have rearranged the contribution of γ_s as:

$$\begin{aligned}
A_c(c_1, a, \alpha_s(\mu)) &\equiv A'_c(c_1, a, \alpha_s(\mu)) - \frac{1}{4}(1-a)\beta(g(\mu))\frac{\partial}{\partial g}\gamma_s(\alpha_s(\mu)), \\
B_c(c_1, c_2, a, \alpha_s(\mu)) &\equiv \gamma_{J_c}(\alpha_s(\mu)) + \left(1 - \frac{a}{2}\right)\gamma_s(\alpha_s(\mu)) + B'_c(c_1, c_2, a, \alpha_s(\mu)).
\end{aligned}
\tag{4.97}$$

Next, we replace the lower limit of the λ' -integral by an explicit θ -function. Then we exchange orders of integration, and change variables in the term containing A from the dimensional variable λ to the dimensionless combination

$$u = \frac{2\lambda\lambda'}{s}.$$
(4.98)

We find

$$\begin{aligned}
\frac{d\sigma^{\text{incl}}(\nu, s, a)}{d\hat{n}_1} &= \frac{d\sigma_0}{d\hat{n}_1} \prod_{c=1}^2 \exp \left\{ - \int_{\sqrt{s}/[2(\nu/2)^{1/(2-a)}]}^{\sqrt{s}/2} \frac{d\lambda}{\lambda} B_c(c_1, c_2, a, \alpha_s(\lambda)) \right\} \\
&\times \prod_{c=1}^2 \exp \left\{ -2 \int_0^{\sqrt{s}} \frac{d\lambda'}{\lambda'} \int_{\lambda'^2/s}^{\lambda'/\sqrt{s}} \frac{du}{u} \theta \left(c_1^{-1} \nu \frac{\lambda'^a u^{1-a}}{s^{a/2}} - 1 \right) A_c(c_1, a, \alpha_s(\lambda')) \right\}.
\end{aligned}
\tag{4.99}$$

Here, the θ -function vanishes for small λ' , and the remaining effects of replacing the lower boundary of the λ' integral by 0 are next-to-next-to-leading logarithmic.

A further change of variables allows us to write the NLL resummed event shapes in a form familiar from the NLL resummed thrust. In the first line of Eq. (4.99), we replace $\lambda^2 \rightarrow us/4$. In the second line we relabel $\lambda' \rightarrow \sqrt{q^2}$,

and exchange orders of integration. Finally, choosing

$$\begin{aligned} c_1 &= e^{-\gamma E}, \\ c_2 &= 2, \end{aligned} \tag{4.100}$$

we find at NLL

$$\begin{aligned} \frac{d\sigma^{\text{incl}}(\nu, s, a)}{d\hat{n}_1} &= \frac{d\sigma_0}{d\hat{n}_1} \\ &\times \prod_{c=1}^2 \exp \left\{ \int_0^1 \frac{du}{u} \left[\int_{u^2 s}^{us} \frac{dq^2}{q^2} A_c(\alpha_s(q^2)) \left(e^{-u^{1-a}\nu(q^2/s)^{a/2}} - 1 \right) \right. \right. \\ &\quad \left. \left. + \frac{1}{2} B_c(\alpha_s(us/4)) \left(e^{-u(\nu/2)^{2/(2-a)} e^{-\gamma E}} - 1 \right) \right] \right\}, \end{aligned} \tag{4.101}$$

and reproduce the well-known coefficients

$$A_c^{(1)} = C_F, \tag{4.102}$$

$$A_c^{(2)} = \frac{1}{2} C_F K, \tag{4.103}$$

$$B_c^{(1)} = -\frac{3}{2} C_F, \tag{4.104}$$

independent of a . In Eq. (4.101), we have made use of the relation

$$e^{-x/y} - 1 \approx -\theta(x - y e^{-\gamma E}), \tag{4.105}$$

which is valid at NLL in the logarithmic integrals. With these choices, when $a = 0$ we reproduce the NLL resummed thrust cross section [57].

The choices of the c_i in Eq. (4.100) cancel all purely soft NLL components (γ_s and K_c). The remaining double logarithms stem from simultaneously soft and collinear radiation, and single logarithms arise from collinear configurations only. At NLL, the cross section is determined by the anomalous dimension A_c , which is the coefficient of the singular $1/[1-x]_+$ term in the nonsinglet evolution kernel [88], and the quark anomalous dimension. All radiation in dijet events thus appears to be emitted coherently by the two jets [57]. This, however, is not necessarily true beyond next-to-leading logarithmic accuracy for dijets, and is certainly not the case for multijet events [65]. Similar considerations apply to the resummed correlation, Eq. (4.69).

4.5.4 Closed expressions

Given the explicit results above, the integrals in the exponents of the resummed correlation, Eq. (4.69), may be easily performed in closed form. We give the analytic results for the exponents of Eq. (4.69), as defined in Eqs. (4.91) and (4.92). As in Eq. (4.70), we identify $p_{J_c} \cdot \hat{\xi}_c$ with $\sqrt{s}/2$.

$$e^{E_1(a)} = \left(\frac{\alpha_s(\sqrt{s}/2)}{\alpha_s(\varepsilon\sqrt{s})} \right)^{\frac{4C_F}{\beta_0}} \left(\frac{\alpha_s\left(\frac{\sqrt{s}}{2\zeta_0}\right)}{\alpha_s(\sqrt{s}/2)} \right)^{\frac{6C_F}{\beta_0}}, \quad (4.106)$$

$$\begin{aligned} e^{E_2(a)} &= \left(\frac{\alpha_s(c_2\sqrt{s}/2)}{\alpha_s\left(\frac{c_2\sqrt{s}}{2\zeta_0}\right)} \right)^{\frac{4C_F}{\beta_0}\kappa_1(a)} \left(\frac{\alpha_s\left(\frac{c_1\sqrt{s}}{2\zeta_0}\right)}{\alpha_s\left(\frac{c_1\sqrt{s}}{\nu}\right)} \right)^{\frac{1}{a-1}\frac{4C_F}{\beta_0}\kappa_2(a)} \\ &\times \left(\frac{\alpha_s(c_2\sqrt{s}/2)}{\alpha_s\left(\frac{c_1\sqrt{s}}{2\zeta_0}\right)} \right)^{\frac{1}{2-a}\frac{8C_F}{\beta_0}\ln(\nu/2)}, \end{aligned} \quad (4.107)$$

with

$$\begin{aligned} \kappa_1(a) &= \ln\left(\frac{4}{c_2^2 e}\right) + \frac{4\pi}{\beta_0} \left[\alpha_s \left(\frac{c_2 \sqrt{s}}{2 \zeta_0} \right) \right]^{-1} - \frac{2K}{\beta_0} \\ &\quad - \frac{\beta_1}{2\beta_0^2} \ln\left(\left(\frac{\beta_0}{4\pi e} \right)^2 \alpha_s \left(\frac{c_2 \sqrt{s}}{2} \right) \alpha_s \left(\frac{c_2 \sqrt{s}}{2 \zeta_0} \right) \right), \end{aligned} \quad (4.108)$$

$$\begin{aligned} \kappa_2(a) &= (1 - a - 2\gamma_E) + \frac{4\pi}{\beta_0} \left[\alpha_s \left(\frac{\sqrt{s}}{\nu} \right) \right]^{-1} - \frac{2K}{\beta_0} \\ &\quad - \frac{\beta_1}{2\beta_0^2} \ln\left(\left(\frac{\beta_0}{4\pi e} \right)^2 \alpha_s \left(\frac{c_1 \sqrt{s}}{\nu} \right) \alpha_s \left(\frac{c_1 \sqrt{s}}{2 \zeta_0} \right) \right). \end{aligned} \quad (4.109)$$

We have used the two-loop running coupling, when appropriate, to derive Eqs. (4.106) - (4.109). The results are expressed in terms of the one-loop running coupling

$$\alpha_s(\mu) = \frac{2\pi}{\beta_0} \frac{1}{\ln\left(\frac{\mu}{\Lambda_{\text{QCD}}}\right)}, \quad (4.110)$$

and the first two coefficients in the expansion of the QCD beta-function, β_0 and

$$\beta_1 = \frac{34}{3} C_A^2 - \left(\frac{20}{3} C_A + 4C_F \right) T_F N_f. \quad (4.111)$$

Combining the expressions for the exponents, Eqs. (4.106) and (4.107), for the Born cross section, Eq. (4.90), and for the soft function, Eq. (4.76), in Eq. (4.69), the complete differential cross section, at LL in ε and at NLL in ν , is

given by

$$\begin{aligned}
\frac{d\sigma(\varepsilon, \nu, s, a)}{d\varepsilon d\hat{n}_1} &= \mathcal{N}_C \left(\sum_{\mathfrak{f}} Q_{\mathfrak{f}}^2 \right) \frac{\pi \alpha_{\text{em}}^2}{2s} (1 + \cos^2 \theta) \\
&\times C_F \frac{\alpha_s(\varepsilon\sqrt{s})}{\pi} \frac{1}{\varepsilon} \int_{\Omega} d\text{PS}_2 \frac{1}{2\pi} \frac{\beta_1 \cdot \beta_2}{\beta_1 \cdot \hat{k} \beta_2 \cdot \hat{k}} \\
&\times \left(\frac{\alpha_s \left(\frac{\sqrt{s}}{2} \right)}{\alpha_s(\varepsilon\sqrt{s})} \right)^{\frac{4C_F}{\beta_0}} \left(\frac{\alpha_s \left(\frac{\sqrt{s}}{2\zeta_0} \right)}{\alpha_s \left(\frac{\sqrt{s}}{2} \right)} \right)^{\frac{6C_F}{\beta_0}} \\
&\times \left(\frac{\alpha_s \left(c_2 \frac{\sqrt{s}}{2} \right)}{\alpha_s \left(\frac{c_2 \sqrt{s}}{2\zeta_0} \right)} \right)^{\frac{4C_F}{\beta_0} \kappa_1(a)} \left(\frac{\alpha_s \left(\frac{c_1 \sqrt{s}}{2\zeta_0} \right)}{\alpha_s \left(\frac{c_1 \sqrt{s}}{\nu} \right)} \right)^{\frac{1}{a-1} \frac{4C_F}{\beta_0} \kappa_2(a)} \\
&\times \left(\frac{\alpha_s \left(c_2 \frac{\sqrt{s}}{2} \right)}{\alpha_s \left(\frac{c_1 \sqrt{s}}{2\zeta_0} \right)} \right)^{\frac{1}{2-a} \frac{8C_F}{\beta_0} \ln\left(\frac{\nu}{2}\right)}. \tag{4.112}
\end{aligned}$$

These are the expressions that we will evaluate in the next section. We note that this is not the only possible closed form for the resummed correlation at this level of accuracy. When a full next-to-leading order calculation for this set of event shapes is given, the matching procedure of [57] may be more convenient.

4.6 Numerical Results

Here we show some representative examples of numerical results for the correlation, Eq. (4.112). We pick the constants c_i as in Eq. (4.100), unless stated otherwise. The effect of different choices is nonleading, and is numerically small, as we will see below. In the following we choose the region Ω to be a ring between the jets, centered in their center-of-mass, with a width of $\Delta\eta = 2$,

or equivalently, opening angle $\delta \approx 50$ degrees (see Eq. (4.14)). The analogous cross section for a cone centered at 90 degrees from the jets (Eq. (4.77)) has a similar behavior. In the following, the center-of-mass energy $Q = \sqrt{s}$ is chosen to be 100 GeV.

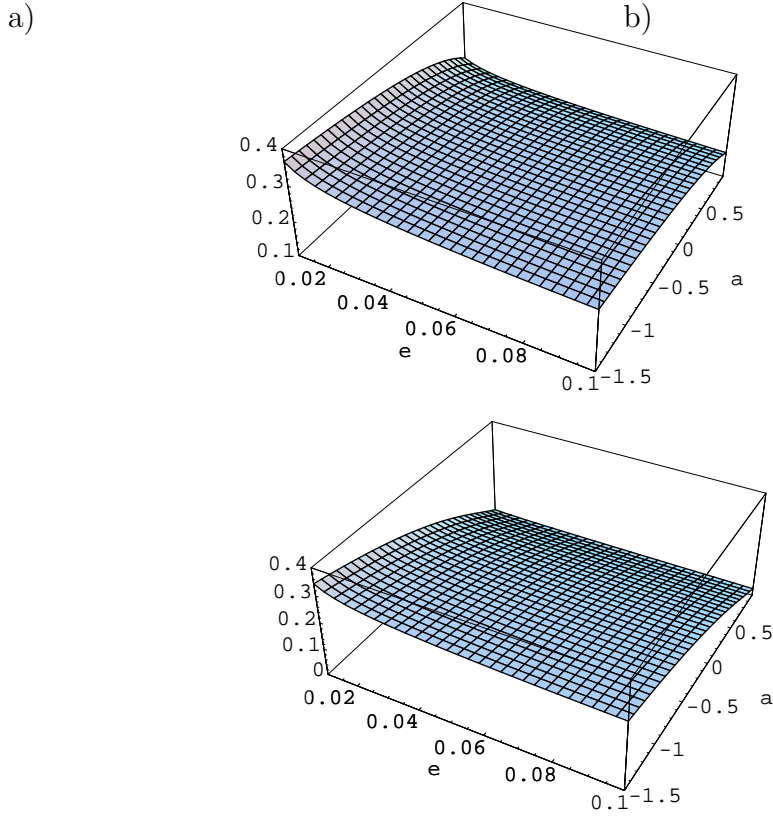


Figure 4.5: Differential cross section $\frac{\varepsilon d\sigma/(d\varepsilon d\hat{n}_1)}{d\sigma_0/d\hat{n}_1}$, normalized by the Born cross section, at $Q = 100$ GeV, as a function of ε and a at fixed ν : a) $\nu = 10$, b) $\nu = 50$. Ω is a ring (slice) centered around the jets, with a width of $\Delta\eta = 2$.

Fig. 4.5 shows the dependence of the differential cross section (4.69), multiplied by ε and normalized by the Born cross section, $\frac{\varepsilon d\sigma/(d\varepsilon d\hat{n}_1)}{d\sigma_0/d\hat{n}_1}$, on the measured energy ε and on the parameter a , at fixed ν . In Fig. 4.5 a), we plot

$\frac{\varepsilon d\sigma/(d\varepsilon d\hat{n}_1)}{d\sigma_0/d\hat{n}_1}$ for $\nu = 10$, in Fig. 4.5 b) for $\nu = 50$. As ν increases, the radiation into the complementary region $\bar{\Omega}$ is more restricted, as illustrated by the comparison of Figs. 4.5 a) and b). Similarly, as a approaches 1, the cross section falls, because the jets are restricted to be very narrow. On the other hand, as a assumes more and more negative values at fixed ε , the correlations (4.69) approach a constant value. For a large and negative, however, non-global dependence on $\ln \varepsilon$ and $|a|$ will emerge from higher order corrections in the soft function, which we do not include in Eq. (4.112).

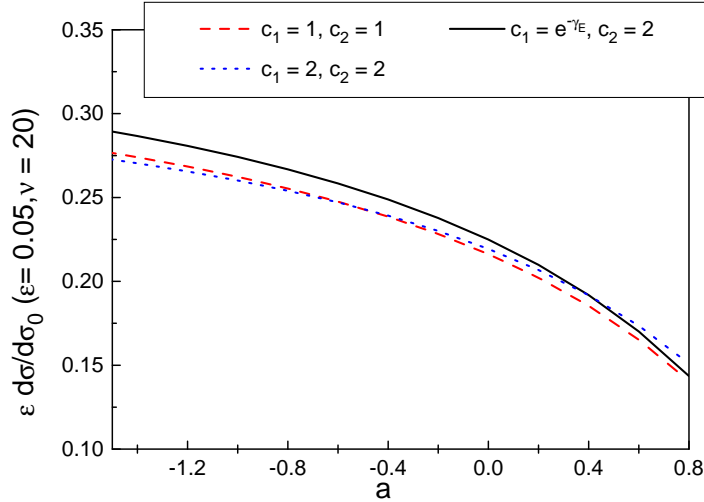


Figure 4.6: Differential cross section $\frac{\varepsilon d\sigma/(d\varepsilon d\hat{n}_1)}{d\sigma_0/d\hat{n}_1}$, normalized by the Born cross section, at $Q = 100$ GeV, as a function of a at fixed $\nu = 20$ and $\varepsilon = 0.05$. Ω is chosen as in Fig. 4.5. Solid line: $c_1 = e^{-\gamma E}$, $c_2 = 2$, as in Eq. (4.100), dashed line: $c_1 = c_2 = 1$, dotted line: $c_1 = c_2 = 2$.

In Fig. 4.6 we investigate the sensitivity of the resummed correlation, Eq. (4.112), to our choice of the constants c_i . The effect of these constants is of next-to-next-to-leading logarithmic order in the event shape. We plot the

differential cross section $\varepsilon \frac{d\sigma/(d\varepsilon d\hat{n}_1)}{d\sigma_0/d\hat{n}_1}$, at $Q = 100$ GeV, for fixed $\varepsilon = 0.05$ and $\nu = 20$, as a function of a . The effects of changes in the c_i are of the order of a few percent for moderate values of a .

Finally, we illustrate the sensitivity of these results to the flavor of the primary partons. For this purpose we study the corresponding ratio of the shape/flow correlation to the cross section for gluon jets produced by a hypothetical color singlet source. Fig. 4.7 displays the ratio of the differential cross section $d\sigma^q(\varepsilon, a)/(d\varepsilon d\hat{n}_1)$, Eq. (4.112), normalized by the lowest-order cross section, to the analogous quantity with gluons as primary partons in the outgoing jets, again at $Q = 100$ GeV. This ratio is multiplied by C_A/C_F in the figure to compensate for the difference in the normalizations of the lowest-order soft functions. Gluon jets have wider angular extent, and hence are suppressed relative to quark jets with increasing ν or a , as can be seen by comparing Figs. 4.7 a) and b). Fig. 4.7 a) shows the ratio at $\nu = 10$, and Fig. 4.7 b) at $\nu = 50$. These results suggest sensitivity to the more complex color and flavor flow characteristic of hadronic scattering [65, 66].

4.7 Summary and Outlook

We have introduced a general class of inclusive event shapes in e^+e^- dijet events which reduce to the thrust and the jet broadening distributions as special cases. We have derived analytic expressions in transform space, and have shown the equivalence of our formalism at NLL with the well-known result for the thrust [57]. Separate studies of this class of event shapes in the untransformed space, at higher orders, and for nonperturbative effects [60] are

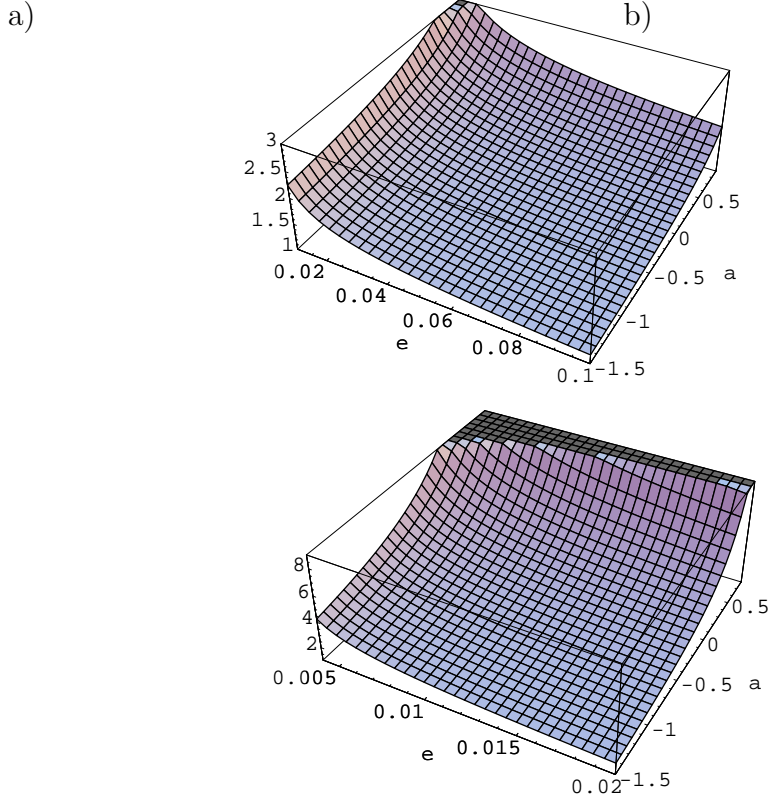


Figure 4.7: Ratios of differential cross sections for quark to gluon jets $\frac{C_A}{C_F} \left(\frac{\varepsilon d\sigma^q / (d\varepsilon d\hat{n}_1)}{d\sigma_0^q / d\hat{n}_1} \right) \left(\frac{\varepsilon d\sigma^g / (d\varepsilon d\hat{n}_1)}{d\sigma_0^g / d\hat{n}_1} \right)^{-1}$ at $Q = 100$ GeV as a function of ε and a at fixed ν : a) $\nu = 10$, b) $\nu = 50$. Ω as in Fig. 4.5, c_1 and c_2 as in Eq. (4.100).

certainly of interest. We reserve these studies for future work.

We have introduced a set of correlations of interjet energy flow for the general class of event shapes, and have shown that for these quantities it is possible to control the influence of secondary radiation and nonglobal logarithms. These correlations are sensitive mainly to radiation emitted directly from the primary hard scattering, through transforms in the weight functions that suppress secondary, or non-global, radiation. We have presented analytic

and numerical studies of these shape/flow correlations at leading logarithmic order in the flow variable and at next-to-leading-logarithmic order in the event shape. The application of our formalism to multijet events and to scattering with initial state hadrons is certainly possible, and may shed light on the relationship between color and energy flow in hard scattering processes with non-trivial color exchange.

Appendix A

A.1 Power counting with contracted vertices

In this appendix we will include the possibility of contracted vertices in the reduced diagram in Fig. 2.1a. These are associated with internal lines (collapsed to a point) which are off-shell by \sqrt{s} . Our analysis closely follows [39] and [43].

If we go back to the argument that led us to Eq. (2.15) for the superficial degree of IR divergence for the soft part, we see that the same reasoning as in the case of elementary vertices applies to the case of contracted vertices since the result (2.15) has been obtained by means of dimensional counting.

The analysis of contracted vertices connecting jet lines only is, however, more subtle. We have to demonstrate that the suppression factors corresponding to the contracted vertices are at least as great as the ones for the elementary vertices. The expression (2.22) tells us that we can restrict ourselves to the two and three point vertices. For these cases, we analyze the full two and three-point subdiagrams, by studying the tensor structures that are found after integration over their internal loop momenta.

Before we discuss all the possible structures, we state some results which will be essential for the upcoming analysis. The first one is the simple Dirac matrix identity

$$\not{a} \not{b} \not{a} = 2(a \cdot b) \not{a} - a^2 \not{b}. \quad (\text{A.1})$$

The other two follow from Eqs. (2.7) and (2.11) for the gluon propagator in Coulomb gauge, and hold for any jet momenta scaling as $l_A \sim l'_A \sim \sqrt{s}(1^+, \lambda^-, \lambda^{1/2})$ collinear to the momentum p_A defined in Eq. (2.2)

$$\begin{aligned} l'_A{}^\alpha N_{\alpha\beta}(l_A, \eta) &= \mathcal{O}(\lambda^{1/2} \sqrt{s}), \\ \bar{l}'_A{}^\alpha N_{\alpha\beta}(l_A, \eta) &= \mathcal{O}(\lambda^{1/2} \sqrt{s}), \end{aligned} \quad (\text{A.2})$$

for all components of β . We now proceed to discuss the particular cases.

Ghost self-energy: The most general covariant structure is, using $p \cdot \bar{p} = \bar{p}^2$,

1

$$\Pi(p, \bar{p}) = p \cdot \bar{p} f(p^2/\mu^2, \bar{p}^2/\mu^2, \alpha_s(\mu)), \quad (\text{A.3})$$

where μ is a scale introduced by a UV/IR regularization of Feynman diagrams and p is the momentum of an internal jet line. Strictly speaking, the covariants should be formed from the vectors p and η , but since p has nonzero light-cone components, we can use Eq. (2.8), to express η in terms of \bar{p} . The maximum degree of divergence for the ghost self-energy occurs when the internal lines become either parallel to the external momentum p or soft. The most general pinch singular surface consists of a subdiagram of collinear lines moving in a direction of the external ghost. This subdiagram can interact with itself

¹In the rest of this subsection we are concerned the momentum factors only, and we omit dependence on the color structure.

through the exchange of soft quanta. Power counting arguments similar to the ones given in Sec. 2.3.2 show, however, that there is no IR divergence for these pinch singular points. This shows that the dimensionless function f in Eq. (A.3) is IR finite. Hence the combination [tree level ghost propagator] - [ghost self-energy] - [tree level ghost propagator], $[1/(p \cdot \bar{p})] \Pi(p, \bar{p}) [1/(p \cdot \bar{p})]$, is suppressed at least as much as a single tree level ghost propagator, $1/(p \cdot \bar{p})$. Therefore the contracted two point ghost vertex within a jet subdiagram contributes at least the same suppression as a single tree level ghost propagator.

Gluon self-energy: With external momentum p , its most general tensor decomposition has the form

$$\Pi_{\mu\nu}(p, \bar{p}) = g_{\mu\nu} p^2 f_1 + p_\mu p_\nu f_2 + \bar{p}_\mu \bar{p}_\nu f_3 + (p_\mu \bar{p}_\nu + \bar{p}_\mu p_\nu) f_4. \quad (\text{A.4})$$

As verified by explicit one-loop calculations in Refs. [49] and [50] the gluon self-energy in Coulomb gauge is not transverse. In Eq. (A.4), the $f_i = f_i(p^2/\mu^2, \bar{p}^2/\mu^2, \alpha_s(\mu))$ are dimensionless functions. Contracting $\Pi_{\mu\nu}$ with tree level gluon propagators, and using Eq. (2.10), the last two terms in Eq. (A.4) drop out and the first and the second terms give at least one factor of p^2 in the numerator, which cancels one of the $(1/p^2)$ denominator factors. Since the maximum degree of IR divergence for the gluon self-energy occurs when all the internal lines become either collinear to the external momentum p or soft, we can use the results of the power counting of Sec. 2.3.2 to demonstrate that the dimensionless functions f_i are at worst logarithmically divergent. Therefore the combination: gluon jet line - 2 point gluon contracted vertex - gluon jet line, behaves the same way as a gluon jet line for the purpose of the jet

power counting.

Fermion self-energy: In the massless fermion limit, the most general matrix structure of the fermion self-energy is

$$\Sigma(p, \bar{p}) = \not{p} g_1 + \not{\bar{p}} g_2, \quad (\text{A.5})$$

with dimensionless functions $g_i = g_i(p^2/\mu^2, \bar{p}^2/\mu^2, \alpha_s(\mu))$, $i = 1, 2$. When we sandwich the fermion self-energy between the tree level fermion denominators, the first term in Eq. (A.5) behaves the same way as the tree level fermion propagator, modulo logarithmic enhancements due to the function g_1 . The second term, however, is absent from the fermion self-energy as was shown in Ref. [43] using the method of induction and Ward identities. The idea was to study a variation of the fermion self-energy by making an infinitesimal Lorentz boost on the external momentum. This implies a relationship between the $(r + 1)$ and the r -loop self energy. Assuming that the term proportional to $\not{\bar{p}}$ is absent from the r -loop expansion Sen shows that it is also absent from the $(r + 1)$ -loop expansion. So the first term in Eq. (A.5) is the only possible structure of the fermion self-energy when its external momentum is jet like and approaches mass shell.

Now let us investigate the 3 point functions.

Fermion-gluon-fermion vertex function: Γ_μ , can depend on vectors that scale as l_A, l'_A in Eq. (A.2), provided all momenta external to the contracted vertex are collinear to momentum p_A given in Eq. (2.2). It has one Lorentz index, μ , and neglecting the fermion masses, it contains an odd number of gamma matrices. This implies that the most general tensor and gamma matrix expansion

of Γ_μ involves

1. γ_μ ,
2. $\gamma_\mu \not{V}_A \bar{V}_A / (l_A \cdot \bar{l}_A)$ and all permutations of γ_μ , \not{V}_A , \bar{V}_A ,
3. $\not{V}_A l_A^\mu / l_A^2$, $\bar{V}_A l_A^\mu / (\bar{l}_A \cdot l_A)$, $\not{V}_A \bar{l}_A^\mu / (l_A \cdot \bar{l}_A)$, $\bar{V}_A \bar{l}_A^\mu / \bar{l}_A^2$.

The differences between the listed set of structures and other possible combinations are $\mathcal{O}(\lambda^{1/2} \sqrt{s})$, as can be shown using Eqs. (A.1)-(A.2). The listed gamma matrix structures are multiplied by dimensionless functions, which can depend on the combinations l_A^2 , \bar{l}_A^2 , $l_A'^2$, $\bar{l}_A'^2$, besides the renormalization scale and the running coupling. Using the arguments similar to the ones leading to Eq. (2.23), we easily verify that the above mentioned dimensionless functions are at most logarithmically divergent. Next we analyze the possible Dirac structures.

1. The first case has the same structure as the elementary vertex, and therefore causes the same suppression as the elementary vertex.
2. The fermion-gluon-fermion composite 3-point vertex is sandwiched between the factors \not{V}_A and \not{V}_A , originating from the numerators of the fermion propagators external to the composite vertex. Therefore the terms from case 2 where \not{V}_A is on the first or third position in the string of the gamma matrices provide a suppression $\sqrt{l_A'^2}$. On the other hand in the case, when \not{V}_A is in the middle of this string of three gamma matrices, we encounter the combination $\not{V}_A \gamma_\mu \not{V}_A$ after taking into account the numerators of the external fermions. Using Eq. (A.1), we can immediately recognize that this combination provides a suppression $\lambda^{1/2}$.

3. Based on the preceding arguments it is obvious that also the structures included in item 3 supply at least the same suppression factor as the elementary vertex.

Therefore, we conclude that the composite 3-point fermion-gluon-fermion vertex behaves as the elementary vertex for the purposes of the jet power counting.

Three gluon vertex: $V_{\mu\nu\rho}$, with external momenta collinear to momentum p_A . This vertex can depend on momenta l_A, \bar{l}_A defined above and the metric tensor $g_{\alpha\beta}$. Taking into account the dimension of the 3 gluon Green function, its only possible tensor structure involves combinations of the form $[g_{\mu\nu} l_A^\rho + \text{perm.} + \mathcal{O}(\lambda^{1/2} \sqrt{s})]$ and $[l_A^\mu l_A^\nu l_A^\rho / l_A^2 + \mathcal{O}(\lambda^{1/2} \sqrt{s})]$, with all possible replacements of $l_A \rightarrow \bar{l}_A$. These tensor structures are multiplied by dimensionless functions. The former is the same as in the case of an elementary vertex and it therefore supplies the same suppression factor as the elementary vertex. The latter also provides the same suppression as the elementary vertex, since the two momenta, say l_A^μ, l_A^ν , after being contracted with the propagators of the external gluons, give suppression factors, as in Eq. (A.2), which cancel the $1/l_A^2$ enhancement. The leftover momentum l_A^ρ provides the same suppression factor as the elementary vertex. Using the collinear power counting of Sec. 2.3.2, one can immediately see that the IR divergence of the dimensionless functions multiplying these tensor structures is not worse than logarithmic. Hence, there is a suppression factor $\lambda^{1/2}$ associated with every contracted 3 gluon vertex.

Ghost - gluon - antighost three point vertex: When all lines external to the contracted vertex are of the order l_A , the most general tensor structure for this

contracted vertex is

$$l_A^\mu h_1 + \bar{l}_A^\mu h_2 + \mathcal{O}(\lambda^{1/2} \sqrt{s}), \quad (\text{A.6})$$

with dimensionless functions $h_i = h_i(l_A^2/\mu^2, \bar{l}_A^2/\mu^2, \alpha_s(\mu))$, $i = 1, 2$, which are at most logarithmically IR divergent. Using Eq. (A.2), we see that when the momenta in Eq. (A.6) are contracted with the tree level gluon propagator, we get a suppression of the order of the transverse jet momentum, and that this contracted vertex gives the same suppression as the elementary three point vertex, at least.

A.2 Varying the Gauge-Fixing Vector

In this appendix we study the effect of an infinitesimal boost, performed on the gauge fixing vector η , on an expectation of a time ordered product of fields, denoted by O , taken between physical states. The gauge-fixing and the ghost terms in the QCD lagrangian are

$$\begin{aligned} \mathcal{L}_{\text{g.f.}}(x) &= -\frac{1}{2\xi} g_a^2(x), \\ \mathcal{L}_{\text{ghost}}(x) &= -b_a(x) \delta_{\text{BRS}} g_a(x) / \delta\Lambda, \end{aligned} \quad (\text{A.7})$$

respectively. In Eq. (A.7), $\delta\Lambda$ is a Grassmann parameter defining the BRS transformation, $b_a(x)$ is an antighost field and

$$g_a(x) \equiv -\bar{\partial} \cdot A_a(x) \equiv -(\partial - (\eta \cdot \partial) \eta) \cdot A_a(x). \quad (\text{A.8})$$

Let us consider an infinitesimal boost with velocity $\delta\beta$ on a gauge fixing vector η performed in the plus-minus plane

$$\eta \rightarrow \eta' \equiv \eta + \tilde{\eta} \delta\beta, \quad (\text{A.9})$$

where the vectors η and $\tilde{\eta}$ are defined in Eqs. (2.9) and (2.35), respectively. Since only the gauge fixing and the ghost terms in the QCD lagrangian depend on η , we can write to accuracy $\mathcal{O}(\delta\beta^2)$

$$\begin{aligned} \delta \langle O \rangle &\equiv \langle O(\eta') \rangle - \langle O(\eta) \rangle = \langle \tilde{\eta}^\alpha \frac{\partial O}{\partial \eta^\alpha} \delta\beta \rangle \\ &= -\frac{i}{\xi} \int d^4x \langle O(\eta) g_a(x) \delta g_a(x) \rangle \\ &\quad - i \int d^4x \langle O(\eta) b_a(x) \delta (\delta_{\text{BRS}} g_a(x)/\delta\Lambda) \rangle. \end{aligned} \quad (\text{A.10})$$

Using the BRS invariance of the QCD lagrangian and the BRS transformation rule for an antighost field

$$\delta_{\text{BRS}} b_a(x)/\delta\Lambda = \frac{1}{\xi} g_a(x), \quad (\text{A.11})$$

we arrive at

$$\delta \langle O \rangle = -i \int d^4x \langle (\delta_{\text{BRS}} O/\delta\Lambda) b_a(x) \delta g_a(x) \rangle. \quad (\text{A.12})$$

Taking a variation of $g_a(x)$ in Eq. (A.12), we obtain

$$\delta \langle O \rangle = -i \int d^4x \langle (\delta_{\text{BRS}} O / \delta \Lambda) b_a(x) ((\tilde{\eta} \cdot \partial) \eta + (\eta \cdot \partial) \tilde{\eta}) \cdot A_a(x) \rangle. \quad (\text{A.13})$$

Substituting for O a product of n gluon fields, we can use Eq. (A.13), together with the rule for the BRS transformation of a gluon field

$$\delta_{\text{BRS}} A_\mu^a(x) / \delta \Lambda = \partial_\mu c^a(x) + g_s f^{abc} A_\mu^b(x) c^c(x), \quad (\text{A.14})$$

with $c^a(x)$ representing the ghost field, to derive the gauge variation for a connected Green function. However, our jet functions are one-particle irreducible in external soft lines and we therefore cannot apply Eq. (A.13) directly, and must find an analog for this subset of diagrams. The modification of Eq. (A.13) due to the restriction to 1PI diagrams is, however, not difficult to identify.

Let us consider the graphical analog of the derivation of Eq. (A.13) just outlined. The variation in η may be implemented as a change in the gluon propagator and, in Coulomb gauge, the ghost-gluon interaction, which is also η -dependent. This is the viewpoint that was taken in axial gauge in Ref. [44]. At lowest order in the variation, the modified gluon propagator produces scalar-polarized gluon lines, which decouple through repeated applications of tree-level Ward identities to the sum over all diagrams. The relevant tree-level identities are given in [46]. We need not describe these identities in detail here. We need only note that they are to be applied to any diagram in which a scalar polarized gluon appears at an internal vertex. Every such application produces a sum of diagrams, each of which fall into one of two sets: 1) diagrams in which

an internal gluon line is transformed to a yet another ghost line ending in a scalar polarization, and 2) diagrams in which one gluon line is contracted to a point. The new vertex formed in the former case is the ghost term, and in the latter case it is the ghost-gluon vertex of the BRS variation (A.14). Eq. (A.13) must result from the cancellation of all diagrams, set 2), in which an internal gluon line is contracted. Contracted external lines provide the ghost-gluon terms, and the ghost lines of set 1) eventually provide the ghost terms of the BRS variations (A.14) of external fields in Eq. (A.13).

The simplicity of the tree level Ward identities puts strong limitations on the sets of diagrams that can combine to form different diagrammatic contributions to Eq. (A.13). For diagrams of set 1), the topology of the original diagram is unchanged, and a 1PI diagram remains 1PI. For diagrams of set 2), generally 1PI diagrams remain 1PI, except in the special case of a diagram that is two-particle reducible, with these two lines separated by a single propagator. In this case, the contraction of the internal line that separates the other two will bring those two lines together at a single vertex, producing a diagram precisely of the topology shown in Fig. 2.4. On the one hand, by Eq. (A.13) all such diagrams must cancel in the full perturbative sum. On the other hand, the same topology results from a diagram that is one-particle *reducible* with respect to a single line, which is then contracted as a result of the tree-level Ward identity. The latter diagram, however, is not included in the set of 1PI diagrams with which we work. The application of the Ward identity to 1PI diagrams only, therefore, results in terms that would cancel this special set of one-particle reducible diagrams, in which the only line that spoils irreducibility is contracted to a point. These are the diagrams shown

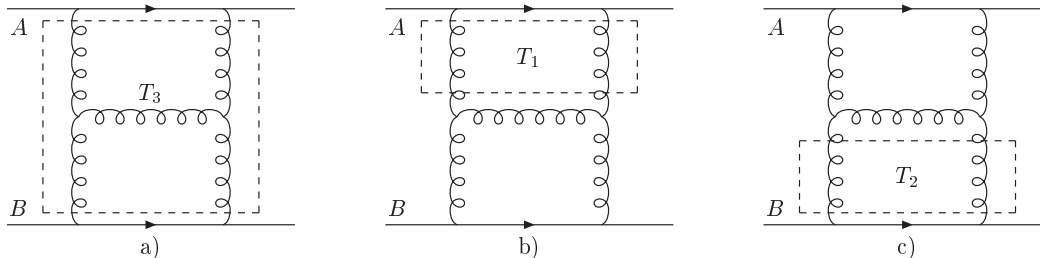


Figure A.1: Two-loop diagram illustrating the idea of the tulip-garden formalism. T_1, T_2, T_3 are the possible tulips.

in Fig. 2.4, in which the ghost-gluon vertex of Eq. (A.14) is inserted between one-particle irreducible subdiagrams in all possible ways. The ghost line ending at this composite vertex is continuously connected to the variation of a gluon propagator, according to Eq. (A.13). The full composite vertex of the Ward identity in Eq. (A.13) appears only at true external lines of the 1PI jet. This vertex is given by the momentum factor in Eq. (2.37) and is represented by the double line crossing a gluon line in Fig. A.2 below. Diagrams that are reducible in one or more internal lines can be treated in a similar manner. The “left-over” terms in the Ward identities for each set of diagrams of definite reducibility properties (1PI, 2PI, etc.), must cancel in the full sum, reproducing the identity for Green functions, Eq. (A.13).

A.3 Tulip-Garden Formalism

In this appendix we illustrate how a given Feynman diagram contributing to the process (2.1) in the leading power can be systematically written in the form (2.27). For concreteness let us consider a two loop diagram where the quarks interact via the exchange of a one rung gluon ladder as in Fig. A.1.

The important contributions of this diagram come from the regions when all of the exchanged gluons are soft, Fig. A.1a or when the gluons attached to the A quark line are soft, while the rest of the gluons carries momenta parallel to the $-$ direction (they belong to jet B), Fig. A.1b, or when the two gluon lines attached to the B quark line are soft and the other gluons are collinear to the $+$ direction (they belong to jet A), Fig. A.1c. The possible central soft exchange parts are called tulips. In our case the possible tulips are denoted as T_1, T_2, T_3 in Fig. A.1. The garden is defined as a nested set of tulips $\{T_1, \dots, T_n\}$ such that $T_i \subset T_{i+1}$ for $i = 1, \dots, n - 1$. In Fig. A.1, $\{T_1\}$, $\{T_2\}$, $\{T_3\}$, $\{T_1, T_3\}$, $\{T_2, T_3\}$ are the possible gardens.

For a given tulip we make the soft approximation, consisting of attaching a soft gluon to jet A via the $-$ component of its polarization only and to jet B via the the $+$ component of its polarization. The result of this soft approximation for a given Feynman diagram F corresponding to a tulip T is denoted $S(T)F$. It has obviously the form of Eq. (2.27). Following the prescription given in Refs. [44] and [16] we write the contribution to a given diagram F in the form

$$F = \sum_G (-1)^{n+1} S(T_1) \dots S(T_n) F + F_R, \quad (\text{A.15})$$

where the sum over inequivalent gardens, as defined bellow, G in Eq. (A.15) is understood. The meaning of this expression is the following. For a given garden consisting of a set of tulips $\{T_1, \dots, T_n\}$, we start with the largest tulip T_n and make the soft approximation for the gluon lines coming out of it. Then for T_{n-1} we proceed the same way as for T_n . If some of the lines coming out of T_{n-1} are identical to the ones coming out of T_n we leave them untouched.

For instance, if we consider a garden $\{T_2, T_3\}$ from Fig. A.1, we first perform the soft approximation on tulip T_3 and then proceed to tulip T_2 . However the lines coming out of T_2 and T_3 which attach to the B quark line are identical so when performing $S(T_2)S(T_3)F$ we leave these gluon lines out of the game and make soft approximations only on the gluon lines attaching to the ladder's rung. Two gardens are equivalent if the soft approximation is identical for both of them. F_R is defined by Eq. (A.15). The contribution to F_R comes from the integration region where $|\vec{k}| \gtrsim \sqrt{s}$ for all gluons coming out of the central soft part. As a result, the contribution to F_R is suppressed by positive powers of $\sqrt{-t}/\sqrt{s}$. Therefore we can ignore the contribution from F_R within the accuracy at which we are working.

We can now rewrite Eq. (A.15), as

$$F = \sum_T \left(\sum_{G, T_n=T} (-1)^{n+1} S(T_1) \dots S(T_{n-1}) \right) S(T) F + F_R. \quad (\text{A.16})$$

This expression is indeed in the form of Eq. (2.27) since the term $S(T)F$ is of that form and the subtractions $\sum(-1)^{n+1}S(T_1)\dots S(T_{n-1})$ modify only the soft function S in Eq. (2.27), but do not alter the form of the equation. We can therefore conclude that the contribution to a given Feynman diagram in leading power can be expressed in the first factorized form given by Eq. (2.27).

A.4 Feynman Rules

In Fig. A.2, we list the Feynman rules for the lines and the vertices encountered in the text. The double lines are eikonal lines, while the dashed lines

$$\begin{aligned}
\begin{array}{c} \overline{\overline{\longrightarrow}} \\ \xrightarrow{k} \end{array} &= \frac{i}{v_{A,B} \cdot k \mp i\epsilon} \\
\begin{array}{c} \text{---} \\ \xrightarrow{k} \end{array} &= \frac{-i}{k \cdot \bar{k} + i\epsilon} \\
\begin{array}{c} \text{---} \\ \xrightarrow{k} \\ \text{---} \end{array} &= -iv^\alpha \\
\begin{array}{c} \text{---} \\ \xrightarrow{k} \\ \text{---} \end{array} &= -i S_\alpha(k) \equiv -i [(\tilde{\eta} \cdot k)\eta_\alpha + (\eta \cdot k)\tilde{\eta}_\alpha] \\
\begin{array}{c} \text{---} \\ \xrightarrow{k} \\ \text{---} \end{array} &= i(k^2 g_{\alpha\beta} - k_\alpha k_\beta) \\
\begin{array}{c} \text{---} \\ \xrightarrow{k} \\ \text{---} \end{array} &= -ig_s f_{abc} g_{\mu\nu} \\
\begin{array}{c} \text{---} \\ \xrightarrow{k} \\ \text{---} \end{array} &= -ig_s f_{abc} g_{\mu\nu} \\
\begin{array}{c} \text{---} \\ \xrightarrow{k} \\ \text{---} \end{array} &= g_s f_{abc} \bar{k}^\mu
\end{aligned}$$

Figure A.2: Feynman rules for the eikonal lines, ghost lines and special vertices.

represent ghosts. The four vectors η , $\tilde{\eta}$ are defined in Eqs. (2.9) and (2.35), respectively. The conventions for the gluon-ghost and gluon-eikonal vertices (third and second from the bottom of Fig. A.2) are the following. We start with a color index of a gluon external to the diagram defining the evolution kernel, see for instance Fig. 3.3a, then proceed to the gluon internal to the diagram and finally to the ghost/eikonal line in order to assign the color indices of f_{abc} . For the three point antighost - gluon - ghost vertex at the bottom of Fig. A.2, we start with an antighost (arrow flowing out of the vertex) then proceed to the ghost and finally we reach the gluon line.

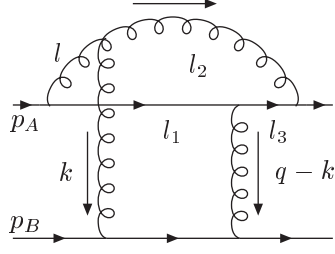


Figure A.3: Two loop diagram demonstrating the origin of the Glauber (Coulomb) region.

A.5 Origin of Glauber Region

In this appendix we exhibit the origin of the Glauber (Coulomb) region using the two-loop diagram shown in Fig. A.3. Consider a situation when the upper gluon loop is a part of J_A . Momentum k of the exchanged gluon flows through jet lines with momenta $l_2 = l - k$ and $l_3 = p_A - l - q + k$. The components of k can be pinched by double poles coming from the denominators of the gluon propagators $k^2 + i\epsilon$ and $(q - k)^2 + i\epsilon$. In addition to these pinches, the component k^- can be pinched by the singularities of the jet lines l_2 and l_3 , at values

$$\begin{aligned}
 k^- &= l^- - \frac{l_{2\perp}^2 - i\epsilon}{2l_2^+}, \\
 k^- &= l^- + \frac{l_{3\perp}^2 - i\epsilon}{2l_3^+}.
 \end{aligned}
 \tag{A.17}$$

The two poles given by Eq. (A.17) are located in opposite half planes since in the region considered $l_2^+, l_3^+ > 0$. This indicates that we must consider the possibility that the different components of the soft momentum k can scale differently. For instance, we can have $k^+ \sim k_\perp \sim \sigma\sqrt{s}$ and $k^- \sim \lambda\sqrt{s}$ where

$\lambda \ll \sigma \ll 1$. Indeed, the power counting performed in Sec. 2.3.2 shows that the singularities originating from these regions can produce a logarithmic enhancement. We also note that it is only minus components that are pinched in this way by the lines in J_A , and plus components by the lines in J_B .

Appendix B

B.1 Symmetry property of the jet functions

Here we prove Eq. (3.45). In order to do so, we first shift the momentum of $\tilde{J}_A^{(n)}$ in the transverse direction: $p_A \rightarrow p_A + q$. This does not effect the logarithmic behavior of the jet function, but it makes easier the comparison of diagrams from $J_A^{(n)}$ and $\tilde{J}_A^{(n)}$.

The general diagram contributing to the jet function $J_A^{(n)}$ has the form shown in Fig. B.1. There are N gluons connecting the quark line to the rest of the diagram, which contains L loops. For every diagram contributing to $J_A^{(n)}$, we identify the corresponding diagram from $\tilde{J}_A^{(n)}$. The guide is that they should be a mirror image of each other, but they should have the same color structure. For instance, in the case of a one loop contribution to $J_A^{(2)}$ shown in Fig. B.2a the related diagram from $\tilde{J}_A^{(2)}$ is the one in Fig. B.2b.

Let us now make a transformation in $\tilde{J}_A^{(n)}(p_A + q, \eta)$:

$$k_i^\pm \rightarrow -k_i^\pm, k_{i\perp} \rightarrow k_{i\perp} \text{ for all } i = 1, \dots, n. \quad (\text{B.1})$$

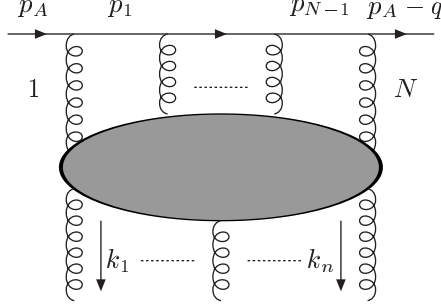


Figure B.1: General class of diagrams contributing to $J_A^{(n)}$.

In the denominators of the propagators this transformation can be compensated by a similar transformation of loop momenta $l_j^\pm \rightarrow -l_j^\pm$ and $l_{j\perp} \rightarrow l_{j\perp}$ for $j = 1, \dots, (L + N - 1)$. The three-point vertices in the L -loop subdiagram generate a factor $(-1)^{v_3}$ under this set of transformations. Using the relationship between the number of loops, vertices and external lines on the L -loop subdiagram:

$$v_3 = N + n + 2(L - v_4 - 1), \quad (\text{B.2})$$

we see that

$$(-1)^{v_3} = (-1)^{N+n}. \quad (\text{B.3})$$

We also have to identify the relationship between the strings of gamma matrices on the fermion line

$$J_A^{(n,0)} \equiv \bar{u}(p_A - q, \lambda_1) \gamma_{\mu_N} \left(\prod_{i=N-1}^1 \not{p}_i \gamma_{\mu_i} \right) u(p_A, \lambda_A), \quad (\text{B.4})$$

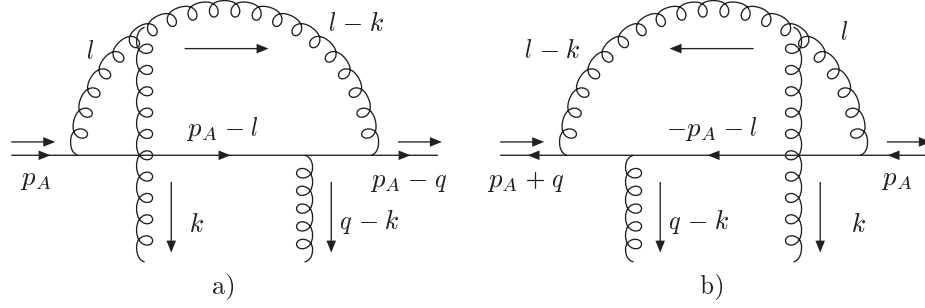


Figure B.2: Identification of a particular one loop diagram between the jet functions $J_A^{(2)}$ and $\tilde{J}_A^{(2)}$.

in $J_A^{(n)}$, and

$$\tilde{J}_A^{(n,0)} \equiv \bar{v}(p_A + q, \lambda_A) \gamma_{\mu_N} \left(\prod_{i=N-1}^1 (-\not{p}_i) \gamma_{\mu_i} \right) v(p_A, \lambda_1), \quad (\text{B.5})$$

in $\tilde{J}_A^{(n)}$. Using the charge conjugation matrix C and its properties, Ref. [51]:

$$\begin{aligned} \gamma_\mu^T &= -C \gamma_\mu C^{-1}, \\ C^T &= -C, \\ \bar{v}_\alpha(p, \lambda) &= (-1)^{\lambda+1/2} C_{\alpha\beta} u_\beta(p, \lambda), \\ \bar{u}_\alpha(p, \lambda) &= (-1)^{\lambda+1/2} C_{\alpha\beta} v_\beta(p, \lambda), \end{aligned} \quad (\text{B.6})$$

we obtain

$$\tilde{J}_A^{(n,0)} = (-1)^N (-1)^{2N-1} (-1)^{\lambda_A+\lambda_1} \bar{u}(p_A, \lambda_1) \left(\prod_{i=1}^{N-1} \gamma_{\mu_i} \not{p}_i \right) \gamma_{\mu_N} u(p_A + q, \lambda_A). \quad (\text{B.7})$$

In the Regge limit, we can neglect the momentum q in the numerators. Since all the momenta p_i are collinear to p_A , $\tilde{J}_A^{(n,0)}$ is symmetric under the exchange of

its external Lorentz indices. Therefore, up to the power-suppressed corrections, we have:

$$\tilde{J}_A^{(n,0)} = (-1)^{N-1} (-1)^{\lambda_A+\lambda_1} J_A^{(n,0)} \quad (\text{B.8})$$

Combining Eqs. (B.3) and (B.8), we immediately recover Eq. (3.45).

B.2 Evolution kernel

In this appendix we provide the calculational details of the results given in Sec. 3.3.2.

The contribution to Fig. 3.9b is:

$$\begin{aligned} \text{Fig. 3.9b} &\equiv ig_s^3 t f_{acb} f_{fbd} f_{cfe} \int \frac{d^D k}{(2\pi)^D} \frac{d^D l}{(2\pi)^D} J_A^{(2)de}(p_A, q; l^+ = 0, l^-, l_\perp) \\ &\times \left(\frac{N^{-\mu}(l)}{l^2} (\bar{l} - \bar{k})_\mu \frac{N^{-\nu}(q-l)}{(q-l)^2} (\bar{q} - \bar{k})_\nu \frac{k^+}{(\bar{l} - \bar{k})^2} \right) (k^+ = 0) \\ &\times \frac{N^{-\rho}(k) S_\rho(k)}{k^2} \frac{1}{k \cdot \bar{k}} \frac{1}{k^- - i\epsilon} \frac{1}{(\bar{q} - \bar{k})^2} = 0. \end{aligned} \quad (\text{B.9})$$

Note that the overall sign in Eq. (B.9) reflects the minus sign explicit in Fig. 3.9b.

We analyze the diagram in Fig. 3.9c in a similar way. It takes the form:

$$\begin{aligned} \text{Fig. 3.9c} &\equiv -ig_s^3 t f_{acb} f_{fbd} f_{cfe} \int \frac{d^D k}{(2\pi)^D} \frac{d^D l}{(2\pi)^D} J_A^{(2)de}(p_A, q; l^+ = 0, l^-, l_\perp) \\ &\times \left(\frac{N^{-\mu}(l)}{l^2} (\bar{l} - \bar{k})_\mu \frac{N^{-+}(q-l)}{(q-l)^2} \frac{1}{(\bar{l} - \bar{k})^2} \right) (k^+ = 0) \\ &\times \frac{N^{-\rho}(k) S_\rho(k)}{k^2} \frac{1}{k \cdot \bar{k}} \frac{1}{k^- - i\epsilon}. \end{aligned} \quad (\text{B.10})$$

Note, again, that the overall sign in Eq. (B.10) reflects the minus sign explicit in Fig. 3.9c. The imaginary part of the eikonal propagator in Eq. (B.10) gives vanishing contribution since the resulting integrand is an odd function under $k^+ \rightarrow -k^+$. Hence only the principal value part contributes. In the Glauber region, $l^- \ll l^+ \sim l_\perp$, the integral vanishes due to the antisymmetry of the integrand under the transformation $l^+ \rightarrow -l^+$, $k^\pm \rightarrow -k^\pm$. In the region $l^- \sim l^+ \sim l_\perp$ we can factor the gluon with momentum l from the jet $J_A^{(2)}$.

The contribution to Fig. 3.10a from a G gluon with momentum k corresponding to the first term in Eq. (3.50) and to Fig. 3.8a is:

$$\begin{aligned} (\text{Fig. 3.10a})_G &\equiv g_s^2 t f_{ade} f_{ebc} \int \frac{d^D k}{(2\pi)^D} \frac{d^D l}{(2\pi)^D} S_G(k, l, q) \\ &\times J_A^{(3) bcd}(p_A, q; k^+ = 0, k^-, k_\perp, l^+ = 0, l^-, l_\perp), \end{aligned} \quad (\text{B.11})$$

with the soft function S_G in Eq. (B.11) defined as

$$\begin{aligned} S_G(k, l, q) &\equiv \left(\frac{N^{-\mu}(l)}{l^2} V_{\mu\rho\nu}(l, -k, k-l) \frac{N^{\nu-}(k-l)}{(k-l)^2} \left(g^{\rho+} - \frac{k^\rho}{k^-} \right) \right) (k^+ = 0) \\ &\times \frac{N^{-\alpha}(k)}{k^2} \frac{S_\alpha(k)}{k \cdot \bar{k}} \frac{N^{-+}(q-k)}{(q-k)^2}. \end{aligned} \quad (\text{B.12})$$

Since, by construction $k^- \sim k^+ \sim k_\perp$ for an external G gluon with momentum k , we can factor the gluon with momentum $q-k$ from $J_A^{(3)}$ in Fig. 3.10a. Then the resulting integrand in Eq. (B.11); $S_G(k, l, q)/k^-$, with S_G defined in Eq. (B.12); is an antisymmetric function under the transformation $k^\pm \rightarrow -k^\pm$, $l^+ \rightarrow -l^+$ in the Glauber region $l^- \ll l^+ \sim l_\perp$. This indicates that the gluon with momentum l can be factored from $J_A^{(3)}$. Therefore the contribution to Fig. 3.10a from a G gluon agrees with a gluon reggeization at NLL.

The contribution to Fig. 3.10c is:

$$\begin{aligned}
(\text{Fig. 3.10c})_G &\equiv ig_s^3 t f_{acb} f_{fdb} f_{cfe} \times \int \frac{d^D k}{(2\pi)^D} \frac{d^D l}{(2\pi)^D} J_A^{(2)de}(p_A, q; l^+ = 0, l^-, l_\perp) \\
&\times \left[\frac{N^{-\mu}(l)}{l^2} V_{\mu\rho\sigma}(l, -k, k-l) \left(g^{\rho+} - \frac{k^\rho}{k^-} \right) \frac{N^{\sigma\lambda}(l-k)}{(l-k)^2} \right. \\
&\times V_{\nu\lambda-}(q-l, l-k, k-q) \frac{N^{\nu-}(q-l)}{(q-l)^2} \left. \right] (k^+ = 0) \\
&\times \frac{N^{-\alpha}(k)}{k^2} \frac{S_\alpha(k)}{k \cdot \bar{k}} \frac{N^{-+}(q-k)}{(q-k)^2}. \tag{B.13}
\end{aligned}$$

In the Glauber region the l^+ integral vanishes due to the antisymmetry of the integrand. In the region $l^- \sim l^+ \sim l_\perp$ the gluon with momentum l factors out and the contribution takes a factorized form.

The diagram in Fig. 3.10d for a G gluon with momentum k is:

$$\begin{aligned}
(\text{Fig. 3.10d})_G &\equiv -ig_s^3 t f_{aed} \times \int \frac{d^D k}{(2\pi)^D} \frac{d^D l}{(2\pi)^D} J_A^{(2)bc}(p_A, q; l^+ = 0, l^-, l_\perp) \\
&\times \frac{N^{-\mu}(q-l)}{(q-l)^2} W_{\mu\rho-\nu}^{bedc} \left(g^{\rho+} - \frac{k^\rho}{k^-} \right) (k^+ = 0) \frac{N^{\nu-}(l)}{l^2} \\
&\times \frac{N^{-\alpha}(k)}{k^2} \frac{S_\alpha(k)}{k \cdot \bar{k}} \frac{N^{-+}(q-k)}{(q-k)^2}, \tag{B.14}
\end{aligned}$$

where

$$\begin{aligned}
W_{\mu\rho-\nu}^{bedc} &\equiv f_{pbe} f_{pdc} (g_{\mu-} g_{\rho\nu} - g_{\mu\nu} g_{\rho-}) + f_{pbd} f_{pce} (g_{\mu\nu} g_{\rho-} - g_{\mu\rho} g_{\nu-}) \\
&+ f_{pbc} f_{ped} (g_{\mu\rho} g_{\nu-} - g_{\mu-} g_{\rho\nu}), \tag{B.15}
\end{aligned}$$

is the Lorentz and the color part of the four point gluon vertex. In the Glauber region the integral over l^+ vanishes due to the antisymmetry of the integrand

in Eq. (B.14). In the region $l^- \sim l^+ \sim l_\perp$ we can factor the gluon with momentum l from the jet function $J_A^{(2)}$. Therefore the contribution from Fig. 3.10d is in accordance with gluon reggeization.

The contribution to Fig. 3.10a from the second term in Eq. (3.50) used in Eq. (3.49) is:

$$\begin{aligned} (\text{Fig. 3.10a})_{\text{soft}} &\equiv g_s^2 t f_{ade} f_{ebc} \int \frac{d^D k}{(2\pi)^D} \frac{d^D l}{(2\pi)^D} S_s^{(a)}(k, l, q) \\ &\times J_A^{(3) bcd}(p_A, q; k^+ = 0, k^-, k_\perp, l^+ = 0, l^-, l_\perp), \end{aligned} \quad (\text{B.16})$$

with the soft function $S_s^{(a)}$ defined by

$$\begin{aligned} S_s^{(a)}(k, l, q) &\equiv \left[\left(\frac{N^{-\mu}(l)}{l^2} V_{\mu\rho\nu}(l, -k, k-l) \frac{N^{\nu-}(k-l)}{(k-l)^2} \right) (k^+) - \right. \\ &\quad \left. \left(\frac{N^{-\mu}(l)}{l^2} V_{\mu\rho\nu}(l, -k, k-l) \frac{N^{\nu-}(k-l)}{(k-l)^2} \right) (k^+ = 0) \right] \\ &\times \frac{N^{-\alpha}(k)}{k^2} \frac{S_\alpha(k)}{k \cdot \bar{k}} \frac{N^{-+}(q-k)}{(q-k)^2}. \end{aligned} \quad (\text{B.17})$$

Eqs. (B.16) and (B.17) immediately follow from Eqs. (B.11) and (B.12). We apply the following identity

$$\begin{aligned} S(l^-, k^-) &= S(l^- = 0, k^- = 0) \theta(M - |l^-|) \theta(M - |k^-|) \\ &+ [S(l^-, k^- = 0) - S(l^- = 0, k^- = 0) \theta(M - |l^-|)] \theta(M - |k^-|) \\ &+ [S(l^- = 0, k^-) - S(l^- = 0, k^- = 0) \theta(M - |k^-|)] \theta(M - |l^-|) \\ &+ [\{S(l^-, k^-) - S(l^-, k^- = 0) \theta(M - |k^-|)\} - \\ &\quad \{S(l^- = 0, k^-) - S(l^- = 0, k^- = 0) \theta(M - |k^-|)\} \theta(M - |l^-|)], \end{aligned} \quad (\text{B.18})$$

to the soft function $S_s^{(a)}$, Eq. (B.17), to analyze the contribution to Eq. (B.16). After using the first term of Eq. (B.18) for the soft function $S_s^{(a)}$ in Eq. (B.16), we arrive at

$$\begin{aligned}
(\text{Fig. 3.10a})_{\text{soft}}^{(1)} &\equiv g_s^2 t f_{ade} f_{ebc} \int \frac{d^{D-2}k_\perp}{(2\pi)^D} \frac{d^{D-2}l_\perp}{(2\pi)^D} \\
&\times \left(\int dk^+ dl^+ S_s^{(a)}(k^+, l^+, k^- = 0, l^- = 0, k_\perp, l_\perp, q) \right) \\
&\times \Gamma_A^{(3)bcd}(p_A, q; k_\perp, l_\perp). \tag{B.19}
\end{aligned}$$

Performing the k^+ and l^+ integrals, we obtain

$$\begin{aligned}
(\text{Fig. 3.10a})_{\text{soft}}^{(1)} &\equiv -\frac{\alpha_s}{8\pi} t f_{ade} f_{ebc} \int \frac{d^{D-2}k_\perp}{(2\pi)^{D-2}} \frac{d^{D-2}l_\perp}{(2\pi)^{D-2}} \frac{(|k_\perp| - |q_\perp - k_\perp - l_\perp|)}{|k_\perp|^2 |q_\perp - k_\perp - l_\perp|^2} \\
&\times \frac{(|k_\perp| - |q_\perp - l_\perp| + |q_\perp - k_\perp - l_\perp|)(|k_\perp| + |l_\perp| + 2|q_\perp - l_\perp| + |q_\perp - k_\perp - l_\perp|)}{|q_\perp - l_\perp| (|l_\perp| + |q_\perp - l_\perp|)^2 (|k_\perp| + |l_\perp| + |q_\perp - k_\perp - l_\perp|)} \\
&\times \frac{1}{(|k_\perp| + |q_\perp - l_\perp| + |q_\perp - k_\perp - l_\perp|)} \Gamma_A^{(3)bcd}(p_A, q; k_\perp, l_\perp). \tag{B.20}
\end{aligned}$$

When analyzing the second (third) term in Eq. (B.18), after used in Eq. (B.16), we can factor the gluon with momentum l (k) from the jet function $J_A^{(3)}$. The resulting l^\pm , k^+ (k^\pm , l^+) integral is over an antisymmetric function under the transformation $l^\pm \rightarrow -l^\pm$, $k^+ \rightarrow -k^+$ ($k^\pm \rightarrow -k^\pm$, $l^+ \rightarrow -l^+$) and therefore it vanishes. In the case of the last term in Eq. (B.18), we can factor both gluons with momenta k and l from the jet $J_A^{(3)}$. So this part is in agreement with gluon reggeization.

The contribution to Fig. 3.10b from the second term in Eq. (3.50) used in

Eq. (3.49) is:

$$\begin{aligned}
(\text{Fig. 3.10b})_{\text{soft}} &\equiv -g_s^2 t f_{aeb} f_{ced} \int \frac{d^D k}{(2\pi)^D} \frac{d^D l}{(2\pi)^D} S_s^{(b)}(k, l, q) \\
&\times J_A^{(3) bcd}(p_A, q; k^+ = 0, k^-, k_\perp, l^+ = 0, l^-, l_\perp),
\end{aligned} \tag{B.21}$$

with the soft function $S_s^{(b)}(k, l, q)$ defined by

$$\begin{aligned}
S_s^{(b)}(k, l, q) &\equiv \left[\left(\frac{N^{-\mu}(k-l)}{(k-l)^2} V_{\mu-\nu}(k-l, l-q, q-k) \frac{N^{\nu-}(q-k)}{(q-k)^2} \right) (k^+) - \right. \\
&\quad \left. \left(\frac{N^{-\mu}(k-l)}{(k-l)^2} V_{\mu-\nu}(k-l, l-q, q-k) \frac{N^{\nu-}(q-k)}{(q-k)^2} \right) (k^+ = 0) \right] \\
&\times \frac{N^{-\alpha}(l)}{l^2} \frac{S_\alpha(l)}{l \cdot \bar{l}} \frac{N^{-+}(q-l)}{(q-l)^2}.
\end{aligned} \tag{B.22}$$

We apply the identity (B.18) to the soft function $S_s^{(b)}$, Eq. (B.22), to analyze the contribution to Eq. (B.21). After using the first term of Eq. (B.18) in Eq. (B.21), we arrive at a contribution

$$\begin{aligned}
(\text{Fig. 3.10b})_{\text{soft}}^{(1)} &\equiv -g_s^2 t f_{aeb} f_{ced} \int \frac{d^{D-2} k_\perp}{(2\pi)^D} \frac{d^{D-2} l_\perp}{(2\pi)^D} \\
&\times \left(\int dk^+ dl^+ S_s^{(b)}(k^+, l^+, k^- = 0, l^- = 0, k_\perp, l_\perp, q) \right) \\
&\times \Gamma_A^{(3) bcd}(p_A, q; k_\perp, l_\perp).
\end{aligned} \tag{B.23}$$

Performing the k^+ and l^+ integrals, we obtain

$$\begin{aligned}
(\text{Fig. 3.10b})_{\text{soft}}^{(1)} &\equiv \frac{\alpha_s}{8\pi} t f_{abe} f_{edc} \int \frac{d^{D-2}k_{\perp}}{(2\pi)^D} \frac{d^{D-2}l_{\perp}}{(2\pi)^D} \\
&\times \frac{(2|k_{\perp}| + |l_{\perp}| + |q_{\perp} - k_{\perp}| + |q_{\perp} - k_{\perp} - l_{\perp}|)}{|k_{\perp}| |l_{\perp}|^2 |q_{\perp} - k_{\perp} - l_{\perp}|^2 (|l_{\perp}| + |q_{\perp} - k_{\perp}| + |q_{\perp} - k_{\perp} - l_{\perp}|)} \\
&\times \frac{(|l_{\perp}|^3 - |l_{\perp}| (|q_{\perp} - k_{\perp}|^2 + |q_{\perp} - k_{\perp} - l_{\perp}|^2) - 2|q_{\perp} - k_{\perp}|^2 |q_{\perp} - k_{\perp} - l_{\perp}|)}{(|k_{\perp}| + |l_{\perp}| + |q_{\perp} - k_{\perp} - l_{\perp}|)^2 (|k_{\perp}| + |q_{\perp} - k_{\perp}|)^2} \\
&\times \Gamma_A^{(3) bcd}(p_A, q; k_{\perp}, l_{\perp}). \tag{B.24}
\end{aligned}$$

When analyzing the second (third) term in Eq. (B.18), when applied to Eq. (B.21), we can factor the gluon with momentum l (k) from the jet function $J_A^{(3)}$. The resulting l^{\pm} , k^+ (k^{\pm} , l^+) integral is over a function antisymmetric under the transformation $l^{\pm} \rightarrow -l^{\pm}$, $k^+ \rightarrow -k^+$ ($k^{\pm} \rightarrow -k^{\pm}$, $l^+ \rightarrow -l^+$) and therefore it vanishes. In the case of the last term in Eq. (B.18), we can factor both gluons with momenta k and l from the jet $J_A^{(3)}$. So this part is in agreement with the gluon reggeization.

The contribution to Fig. 3.10c from the second term in Eq. (3.50) used in Eq. (3.49) is:

$$\begin{aligned}
(\text{Fig. 3.10c})_{\text{soft}} &\equiv i g_s^3 t f_{acb} f_{fbd} f_{cfe} \times \int \frac{d^D k}{(2\pi)^D} \frac{d^D l}{(2\pi)^D} J_A^{(2) de}(p_A, q; l^+ = 0, l^-, l_{\perp}) \\
&\times \left[\left(\frac{N^{-\mu}(l)}{l^2} V_{\mu-\sigma}(l, -k, k-l) \frac{N^{\sigma\lambda}(l-k)}{(l-k)^2} V_{\nu\lambda-}(q-l, l-k, k-q) \frac{N^{\nu-}(q-l)}{(q-l)^2} \right) (k^+) \right. \\
&- \left. \left(\frac{N^{-\mu}(l)}{l^2} V_{\mu-\sigma}(l, -k, k-l) \frac{N^{\sigma\lambda}(l-k)}{(l-k)^2} V_{\nu\lambda-}(q-l, l-k, k-q) \frac{N^{\nu-}(q-l)}{(q-l)^2} \right) (k^+ = 0) \right] \\
&\times \frac{N^{-\alpha}(k)}{k^2} \frac{S_{\alpha}(k)}{k \cdot \bar{k}} \frac{N^{-+}(q-k)}{(q-k)^2}. \tag{B.25}
\end{aligned}$$

This follows immediately from Eq. (B.13). In the Glauber region, $l^- \ll l^+ \sim l_\perp$, the integrand is an antisymmetric function of k^\pm and l^+ and therefore the k^\pm, l^+ integral vanishes. In the region $l^- \sim l^+ \sim l_\perp$, we can factor the gluon with momentum l from the jet function $J_A^{(2)}$. Hence this contribution is in agreement with gluon reggeization.

The contribution to Fig. 3.10a from the third term in Eq. (3.50) used in Eq. (3.49) is:

$$\begin{aligned}
(\text{Fig. 3.10a})_{\text{soft}'} &\equiv g_s^2 t f_{ade} f_{ebc} \int \frac{d^D k}{(2\pi)^D} \frac{d^D l}{(2\pi)^D} S_{s'}^{(a)} \\
&\times J_A^{(3) bcd}(p_A, q; k^+ = 0, k^-, k_\perp, l^+ = 0, l^-, l_\perp),
\end{aligned} \tag{B.26}$$

with the soft function $S_{s'}^{(a)}$ defined by

$$\begin{aligned}
S_{s'}^{(a)} &\equiv \frac{N^{-\mu}(l)}{l^2} (V_{\mu\rho\nu}(l, -k, k-l) - g_{+\rho} V_{\mu-\nu}(l, -k, k-l)) \frac{N^{\nu-}(k-l)}{(k-l)^2} \\
&\times \frac{N^{\rho\alpha}(k)}{k^2} \frac{S_\alpha(k)}{k \cdot \bar{k}} \frac{N^{-+}(q-k)}{(q-k)^2}.
\end{aligned} \tag{B.27}$$

This follows immediately from Eqs. (B.11) and (B.12). We apply the identity (B.18) to the soft function $S_{s'}^{(a)}$, Eq. (B.27), to analyze the contribution to Eq. (B.26). After using the first term of Eq. (B.18) in Eq. (B.26), we arrive at

$$\begin{aligned}
(\text{Fig. 3.10a})_{\text{soft}'}^{(1)} &\equiv g_s^2 t f_{ade} f_{ebc} \int \frac{d^{D-2} k_\perp}{(2\pi)^D} \frac{d^{D-2} l_\perp}{(2\pi)^D} \\
&\times \left(\int dk^+ dl^+ S_{s'}^{(a)}(k^+, l^+, k^- = 0, l^- = 0, k_\perp, l_\perp, q) \right) \\
&\times \Gamma_A^{(3) bcd}(p_A, q; k_\perp, l_\perp).
\end{aligned} \tag{B.28}$$

The integrand $S_{s'}^{(a)}$ in Eq. (B.28) is an antisymmetric function of l^+ and k^+ and therefore the integral over k^+ and l^+ in Eq. (B.28) vanishes. In order to show this antisymmetry, we have used that the component

$$N^{+\alpha}(k^- = 0, k^+, k_\perp) S_\alpha(k^- = 0, k^+, k_\perp) = 0, \quad (\text{B.29})$$

in the Glauber region, $k^- \sim 0$. We have also used the Ward identity

$$l^\mu k^\rho V_{\mu\rho\nu}(l, -k, k-l)(k-l)^\nu = 0, \quad (\text{B.30})$$

when analyzing the contribution from the transverse polarization of the gluon with momentum k in Fig. 3.10a. When studying the second (third) term in Eq. (B.18), after applied to Eq. (B.26), we can factor the gluon with momentum l (k) from the jet function $J_A^{(3)}$. The resulting l^\pm, k^+ (k^\pm, l^+) integral is over an antisymmetric function under the transformation $l^\pm \rightarrow -l^\pm, k^+ \rightarrow -k^+$ ($k^\pm \rightarrow -k^\pm, l^+ \rightarrow -l^+$) and therefore it vanishes. In the case of the last term in Eq. (B.18), we can factor both gluons with momenta k and l from the jet $J_A^{(3)}$. Therefore the contribution from (Fig. 3.10a)_{soft'}, Eq. (B.26), is in an agreement with gluon reggeization at NLL.

The contribution to Fig. 3.10b from the third term in Eq. (3.50) used in Eq. (3.49) is:

$$\begin{aligned} (\text{Fig. 3.10b})_{\text{soft}'} &\equiv -g_s^2 t f_{acb} f_{ced} \int \frac{d^D k}{(2\pi)^D} \frac{d^D l}{(2\pi)^D} S_{s'}^{(b)} \\ &\times J_A^{(3) bcd}(p_A, q; k^+ = 0, k^-, k_\perp, l^+ = 0, l^-, l_\perp), \quad (\text{B.31}) \end{aligned}$$

with the soft function $S_{s'}^{(b)}$ defined by

$$\begin{aligned}
S_{s'}^{(b)} &\equiv \frac{N^{-\mu}(k-l)}{(k-l)^2} (V_{\mu\rho\nu}(k-l, l-q, q-k) - g_{+\rho} V_{\mu-\nu}(k-l, l-q, q-k)) \\
&\times \frac{N^{\nu-}(q-k)}{(q-k)^2} \frac{N^{-\alpha}(l)}{l^2} \frac{S_\alpha(l)}{l \cdot \bar{l}} \frac{N^{\rho+}(q-l)}{(q-l)^2}.
\end{aligned} \tag{B.32}$$

This follows from Eqs. (B.21) and (B.22). We apply the identity (B.18) to the soft function, Eq. (B.32), to analyze the contribution to Eq. (B.31). After using the first term of Eq. (B.18) in Eq. (B.31), we arrive at

$$\begin{aligned}
(\text{Fig. 3.10b})_{\text{soft}}^{(1)} &\equiv -g_s^2 t f_{acb} f_{ced} \int \frac{d^{D-2}k_\perp}{(2\pi)^D} \frac{d^{D-2}l_\perp}{(2\pi)^D} \\
&\times \left(\int dk^+ dl^+ S_{s'}^{(b)}(k^+, l^+, k^- = 0, l^- = 0, k_\perp, l_\perp, q) \right) \\
&\times \Gamma_A^{(3) bcd}(p_A, q; k_\perp, l_\perp).
\end{aligned} \tag{B.33}$$

The integrand $S_{s'}^{(b)}$ in Eq. (B.33) is an antisymmetric function of l^+ and k^+ and therefore the integral over k^+ and l^+ in Eq. (B.33) vanishes. In order to show this antisymmetry, we have used that the component $N^{++}(q-l) = 0$ in the Glauber region, $l^- \sim 0$. We have also used the Ward identity

$$(k-l)^\mu (l-q)^\rho V_{\mu\rho\nu}(k-l, l-q, q-k) (q-k)^\nu = 0, \tag{B.34}$$

when analyzing the contribution from the transverse polarization of the gluon with momentum $q-l$ in Fig. 3.10b. When analyzing the second (third) term in Eq. (B.18), applied to Eq. (B.31), we can factor the gluon with momentum l (k) out the jet function $J_A^{(3)}$. The resulting l^\pm, k^+ (k^\pm, l^+) integral is over an antisymmetric function under the transformation $l^\pm \rightarrow -l^\pm, k^+ \rightarrow -k^+$

($k^\pm \rightarrow -k^\pm$, $l^+ \rightarrow -l^+$) and therefore it vanishes. In the case of the last term in Eq. (B.18), we can factor both gluons with momenta k and l from the jet $J_A^{(3)}$. Therefore the contribution from (Fig. 3.10b)_{soft'}, Eq. (B.31), is in an agreement with gluon reggeization at NLL.

The contribution to Fig. 3.10c from the third term in Eq. (3.50) used in Eq. (3.49) is:

$$\begin{aligned}
(\text{Fig. 3.10c})_{\text{soft}'} &\equiv ig_s^3 t f_{acb} f_{fdb} f_{cfe} \times \int \frac{d^D k}{(2\pi)^D} \frac{d^D l}{(2\pi)^D} \\
&\times J_A^{(2)de}(p_A, q; l^+ = 0, l^-, l_\perp) \frac{N^{-\mu}(l)}{l^2} \\
&\times (V_{\mu\beta\sigma}(l, -k, k-l) - g_{-\beta} V_{\mu-\sigma}(l, -k, k-l)) \frac{N^{\sigma\lambda}(l-k)}{(l-k)^2} \\
&\times (V_{\nu\lambda\gamma}(q-l, l-k, k-q) - g_{-\gamma} V_{\nu\lambda-}(q-l, l-k, k-q)) \\
&\times \frac{N^{\nu-}(q-l)}{(q-l)^2} \frac{N^{\beta\alpha}(k)}{k^2} \frac{S_\alpha(k)}{k \cdot \bar{k}} \frac{N^{\gamma+}(q-k)}{(q-k)^2}. \tag{B.35}
\end{aligned}$$

In the Glauber region, $l^- \ll l^+ \sim l_\perp$, the integrand is an antisymmetric function of k^\pm and l^+ and therefore the k^\pm, l^+ integral vanishes. In the region $l^- \sim l^+ \sim l_\perp$, we can factor the gluon with momentum l out the jet function $J_A^{(2)}$. Hence this contribution is in agreement with gluon reggeization.

The diagram in Fig. 3.10d from the third term in Eq. (3.50) used in Eq. (3.49) is:

$$\begin{aligned}
(\text{Fig. 3.10d})_{\text{soft}'} &\equiv -ig_s^3 t f_{aed} \times \int \frac{d^D k}{(2\pi)^D} \frac{d^D l}{(2\pi)^D} J_A^{(2)bc}(p_A, q; l^+ = 0, l^-, l_\perp) \\
&\times \frac{N^{-\mu}(q-l)}{(q-l)^2} (W_{\mu\rho\sigma\nu}^{bedc} - g_{-\rho} g_{-\sigma} W_{\mu--\nu}^{bedc}) \frac{N^{\nu-}(l)}{l^2} \frac{N^{\rho\alpha}(k)}{k^2} \\
&\times \frac{S_\alpha(k)}{k \cdot \bar{k}} \frac{N^{\sigma+}(q-k)}{(q-k)^2}, \tag{B.36}
\end{aligned}$$

In the Glauber region, $l^- \ll l^+ \sim l_\perp$, the integrand is an antisymmetric function of k^\pm and l^+ and therefore the k^\pm, l^+ integral vanishes. In the region $l^- \sim l^+ \sim l_\perp$, we can factor the gluon with momentum l out the jet function $J_A^{(2)}$. Hence this contribution is in agreement with gluon reggeization.

The contribution from the first term in Eq. (3.51) is:

$$\begin{aligned}
(\text{Fig. 3.8c})_{\text{jet}} &\equiv g_s^2 t f_{ade} f_{ebc} \int \frac{d^D k}{(2\pi)^D} \frac{d^D l}{(2\pi)^D} S_{\text{jet}}(k, l, q) \\
&\times J_A^{(3) bcd}(p_A, q; k^+ = 0, k^-, k_\perp, l^+ = 0, l^-, l_\perp),
\end{aligned} \tag{B.37}$$

with a soft function S_{jet} defined

$$S_{\text{jet}}(k, l, q) \equiv \frac{N^{-\mu}(k)}{k^2} \frac{S_\mu(k)}{k \cdot \bar{k}} \frac{N^{-\alpha}(q-l-k)}{(q-l-k)^2} \frac{(\bar{q}-\bar{l})_\alpha}{(l-q) \cdot (\bar{l}-\bar{q})} \frac{N^{-+}(l)}{l^2}. \tag{B.38}$$

Next we use an identity (B.18) for $S_{\text{jet}}(k^-, l^-)$, defined in Eq. (B.38). After performing the k^+ and l^+ integrals in the first term of Eq. (B.18), when used

in Eq. (B.37), we obtain the following contribution:

$$\begin{aligned}
(\text{Fig. 3.8c})_{\text{jet}}^{(1)} &\equiv -\frac{\alpha_s}{8\pi} t f_{ade} f_{ebc} \int \frac{d^{D-2}k_{\perp}}{(2\pi)^{D-2}} \frac{d^{D-2}l_{\perp}}{(2\pi)^{D-2}} \Gamma_A^{(3) bcd}(p_A, q; k_{\perp}, l_{\perp}) \\
&\times \left[\frac{(|k_{\perp}| + |l_{\perp}| + |q_{\perp} - l_{\perp}| + 2|q_{\perp} - k_{\perp} - l_{\perp}|)}{(|k_{\perp}| |q_{\perp} - k_{\perp} - l_{\perp}| (|l_{\perp}| + |q_{\perp} - l_{\perp}|) (|k_{\perp}| + |q_{\perp} - k_{\perp}| + |q_{\perp} - k_{\perp} - l_{\perp}|)^2)} \right. \\
&\times \frac{(|k_{\perp}|^2 - |q_{\perp} - l_{\perp}|^2 + |q_{\perp} - k_{\perp} - l_{\perp}|^2)}{(|k_{\perp}| + |q_{\perp} - l_{\perp}| + |q_{\perp} - k_{\perp} - l_{\perp}|)^2 |q_{\perp} - k_{\perp} - l_{\perp}|^2} \\
&+ \left(\frac{|l_{\perp}| + 2|q_{\perp} - k_{\perp} - l_{\perp}|}{(|l_{\perp}| + |q_{\perp} - k_{\perp} - l_{\perp}|) (|k_{\perp}| + |l_{\perp}| + |q_{\perp} - k_{\perp} - l_{\perp}|)^2} \right. \\
&\left. \left. - \frac{|q_{\perp} - l_{\perp}| + 2|q_{\perp} - k_{\perp} - l_{\perp}|}{(|q_{\perp} - l_{\perp}| + |q_{\perp} - k_{\perp} - l_{\perp}|) (|k_{\perp}| + |q_{\perp} - l_{\perp}| + |q_{\perp} - k_{\perp} - l_{\perp}|)^2} \right) \right. \\
&\left. \times \frac{(|k_{\perp}|^2 - |q_{\perp} - l_{\perp}|^2 - |q_{\perp} - k_{\perp} - l_{\perp}|^2)}{|k_{\perp}| (|l_{\perp}|^2 - |q_{\perp} - l_{\perp}|^2) |q_{\perp} - k_{\perp} - l_{\perp}|^3} \right]. \tag{B.39}
\end{aligned}$$

In the second (third) term of Eq. (B.18), we can factor the gluon with momentum l (k) from the jet function $J_A^{(3)}$. The resulting l^{\pm} , k^{\pm} (k^{\pm} , l^{\pm}) integrals are over antisymmetric functions and therefore they vanish. In the last term of Eq. (B.18), we can factor both gluons with momenta k and l from the jet function $J_A^{(3)}$. Hence this contribution is in a factorized form, in agreement with the gluon reggeization.

The contribution to the second term in Eq. (3.51) comes from a diagram in Fig. 3.10e:

$$\begin{aligned}
\text{Fig. 3.10e} &= ig_s^3 t f_{aeb} f_{bcf} f_{fdc} \times \int \frac{d^D k}{(2\pi)^D} \frac{d^D l}{(2\pi)^D} J_A^{(2) de}(p_A, q; l^+ = 0, l^-, l_{\perp}) \\
&\times \frac{N^{-\mu}(q-l)}{(q-l)^2} V_{\mu\nu\rho}(q-l, -k, k+l-q) \frac{N^{\nu\alpha}(k)}{k^2} \frac{S_{\alpha}(k)}{k \cdot k} \\
&\times \frac{N^{\rho\sigma}(q-l-k)}{(q-l-k)^2} \frac{(\bar{l}-\bar{q})_{\sigma}}{(l-q) \cdot (\bar{l}-\bar{q})} \frac{N^{-+}(l)}{l^2}. \tag{B.40}
\end{aligned}$$

In the Glauber region $l^- \ll l^+ \sim l_{\perp}$, the integrand is an antisymmetric function

under the transformation $k^\pm \rightarrow -k^\pm$ and $l^+ \rightarrow -l^+$, so the integral over k^\pm and l^+ vanishes. In the region $l^- \sim l^+ \sim l_\perp$ we can factor the gluon with momentum l from the jet function $J_A^{(2)}$ using the K - G decomposition. Therefore the contribution from Fig. 3.10e takes a factorized form.

The same reasoning applies to the diagram in Fig. 3.10f, which is due to the third term in Eq. (3.51):

$$\begin{aligned}
\text{Fig. 3.10f} &= ig_s^3 t f_{abc} f_{cdf} f_{fbe} \times \int \frac{d^D k}{(2\pi)^D} \frac{d^D l}{(2\pi)^D} J_A^{(2)de}(p_A, q; k^+ = 0, k^-, k_\perp) \\
&\times \frac{N^{-\alpha}(k)}{k^2} \frac{S_\alpha(k)}{k \cdot \bar{k}} \frac{N^{-\mu}(q-k)}{(q-k)^2} V_{\mu\nu\rho}(q-k, k+l-q, -l) \frac{N^{\rho+}(l)}{l^2} \\
&\times \frac{N^{\nu\sigma}(q-l-k)}{(q-l-k)^2} \frac{(\bar{l}-\bar{q})_\sigma}{(l-q) \cdot (\bar{l}-\bar{q})}. \tag{B.41}
\end{aligned}$$

It also factorizes in agreement with the gluon reggeization hypothesis.

Appendix C

C.1 Eikonal Example

In this appendix, we give details of the calculation of the logarithmic behavior in the diagrams of Fig. 4.3. We choose the reference frame such that the momenta of the final state particles are given by:

$$\begin{aligned}\beta_1 &= (1, 0, 0, 1), \\ \beta_2 &= (1, 0, 0, -1), \\ l &= \omega_l(1, s_l, 0, c_l), \\ k &= \omega_k(1, s_k \cos \phi, s_k \sin \phi, c_k).\end{aligned}\tag{C.1}$$

Here we define $s_{l,k} \equiv \sin \theta_{l,k}$ and $c_{l,k} \equiv \cos \theta_{l,k}$. θ_l is the angle between the vectors \vec{l} and $\vec{\beta}_1$, θ_k is the angle between the vectors \vec{k} and $\vec{\beta}_1$ and ϕ is the azimuthal angle of the gluon with momentum k relative to the plane defined by β_1 , β_2 and l . The available phase space in polar angle for the radiated gluons is $\theta_k \in (\pi/2 - \delta, \pi/2 + \delta)$ and $\theta_l \in (0, \pi/2 - \delta) \cup (\pi/2 + \delta, \pi)$.

Using the diagrammatic rules for eikonal lines and vertices, as listed for ex-

ample in [8], we can write down the expressions corresponding to each diagram separately. For example, diagram 4.3 a) gives

$$\begin{aligned}
a) + (k \leftrightarrow l) &= [f_{abc} \text{Tr}(t_a t_b t_c)] \left(-ig_s^4 \beta_1^\alpha \beta_2^\beta \beta_1^\gamma \right) V_{\alpha\beta\gamma}(k+l, -k, -l) \\
&\times \frac{1}{\beta_1 \cdot (k+l)} \frac{1}{2k \cdot l} \frac{1}{\beta_1 \cdot l} \frac{1}{\beta_2 \cdot k} \\
&+ (k \leftrightarrow l). \tag{C.2}
\end{aligned}$$

$V_{\alpha\beta\gamma}(k+l, -k, -l) = [(2k+l)_\gamma g_{\alpha\beta} + (l-k)_\alpha g_{\beta\gamma} - (2l+k)_\beta g_{\alpha\gamma}]$ is the momentum-dependent part of the three gluon vertex. Using the color identity $f_{abc} \text{Tr}(t_a t_b t_c) = iC_F \mathcal{N}_C C_A / 2$, and the approximation $\beta_j \cdot l \gg \beta_j \cdot k$ for $j = 1, 2$, which is valid due to the strong ordering of the final state gluon energies, we arrive at

$$a) + (k \leftrightarrow l) = \frac{1}{4} C_F \mathcal{N}_C C_A g_s^4 \frac{\beta_1 \cdot \beta_2}{k \cdot l} \left(\frac{1}{\beta_1 \cdot k \beta_2 \cdot l} + \frac{2}{\beta_1 \cdot l \beta_2 \cdot k} \right). \tag{C.3}$$

We proceed in a similar manner for the rest of the diagrams. The results are:

$$\begin{aligned}
b) + (k \leftrightarrow l) &= \frac{1}{4} C_F \mathcal{N}_C C_A g_s^4 \frac{\beta_1 \cdot \beta_2}{k \cdot l} \left(\frac{2}{\beta_1 \cdot k \beta_2 \cdot l} + \frac{1}{\beta_1 \cdot l \beta_2 \cdot k} \right), \\
c) &= \frac{1}{4} C_F \mathcal{N}_C C_A g_s^4 \frac{\beta_1 \cdot \beta_2}{k \cdot l} \frac{1}{\beta_1 \cdot l} \frac{1}{\beta_2 \cdot k}, \\
d) &= \frac{1}{4} C_F \mathcal{N}_C C_A g_s^4 \frac{\beta_1 \cdot \beta_2}{k \cdot l} \frac{1}{\beta_1 \cdot k} \frac{1}{\beta_2 \cdot l}, \\
e) &= C_F \mathcal{N}_C (C_F - C_A / 2) g_s^4 \frac{(\beta_1 \cdot \beta_2)^2}{\beta_1 \cdot l \beta_2 \cdot l} \frac{1}{\beta_1 \cdot k \beta_2 \cdot k}, \\
f) + (k \leftrightarrow l) &= C_F \mathcal{N}_C (C_F - C_A / 2) g_s^4 \frac{(\beta_1 \cdot \beta_2)^2}{\beta_1 \cdot l \beta_2 \cdot l} \frac{2}{\beta_1 \cdot k \beta_2 \cdot k}. \tag{C.4}
\end{aligned}$$

The color factors in the last two equations of (C.4) are obtained from the identity $\text{Tr}(t_a t_b t_a t_b) = C_F \mathcal{N}_C (C_F - C_A / 2)$. Combining the terms proportional

to the color factor $C_F \mathcal{N}_C C_A$, and including the complex conjugate diagrams, we find for the squared amplitude

$$\begin{aligned}
|M|^2 &= 2g_s^4 C_F \mathcal{N}_C C_A \beta_1 \cdot \beta_2 \\
&\times \left(\frac{1}{k \cdot l \beta_1 \cdot k \beta_2 \cdot l} + \frac{1}{k \cdot l \beta_1 \cdot l \beta_2 \cdot k} - \frac{\beta_1 \cdot \beta_2}{\beta_1 \cdot l \beta_2 \cdot l \beta_1 \cdot k \beta_2 \cdot k} \right).
\end{aligned} \tag{C.5}$$

Having determined the amplitude, we need to integrate $|M|^2$ over the phase space corresponding to the geometry given in Fig. 4.2. Specifically, we have to evaluate:

$$I \equiv \frac{1}{\mathcal{N}_C} \int d\bar{\varepsilon} e^{-\nu \bar{\varepsilon}} \int_{\Omega} \frac{d^3 k}{(2\pi)^3 2\omega_k} \int_{\bar{\Omega}} \frac{d^3 l}{(2\pi)^3 2\omega_l} \delta(\varepsilon - \omega_k/\sqrt{s}) \delta(\bar{\varepsilon} - \bar{f}(l, a)) |M|^2, \tag{C.6}$$

where the weight function $\bar{f}(l, a)$ is given, as in Eqs. (4.4) and (4.11), by

$$\bar{f}(l, a) = \begin{cases} \frac{\omega_l}{\sqrt{s}} (1 - c_l)^{1-a} s_l^a & : \theta_l \in (0, \pi/2 - \delta) \\ \frac{\omega_l}{\sqrt{s}} (1 + c_l)^{1-a} s_l^a & : \theta_l \in (\pi/2 + \delta, \pi), \end{cases} \tag{C.7}$$

with $a < 1$.

Using the equalities: $\beta_1 \cdot \beta_2 = 2$, $\beta_1 \cdot l = \omega_l(1 - c_l)$, $\beta_2 \cdot l = \omega_l(1 + c_l)$, $\beta_1 \cdot k = \omega_k(1 - c_k)$, $\beta_2 \cdot k = \omega_k(1 + c_k)$ and $k \cdot l = \omega_k \omega_l (1 - c_k c_l - s_k s_l \cos \phi)$ in Eq. (C.5), performing the integration over ϕ , and changing the integration variable $c_l \rightarrow -c_l$ in the angular region $\theta_l \in (\pi/2 + \delta, \pi)$, we easily arrive at

the following three-dimensional integral:

$$I = C_F C_A \left(\frac{\alpha_s}{\pi} \right)^2 \frac{1}{\varepsilon} \int_{-\sin \delta}^{\sin \delta} dc_k \int_{\sin \delta}^1 dc_l \int_{\varepsilon \sqrt{s}}^{\sqrt{s}} \frac{d\omega_l}{\omega_l} e^{-\nu \omega_l (1-c_l)^{1-a} s_l^a / \sqrt{s}} \left[\frac{1}{c_k + c_l} \frac{1}{1 + c_k} \left(\frac{1}{1 + c_l} + \frac{1}{1 - c_k} \right) - \frac{1}{s_k^2} \frac{1}{1 + c_l} \right]. \quad (\text{C.8})$$

We are interested in the $(1/\varepsilon) \ln(1/\varepsilon)$ behavior of I . This is obtained after performing the ω_l integral with the replacement $e^{-\nu \omega_l (1-c_l)^{1-a} s_l^a / \sqrt{s}} \rightarrow \theta(1 - \nu \omega_l (1 - c_l)^{1-a} s_l^a / \sqrt{s})$. Remainders do not contain terms proportional to $\ln \varepsilon$. In this approximation, the c_l integration can be carried out, and we obtain the integral representation for the term containing $(1/\varepsilon) \ln(1/\varepsilon)$:

$$I = 2 C_F C_A \left(\frac{\alpha_s}{\pi} \right)^2 \frac{1}{\varepsilon} \ln \left(\frac{1}{\varepsilon \nu} \right) \times \left[\int_0^{\sin \delta} \frac{dc_k}{s_k^2} \ln \left(\frac{s_k^2}{s_k^2 - \cos^2 \delta} \right) - \ln \left(\frac{2}{1 + \sin \delta} \right) \ln \left(\frac{1 + \sin \delta}{1 - \sin \delta} \right) \right]. \quad (\text{C.9})$$

The potential non-global logarithm of ε is replaced by $\ln(\varepsilon \nu)$. The angular integral over c_k can be expressed in terms of dilogarithmic functions. The final expression for the term proportional to $\ln(\varepsilon \nu)/\varepsilon$ takes the form:

$$I = C_F C_A \left(\frac{\alpha_s}{\pi} \right)^2 \frac{1}{\varepsilon} \ln \left(\frac{1}{\varepsilon \nu} \right) \left[\frac{\pi^2}{6} + \ln \left(\frac{\cot \delta (1 + \sin \delta)}{4} \right) \ln \left(\frac{1 + \sin \delta}{1 - \sin \delta} \right) + \text{Li}_2 \left(\frac{1 - \sin \delta}{2} \right) - \text{Li}_2 \left(\frac{1 + \sin \delta}{2} \right) - \text{Li}_2 \left(-\frac{2 \sin \delta}{1 - \sin \delta} \right) - \text{Li}_2 \left(\frac{1 - \sin \delta}{1 + \sin \delta} \right) \right]. \quad (\text{C.10})$$

Equivalently, we can express our results in terms of the rapidity width of the

region Ω , Eq. (4.14), and we obtain

$$\begin{aligned}
I &= C_F C_A \left(\frac{\alpha_s}{\pi}\right)^2 \frac{1}{\varepsilon} \ln\left(\frac{1}{\varepsilon\nu}\right) \left[\frac{\pi^2}{6} + \Delta\eta \left(\frac{\Delta\eta}{2} - \ln(2 \sinh(\Delta\eta)) \right) \right] \\
&+ \operatorname{Li}_2\left(\frac{e^{-\Delta\eta/2}}{2 \cosh(\Delta\eta/2)}\right) - \operatorname{Li}_2\left(\frac{e^{\Delta\eta/2}}{2 \cosh(\Delta\eta/2)}\right) \\
&- \operatorname{Li}_2(-2 \sinh(\Delta\eta/2) e^{\Delta\eta/2}) - \operatorname{Li}_2(e^{-\Delta\eta})].
\end{aligned} \tag{C.11}$$

The coefficient

$$C(\Delta\eta) \equiv - \left(\frac{\pi}{\alpha_s}\right)^2 \frac{\varepsilon I}{C_F C_A \ln(\varepsilon\nu)} \tag{C.12}$$

as a function of $\Delta\eta$ is shown in Fig. C.1. Naturally, C is a monotonically increasing function of $\Delta\eta$. For $\Delta\eta \rightarrow 0$,

$$C \sim \mathcal{O}(\Delta\eta \ln \Delta\eta), \tag{C.13}$$

and the cross section vanishes, as expected. On the other hand, as the size of region Ω increases, C rapidly saturates and reaches its limiting value [68]

$$\lim_{\Delta\eta \rightarrow \infty} C = \frac{\pi^2}{6}. \tag{C.14}$$

C.2 Recoil

In this appendix, we return to the justification of the technical step represented by Eq. (4.23). According to this approximation, we may compute the jet functions by identifying axes that depend only upon particles in the final states N_{J_c} associated with those functions, rather than the full final state N .

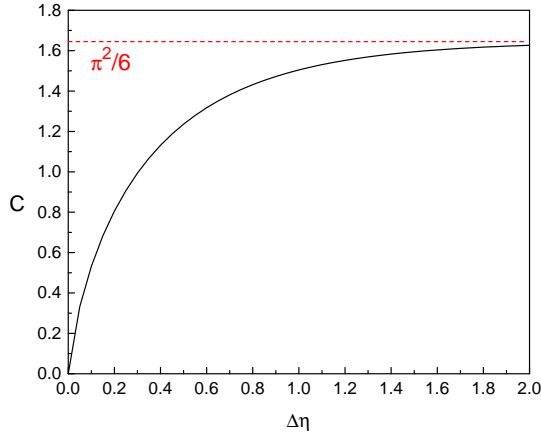


Figure C.1: $C(\Delta\eta)$, as defined in (C.12), as a function of rapidity width $\Delta\eta$ of the region Ω . The dashed line is its limiting value, $C(\Delta\eta \rightarrow \infty) = \pi^2/6$.

Intuitively, this is a reasonable estimate, given that the jet axis should be determined by a set of energetic, nearly collinear particles. When we make this replacement, however, the contributions to the event shape from energetic particles near the jet axis may change. This change is neglected in going from the original factorization, Eq. (4.21), to the factorization in convolution form, Eq. (4.27), which is the starting point for the resummation techniques that we employ in this paper. The weight functions $\bar{f}^N(N_i, a)$ in Eq. (4.21) are defined relative to the unit vector \hat{n}_1 corresponding to $a = 0$, the thrust-like event shape. The factorization of Eq. (4.21) applies to any $a < 2$, but as indicated by the superscript, individual contributions to $\bar{f}^N(N_i, a)$ on the right-hand side continue to depend on the full final state N , through the identification of the jet axis.

To derive the factorization of Eq. (4.27) in a simple convolution form, we must be able to treat the thrust axis, \hat{n}_1 , as a fixed vector for each of the states N_s, N_{J_c} . This is possible if we can neglect the effects of recoil from soft,

wide-angle radiation on the direction of the axis. Specifically, we must be able to make the replacement

$$\bar{f}_{\bar{\Omega}_c}^N(N_{J_c}, a) \rightarrow \bar{f}_c(N_{J_c}, a), \quad (\text{C.15})$$

where $\bar{f}_c(N_{J_c}, a)$ is the event shape variable for jet c , in which the axis \hat{n}_c is specified by state N_{J_c} *only*. Of course, this replacement changes the value of the weight, $\bar{\varepsilon}$, $\bar{f}_{\bar{\Omega}_c}^N(N_{J_c}, a) \neq \bar{f}_c(N_{J_c}, a)$. As we now show, the error induced by this replacement is suppressed by a power of $\bar{\varepsilon}$ so long as $a < 1$. In general, the error is nonnegligible for $a \geq 1$. The importance of recoil for jet broadening, at $a = 1$, was pointed out in [59]. We now discuss how the neglect of such radiation affects the jet axis (always determined from $a = 0$) and hence the value of the event shape for arbitrary $a < 2$.

The jet axis is found by minimizing $\bar{f}(a = 0)$ in each state. The largest influence on the axis \hat{n}_c for jet c is, of course, the set of fast, collinear particles within the state N_{J_c} associated with the jet function in Eq. (4.21). Soft, wide-angle radiation, however, does affect the precise direction of the axis. This is what we mean by ‘recoil’.

Let us denote by ω_s the energy of the soft wide-angle radiation that is neglected in the factorization (4.27). Neglecting this soft radiation in the determination of the jet axis will result in an axis $\hat{n}_1(N_{J_c})$, which differs from the axis $\hat{n}_1(N)$ determined from the complete final state (N) by an angle $\Delta_s\phi$:

$$\angle(\hat{n}_1(N), \hat{n}_1(N_{J_c})) \equiv \Delta_s\phi \sim \frac{\omega_s}{Q}. \quad (\text{C.16})$$

At the same time, the soft, wide-angle radiation also contributes to the total

event shape $\bar{f}(N, a) \sim (1/Q)k_{\perp}^a (k^-)^{1-a}$ at the level of

$$\bar{\varepsilon}_s \sim \frac{\omega_s}{Q}, \quad (\text{C.17})$$

because for such wide-angle radiation, we may take $k_s^- \sim k_{s,\perp} \sim \omega_s$. In summary, the neglect of wide-angle soft radiation rotates the jet axis by an angle that is of the order of the contribution of the same soft radiation to the event shape.

In the factorization (4.27), the contribution of each final-state particle is taken into account, just as in Eq. (4.21). The question we must answer is how the rotation of the jet axis affects these contributions, and hence the value of the event shape.

For a wide-angle particle, the rotation of the jet axis by an angle of order $\Delta_s \phi$ in Eq. (C.16) leads to a negligible change in its contributions to the event shape, because its angle to the axis is a number of order unity, and the jet axis is rotated only by an angle of order $\bar{\varepsilon}_s$. Contributions from soft radiation are therefore stable under the approximation (4.23). The only source of large corrections is then associated with energetic jet radiation, because these particles are nearly collinear to the jet axis.

It is easy to see from the form of the shape function in terms of angles, Eq. (4.11), that for any value of parameter a , a particle of energy ω_i at a small angle θ_i to the jet axis $\hat{n}_1(N)$ contributes to the event shape at the level

$$\bar{\varepsilon}_i \sim \frac{\omega_i}{Q} \theta_i^{2-a}. \quad (\text{C.18})$$

The rotation of the jet axis by the angle $\Delta_s\phi$ due to neglect of soft radiation may be as large as, or larger than, θ_i . Assuming the latter, we find a shift in the $\bar{\varepsilon}_i$ of order

$$\delta\bar{\varepsilon}_i \equiv \bar{\varepsilon}_i(\hat{n}_1(N)) - \bar{\varepsilon}_i(\hat{n}_1(N_{J_c})) \sim \frac{\omega_i}{Q} (\Delta_s\phi)^{2-a} \sim \frac{\omega_i}{Q} \left(\frac{\omega_s}{Q}\right)^{2-a} \sim \frac{\omega_i}{Q} \bar{\varepsilon}_s^{2-a}. \quad (\text{C.19})$$

The change in $\bar{\varepsilon}_i$ is thus suppressed by at least a factor $\bar{\varepsilon}_s^{1-a}$ compared to $\bar{\varepsilon}_s$, which is the contribution of the wide-angle soft radiation to the event shape. The contributions of nearly-collinear, energetic radiation to the event shape thus change significantly under the replacement (4.23), but so long as $a < 1$, these contributions are power-suppressed in the value of the event shape, both before and after the approximation that leads to a rotation of the axis. For this reason, when $a < 1$ (and only when $a < 1$), the value of the event shape is stable whether or not we include soft radiation in the determination of the jet axes, up to corrections that are suppressed by a power of the event shape. In this case, the transition from Eq. (4.21) to Eq. (4.27) is justified.

Bibliography

- [1] M. Gell-Mann, *Phys. Lett.* **8** 214 (1964).
G. Zweig, *Preprints CERN-TH* **401** and **412** (1964).
- [2] H. Fritzsch, M. Gell-Mann, H. Leutwyler, *Phys. Lett.* **47 B** 365 (1973).
- [3] C. Becchi, A. Rouet, R. Stora, *Commun. Math Phys.* **42**, 127 (1975);
Ann. Phys. **98**, 287 (1976).
- [4] G. 't Hooft, *Proc. Colloquium on Renormalization of Yang-Mills Fields and Applications in Particle Physics*, Marseilles, 1972 (ed. C. P. Korthals-Altes).
- D. J. Gross, F. Wilczek, *Phys. Rev. Lett.* **30** 1343 (1973).
H. D. Politzer, *Phys. Rev. Lett.* **30** 1346 (1973).
- [5] G. 't Hooft, *Nucl. Phys.* **B 33** 173 (1971).
- [6] F. Bloch, A. Nordsieck, *Phys. Rev.* **D 31** 2616 (1937).
- [7] T. Kinoshita, *J. Math. Phys.* **3** 650 (1962).
T. D. Lee, M. Nauenberg, *Phys. Rev.* **133 B** 1549 (1964).

- [8] J. C. Collins, D. E. Soper, G. Sterman, *Factorization of hard processes in QCD*, in *Perturbative Quantum Chromodynamics*, ed. A. H. Mueller (World Scientific, Singapore, 1989), p. 1.
- [9] G. Altarelli, G. Parisi, *Nucl. Phys.* **B 126** 298 (1977).
 V. N. Gribov, L. N. Lipatov, *Sov. J. Nucl. Phys.* **15** 438 (1972).
 L. N. Lipatov, *Sov. J. Nucl. Phys.* **20** 94 (1975).
- [10] T. Kúcs, *Scattering Amplitudes in High Energy QCD*, [hep-ph/0307141].
- [11] T. Kúcs *Gluon Reggeization*, In preparation.
- [12] C. F. Berger, T. Kúcs, G. Sterman, *Phys. Rev.* **D 68** 014012 (2003) [hep-ph/0303051].
 C. F. Berger, *Soft Gluon Exponentiation and Resummation*, Ph.D. Thesis [hep-ph/0305076].
- [13] L.N. Lipatov, in “*Perturbative QCD*”, ed. A. H. Mueller (World Scientific, Singapore, 1989).
- [14] H. Cheng, T.T. Wu, “*Expanding Protons: Scattering at High Energies*”, (MIT Press, Cambridge, Massachusetts, 1987).
- [15] J.R. Forshaw, D.A. Ross, *Quantum Chromodynamics and the Pomeron*, (Cambridge University Press, 1997).
- [16] A. Sen, *Phys. Rev.* **D 27**, 2997 (1983).
- [17] T. Jaroszewicz, *Acta Phys. Pol.* **B 11**, 965 (1980).

- [18] M. Gell-Man, M.L. Goldberger, F.E. Low, E. Marx, F. Zachariasen, *Phys. Rev.* **133**, B145 (1964).
 J.C. Polkinghorne, *J. Math. Phys.* **5**, 1491 (1964).
 H. Cheng and T.T. Wu, *Phys. Rev.* **140**, B465 (1965).
- [19] B.M. McCoy and T.T. Wu, *Phys. Rev.* **D 13**, 369 (1976); 379 (1976); 395 (1976); 424 (1976); 484 (1976); 508 (1976).
- [20] A.L. Mason, *Nucl. Phys.* **B 104**, 141 (1976); **B 117** 493 (1976); **B 120**, 275 (1977).
- [21] L.N. Lipatov, *Sov. J. Nucl. Phys.* **23**, 338 (1976).
 E.A. Kuraev, L.N. Lipatov, V.S. Fadin, *Sov. Phys. JETP* **44**, 443 (1976).
 E.A. Kuraev, L.N. Lipatov, V.S. Fadin, *Sov. Phys. JETP* **45**, 199 (1977).
 Ya. Balitskii, L.N. Lipatov, *Sov. J. Nucl. Phys.* **28**, 822 (1978).
- [22] J. Kwiecinski, M. Praszalowicz, *Phys. Lett.* **B 94**, 413 (1980).
- [23] J. Bartels, *Nucl. Phys.* **B 151**, 293 (1979); **B 175**, 365 (1980).
- [24] H. Cheng, J. Dickinson, C.Y. Lo, K. Olausson, P.S. Yeung, *Phys. Lett.* **B 76** 129 (1978).
- [25] G.P. Salam, *Acta Phys. Pol.* **B 30**, 3679 (1999).
- [26] V.S. Fadin, L.N. Lipatov, *Sov. J. Nucl. Phys.* **50**, 712 (1989); *Nucl. Phys.* **B 477**, 767 (1996) [hep-ph/9602287].
 V. del Duca, *Phys. Rev.* **D 54**, 989 (1996) [hep-ph/9601211]; 4474 (1996) [hep-ph/9604250].

- [27] V.S. Fadin, L.N. Lipatov, *Nucl. Phys.* **B 406**, 259 (1993).
 V.S. Fadin, R. Fiore, A. Quartarolo, *Phys. Rev.* **D 50**, 5893 (1994) [hep-ph/9405127].
 V.S. Fadin, R. Fiore, M.I. Kotsky, *Phys. Lett.* **B 389**, 737 (1996) [hep-ph/9608229].
 V. Del Duca, C.R. Schmidt, *Phys. Rev.* **D 59**, 074004 (1999) [hep-ph/9810215].
 Z. Bern, V. Del Duca, C.R. Schmidt, *Phys. Lett.* **B 445**, 168 (1998) [hep-ph/9810409].
- [28] V.S. Fadin, R. Fiore, M.I. Kotsky, *Phys. Lett.* **B 359**, 181 (1995).
 V.S. Fadin, R. Fiore, A. Quartarolo, *Phys. Rev.* **D 53**, 2729 (1996).
 V.S. Fadin, R. Fiore, *Phys. Rev.* **D 64**, 114012 (2001).
 J. Blumlein, V. Ravindran, W.L. van Neerven, *Phys. Rev.* **D 58**, 091502 (1998) [hep-ph/9806357].
- [29] G.P. Korchemsky, *Phys. Lett.* **B 325**, 459 (1994).
 I.A. Korchemskaya, G.P. Korchemsky, *Nucl. Phys.* **B437**, 127 (1995);
Phys. Lett. **B 387**, 346 (1996).
- [30] V. del Duca, E.W.N. Glover, *JHEP* **0110**, 035 (2001) [hep-ph/0109028].
- [31] J. Bartels, V.S. Fadin, R. Fiore, *The Bootstrap Conditions for the Gluon Reggeization* [hep-ph/0307076].
- [32] V.S. Fadin, L.N. Lipatov, *Phys. Lett.* **B 429**, 127 (1998) [hep-ph/9802290].

- G. Camici, M. Ciafaloni, *Phys. Lett.* **B 412** 396 (1997); Erratum **B 417** 390 (1998) [hep-ph/9707390]; **B 430** 349 (1998) [hep-ph/9803389].
- [33] A.V. Bogdan, V. del Duca, V.S. Fadin, E.W.N. Glover, *JEHP* **0203** 032, (2002) [hep-ph/0201240].
- [34] C. Anastasiou, E.W.N. Glover, C. Oleari, M.E. Tejeda-Yeomans, *Nucl. Phys.* **B 601**, 318 (2001) [hep-ph/0010212]; **B 601**, 341 (2001) [hep-ph/0011094]; **B 605**, 486 (2001) [hep-ph/0101304].
E.W.N. Glover, C. Oleari, M.E. Tejeda-Yeomans, *Nucl. Phys.* **B 605**, 467 (2001) [hep-ph/0102201].
- [35] L.V. Gribov, E.M. Levin, M.G. Ryskin, *Phys. Rept.* **100** 1 (1983).
A.H. Mueller, J.W. Qiu, *Nucl. Phys.* **B 268** 427 (1986).
L. McLerran, R. Venugopalan, *Phys. Rev.* **D 49** 2233 (1994); **D 49** 3352 (1994); **D 50** 2225 (1994).
- [36] I. Balitsky, *Nucl. Phys.* **B 463** 99 (1996); *Phys. Rev. Lett.* **81** 2024 (1998) [hep-ph/9807434].
A.H. Mueller, *Nucl. Phys.* **B 558** 285 (1999).
Yu.V. Kovchegov, *Phys. Rev.* **D 60** 034008 (1999); **D 61** 074018 (2000).
J. Jalilian-Marian, A. Kovner, L. McLerran, H. Weigert, *Nucl. Phys.* **B 504** 415 (1997); *Phys. Rev.* **D 59** 014014 (1999); *Phys. Rev.* **D 59** 034007 (1999).
- [37] L.N. Lipatov *JETP Lett.* **59** 596 (1994); *Pisma Zh. Eksp. Teor. Fiz.* **59** (571) 1994 [hep-th/9311037].

- L.D. Faddeev, G.P. Korchemsky, *Phys. Lett.* **B 342** 311 (1995) [hep-th/9404173].
- [38] L. Baulieu and D. Zwanziger, *Nucl. Phys.* **B 548** 527 (1999) [hep-th/9807024].
- [39] G. Sterman, *Phys. Rev.* **D 17**, 2773 (1978).
- [40] G. Sterman, S.B. Libby, *Phys. Rev.* **D 18**, 3252 (1978).
 G. Sterman, *An Introduction to Quantum Field Theory*, Cambridge Univ. Press, 1993.
 G. Sterman, *QCD and Beyond, Proceedings of the Theoretical Advanced Study Institute in Elementary Particle Physics (TASI 95)*, ed. D.E. Soper (World Scientific, 1996), hep-ph/9606312.
- [41] J.C. Collins, G. Sterman, *Nucl. Phys.* **B 185** 172 (1981).
 G.T. Bodwin, S.J. Brodsky, G.P. Lepage, *Phys. Rev. Lett.* **47** 1799 (1981).
- [42] S. Coleman, R.E. Norton, *Nuovo Cimento* **38**, 438 (1965).
- [43] A. Sen, *Phys. Rev.* **D 24**, 3281 (1981).
- [44] J.C. Collins, D.E. Soper, *Nucl. Phys.* **B 193**, 381 (1981).
- [45] G. Grammer, D.R. Yennie, *Phys. Rev.* **D 8**, 4332 (1973).
- [46] G. 't Hooft, *Nucl. Phys.* **B33**, 173 (1971).
 G. 't Hooft, M. Veltman, *Nucl. Phys.* **B50**, 318 (1972).
- [47] C. Becchi, A. Rouet, R. Stora, *Commun. Math Phys.* **42**, 127 (1975);
Ann. Phys. **98**, 287 (1976).

- [48] H. Kluberg-Stern, J. B. Zuber, *Phys. Rev. D* **12**, 476 (1975); **12**, 482 (1975).
N. K. Nielsen, *Nucl. Phys. B* **101**, 173 (1975).
- [49] G. Leibbrandt, J. Williams, *Nucl. Phys. B* **475**, 469 (1996).
- [50] G. Leibbrandt, *Nucl. Phys. B* **64** (Proc. Suppl.), 101 (1998).
- [51] G. Sterman, *An Introduction to Quantum Field Theory*, Cambridge Univ. Press, 1993.
- [52] S. Bethke, in *Barcelona 1998, Radiative corrections: Application of quantum field theory to phenomenology*, p. 243, [hep-ex/9812026].
CDF Collaboration and D0 Collaboration (Sally Seidel for the collaborations), *Jet physics at the Tevatron*, hep-ex/0205013.
H1 Collaboration and ZEUS Collaboration (Oscar Gonzalez for the collaboration), *Jet physics at HERA*, hep-ex/0211063.
- [53] Yu. L. Dokshitzer, V. A. Khoze, S. I. Troyan, in *Perturbative quantum chromodynamics*, ed. A. H. Mueller (World Scientific, Singapore, 1989), p. 241.
Yu. L. Dokshitzer, V. A. Khoze, S. I. Troyan, A. H. Mueller, *Rev. Mod. Phys.* **60**, 373 (1988).
- [54] H. Georgi, M. Machacek, *Phys. Rev. Lett.* **39**, 1237 (1977).
C. L. Basham, L. S. Brown, S. D. Ellis, S. T. Love, *Phys. Rev. Lett.* **41**, 1585 (1978).
A. De Rujula, J. R. Ellis, E.G. Floratos, M. K. Gaillard, *Nucl. Phys. B*

- 138**, 387 (1978).
- G. C. Fox, S. Wolfram, Phys. Rev. Lett. **41**, 1581 (1978).
- G. Parisi, Phys. Lett. **B 74**, 65 (1978).
- J. F. Donoghue, F. E. Low, S.-Y. Pi, Phys. Rev. **D 20**, 2759 (1979).
- R. K. Ellis, D. A. Ross, A. E. Terrano, Phys. Rev. Lett. **45**, 1226 (1980).
- [55] E. Farhi, Phys. Rev. Lett. **39**, 1587 (1977).
- [56] G. Sterman, Phys. Rev. **D 19**, 3135 (1979).
- [57] S. Catani, G. Turnock, B. R. Webber, L. Trentadue, Phys. Lett. **B 263**, 491 (1991).
- S. Catani, L. Trentadue, G. Turnock, B. R. Webber, Nucl. Phys. **B 407**, 3 (1993).
- [58] S. Catani, G. Turnock, B. R. Webber, Phys. Lett. **B 295**, 269 (1992).
- [59] Yu. L. Dokshitzer, A. Lucenti, G. Marchesini, G. P. Salam, JHEP **9801**, 011 (1998) [hep-ph/9801324].
- [60] G. P. Korchemsky, G. Sterman, in *Moriond 1995: Hadronic:0383-392* [hep-ph/9505391]; Nucl. Phys. **B 437**, 415 (1995) [hep-ph/9411211]; Nucl. Phys. **B 555**, 335 (1999) [hep-ph/9902341].
- Yu. L. Dokshitzer, B. R. Webber, Phys. Lett. **B 404**, 321 (1997) [hep-ph/9704298].
- A. V. Belitsky, G. P. Korchemsky, G. Sterman, Phys. Lett. **B 515**, 297 (2001) [hep-ph/0106308].
- E. Gardi, J. Rathsman, Nucl. Phys. **B 638**, 243 (2002) [hep-ph/0201019].

- C. F. Berger, G. Sterman, JHEP **0309**, 058 (2003) [hep-ph/0307394]; [hep-ph/0310058].
- [61] N. A. Sveshnikov, F. V. Tkachov, Phys. Lett. **B 382**, 403 (1996) [hep-ph/9512370].
 F.V. Tkachov, Int. J. Mod. Phys. **A 12**, 5411 (1997) [hep-ph/9601308].
 G. P. Korchemsky, G. Oderda, G. Sterman, in *5th International Workshop on Deep Inelastic Scattering and QCD (DIS 97)*, AIP Conference Proceedings 407, ed. J. Repond, D. Krakauer (American Institute of Physics, Woodbury, NY 1978), p. 988, [hep-ph/9708346].
 C. F. Berger *et al.*, in *Proc. of the APS/DPF/DPB Summer Study on the Future of Particle Physics (Snowmass 2001)* ed. N. Graf, eConf **C010630**, P512 (2001) [hep-ph/0202207].
- [62] W. Bartel *et al.* [JADE Collaboration], Phys. Lett. **B 101**, 129 (1981); Z. Phys. **C 21**, 37 (1983).
 M. Althoff *et al.* [TASSO Collaboration], Z. Phys. **C 29**, 29 (1985).
 M. Z. Akrawy *et al.* [OPAL Collaboration], Phys. Lett. **B 261**, 334 (1991).
 R. Akers *et al.* [OPAL Collaboration], Z. Phys. **C 68**, 531 (1995).
- [63] J. R. Ellis, V. A. Khoze, W. J. Stirling, Z. Phys. **C75**, 287 (1997) [hep-ph/9608486].
- [64] B. Abbott *et al.* [D0 Collaboration], Phys. Lett. **B 464**, 145 (1999) [hep-ex/9908017].
- [65] N. Kidonakis, G. Oderda, G. Sterman, Nucl. Phys. **B 531**, 365 (1998) [hep-ph/9803241].

- [66] C. F. Berger, T. Kúcs, G. Sterman, Phys. Rev. **D 65**, 094031 (2002) [hep-ph/0110004].
- [67] J. Huston (CDF Collaboration), Int. J. Mod. Phys. **A16S1A**, 219 (2001).
V. Tano, *The underlying event in hadron-hadron collisions*, hep-ex/0205023.
- [68] M. Dasgupta, G. P. Salam, Phys. Lett. **B 512**, 323 (2001) [hep-ph/0104277]; JHEP **0203**, 017 (2002) [hep-ph/0203009]; JHEP **0208**, 032 (2002) [hep-ph/0208073].
- [69] C. F. Berger, T. Kúcs, G. Sterman, Int. J. Mod. Phys. **A 18** 4159 (2003) [hep-ph/0212343].
- [70] A. Banfi, G. Marchesini, Yu. L. Dokshitzer, G. Zanderighi, JHEP **0007**, 001 (2000) [hep-ph/0004027].
S. J. Burby, N. Glover, JHEP **0104**, 029 (2001) [hep-ph/0101226].
R. B. Appleby, M. H. Seymour, JHEP **0212**, 063 (2002) [hep-ph/0211426].
- [71] A. Banfi, G. Marchesini, G. Smye, JHEP **0208**, 006 (2002) [hep-ph/0206076].
- [72] J. C. Collins, D. E. Soper, Nucl. Phys. **B 193**, 381 (1981).
- [73] A. V. Manohar, M. B. Wise, Phys. Lett. **B 344**, 407 (1995) [hep-ph/9406392].
- [74] R. B. Appleby, M. H. Seymour, Ref. [70].
- [75] G. Sterman, Phys. Rev. **D 17**, 2773 (1978).

- [76] G. Sterman, in *QCD & Beyond*, proceedings of the Theoretical Advanced Study Institute in Elementary Particle Physics (TASI '95), ed. D.E. Soper (World Scientific, Singapore, 1996) [hep-ph/9606312].
- [77] J. C. Collins, D. E. Soper, Nucl. Phys. B **194**, 445 (1982).
- [78] N. Kidonakis, G. Sterman, Nucl. Phys. B **505**, 321 (1997) [hep-ph/9705234].
N. Kidonakis, G. Oderda and G. Sterman, Nucl. Phys. B **525**, 299 (1998) [hep-ph/9801268].
- [79] J. C. Collins, G. Sterman, Nucl. Phys. B **185**, 172 (1981).
- [80] H. Contopanagos, E. Laenen, G. Sterman, Nucl. Phys. B **484**, 303 (1997) [hep-ph/9604313].
- [81] Y. L. Dokshitzer, G. Marchesini, JHEP **0303**, 040 (2003) [hep-ph/0303101].
- [82] G. Oderda, Phys. Rev. D **61**, 014004 (2000) [hep-ph/9903240].
- [83] A. Sen, Phys. Rev. D **24**, 3281 (1981).
G. P. Korchemsky, A. V. Radyushkin, Nucl. Phys. B **283**, 342 (1987).
- [84] J. C. Collins, D. E. Soper, G. Sterman, Nucl. Phys. B **250**, 199 (1985).
- [85] A. Gonzalez-Arroyo, C. Lopez, F. J. Yndurain, Nucl. Phys. B **153**, 161 (1979).
G. Curci, W. Furmanski, R. Petronzio, Nucl. Phys. B **175**, 27 (1980).
E. G. Floratos, C. Kounnas, R. Lacaze, Nucl. Phys. B **192**, 417 (1981).
J. Kodaira, L. Trentadue, Phys. Lett. B **112**, 66 (1982).

- [86] S. Catani, L. Trentadue, Nucl. Phys. **B 353**, 183 (1991).
- [87] G. Sterman, Nucl. Phys. **B 281**, 310 (1987).
S. Catani, L. Trentadue, Nucl. Phys. **B 327**, 323 (1989).
- [88] G. P. Korchemsky, Mod. Phys. Lett. **A 4**, 1257 (1989).
S. Albino, R. D. Ball, Phys. Lett. **B 513**, 93 (2001) [hep-ph/0011133].
C. F. Berger, Phys. Rev. **D 66**, 116002 (2002) [hep-ph/0209107].